Measurement of total and differential W^+W^- production cross sections in proton-proton collisions at $\sqrt{s} = 8$ TeV with the ATLAS detector and limits on anomalous triple-gauge-boson couplings

The ATLAS collaboration

E-mail: atlas.publications@cern.ch

ABSTRACT: The production of W boson pairs in proton-proton collisions at $\sqrt{s} = 8$ TeV is studied using data corresponding to $20.3\,\mathrm{fb}^{-1}$ of integrated luminosity collected by the ATLAS detector during 2012 at the CERN Large Hadron Collider. The W bosons are reconstructed using their leptonic decays into electrons or muons and neutrinos. Events with reconstructed jets are not included in the candidate event sample. A total of 6636 WW candidate events are observed. Measurements are performed in fiducial regions closely approximating the detector acceptance. The integrated measurement is corrected for all acceptance effects and for the W branching fractions to leptons in order to obtain the total WW production cross section, which is found to be $71.1 \pm 1.1(\mathrm{stat})\,^{+5.7}_{-5.0}(\mathrm{syst}) \pm 1.4(\mathrm{lumi})$ pb. This agrees with the next-to-next-to-leading-order Standard Model prediction of $63.2^{+1.6}_{-1.4}(\mathrm{scale}) \pm 1.2(\mathrm{PDF})$ pb. Fiducial differential cross sections are measured as a function of each of six kinematic variables. The distribution of the transverse momentum of the leading lepton is used to set limits on anomalous triple-gauge-boson couplings.

Contents

1 Introduction

The measurement of the production of pairs of electroweak gauge bosons plays a central role in tests of the Standard Model (SM) and in searches for new physics at the TeV scale [1]. The WW production cross section would grow arbitrarily large as a function of the centre-of-mass energy of the production process, $\sqrt{\hat{s}}$, were it not for the cancellations of s- and t-channel W^+W^- (henceforth denoted WW) processes. New physics phenomena can occur as deviations from the gauge structure of the Standard Model in the triple-gauge-boson couplings ZWW or γWW [2], termed anomalous triple-gauge-boson couplings (aTGCs). As the cross section for WW production is one of the largest among those involving a triple-gauge-boson vertex, it allows tests of the self-interaction of the gauge bosons to be made with high precision through measurements of differential kinematic distributions. Studies of the WW production process are particularly important as it constitutes a large irreducible background to searches for physics beyond the SM as well as to resonant $H \to W^+W^-$ production.

A precise measurement of WW production also tests the validity of the theoretical calculations. Perturbative quantum chromodynamics (pQCD) is the essential ingredient in all these calculations and a recent calculation of non-resonant WW production has been performed up to next-to-next-to-leading order (NNLO) [3]. However, fixed-order calculations may fail to describe effects that arise from restrictions imposed on the phase space of the measurement. In this analysis, it is required that there be no jets above a certain transverse momentum threshold, which introduces an additional momentum scale in the theoretical calculation. Resumming the resulting large logarithms can improve the accuracy of the prediction. Several calculations including resummation effects up to next-to-next-to-leading logarithms (NNLL) have appeared recently in the literature [4–7]. Both the fixed-order and resummed predictions are compared to the measurements in this paper, except for ref. [4] which coincides with the central prediction of the NNLO fixed-order prediction.

The existence of a non-zero self-coupling of the Standard Model gauge bosons has been proved by measurements of WW production in electron-positron collisions at LEP [8]. The first measurement of the production of W boson pairs at a hadron collider was conducted by the CDF experiment using Tevatron Run I data [9]. Since then, more precise results have been published by the CDF [10] and DØ experiments [11]. The WW production cross sections have already been measured at the LHC for a centre-of-mass energy of $\sqrt{s} = 7$ TeV by the ATLAS Collaboration [12] and for centre-of-mass energies of $\sqrt{s} = 7$ TeV and 8 TeV
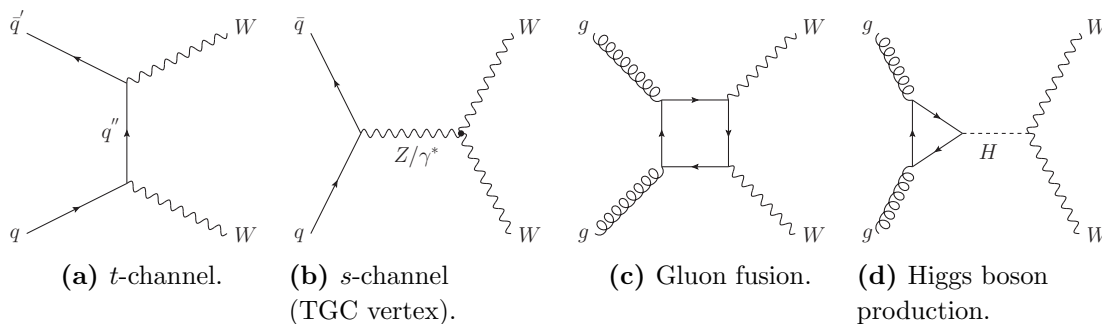
(a) *t*-channel. **(b)** *s*-channel (TGC vertex). **(c)** Gluon fusion. **(d)** Higgs boson production.

Figure 1. (a) The SM tree-level Feynman diagram for WW production through the $q\bar{q}$ initial state in the t-channel. (b) The corresponding tree-level diagram in the s-channel, which contains the WWZ and $WW\gamma$ TGC vertices. (c) The gluon fusion process, which is mediated by a quark loop. (d) The Higgs boson production process through gluon fusion and the subsequent decay of the Higgs boson to WW.

by the CMS Collaboration [13, 14]. Limits on anomalous couplings have been reported in these publications as well and, in several cases, are comparable to the most stringent aTGC limits set by the LEP experiments [8].

The present analysis uses a data sample with an integrated luminosity of $20.3\,\mathrm{fb}^{-1}$ at a centre-of-mass energy of $\sqrt{s} = 8$ TeV. The total and fiducial WW production cross sections are measured using $W \to e\nu$ and $W \to \mu\nu$ decays. Furthermore, measurements of differential cross sections are presented and limits on anomalous triple-gauge-boson couplings are reported.

2 Analysis overview

The production of WW signal events takes place dominantly through quark-antiquark t-channel scattering and s-channel annihilation, denoted by $q\bar{q} \to W^+W^-$,[1] and are shown in figures 1(a) and 1(b), where the latter process involves a triple-gauge-boson vertex. In addition, W boson pairs can be produced via gluon fusion through a quark loop; these are the non-resonant $gg \to W^+W^-$ and the resonant Higgs boson $gg \to H \to W^+W^-$ production processes in figures 1(c) and 1(d). All of these are considered as signal processes in this analysis.

The WW candidate events are selected in fully leptonic decay channels, resulting in final states of $e^{\pm}\overset{(-)}{\nu_e}\mu^{\mp}\overset{(-)}{\nu_\mu}$, $e^+\nu_e e^-\bar{\nu}_e$ and $\mu^+\nu_\mu\mu^-\bar{\nu}_\mu$. In the following, the different final states are referred to as $e\mu$, ee and $\mu\mu$.

Backgrounds to these final states originate from a variety of processes. Top-quark production ($t\bar{t}$ and the associated production of a single top quark and a W boson) also results in events with W pairs. In this case, the W bosons are, however, accompanied by b-quarks that hadronise into jets. To enhance the purity of the signal candidates, events are rejected if any jets above a certain transverse momentum threshold are present in the final state.

---

[1]In the following, $q\bar{q} \to W^+W^-$ is taken to also include qg initial states contributing to t-channel and s-channel WW production.

The Drell-Yan background is suppressed by requirements on missing transverse momentum, caused in WW events by final-state neutrinos. For final states with same-flavour leptons, a veto on dilepton invariant masses close to the Z pole mass is used. Other backgrounds stem from the W+jets or multijet production processes where one or more jets are misidentified as leptons. Diboson processes such as production of a heavy boson with an off- or on-shell photon or a Z boson, $WZ(\gamma^*)$, $W/Z + \gamma$ and ZZ production, where one of the leptons falls outside the acceptance of the detector or a photon converts to an electron-positron pair, are additional sources of backgrounds. Backgrounds stemming from top-quark, Drell-Yan, W+jets and multijet production are evaluated using partially data-driven methods, where simulated event samples are only used to describe the shape of kinematic distributions or to validate the methods. The background from diboson production processes is modelled using Monte Carlo samples normalised to the expected production cross section using theoretical calculations at the highest available order. Other processes, such as double parton interactions, vector-boson fusion processes or associated WH production, resulting in $e\mu$, ee and $\mu\mu$ final states are not considered explicitly in the analysis as their contribution to the selected event sample is expected to be negligible ($<0.6\%$).

The $e\mu$, ee and $\mu\mu$ measurements of the total WW production cross section are combined using a likelihood fit that includes the branching fractions into electrons or muons, whereas the fiducial cross sections are calculated per final state. Contributions from leptonic τ-decays are not included in the definitions of the fiducial cross sections in order to allow comparisons with existing theoretical predictions. Because of its larger signal acceptance and smaller background, only the $e\mu$ final state is used to measure differential cross sections and to set limits on anomalous triple-gauge-boson-couplings.

The differential cross sections are reported as a function of the transverse momentum of the leading lepton, $p_{\mathrm{T}}^{\mathrm{lead}}$, the transverse momentum of the dilepton system, $p_{\mathrm{T}}(\ell\ell)$, and the dilepton invariant mass, $m_{\ell\ell}$, all of which are correlated with the centre-of-mass energy of the interaction and thus sensitive to contributions from new physics processes at high values of $\sqrt{\hat{s}}$. Differential cross sections are also reported as a function of the azimuthal angle between the decay leptons, $\Delta\phi_{\ell\ell}$, which is correlated with the polarisation of the W bosons and plays a special role in the extraction of the scalar Higgs boson signal. Additional measurements are presented as a function of the rapidity of the dilepton system, $|y_{\ell\ell}|$, and the observable $|\cos(\theta^*)|$, which is defined using the difference between the pseudorapidities of the leptons, $\Delta\eta_{\ell\ell}$, as follows:

$$|\cos(\theta^*)| = \left|\tanh\left(\frac{\Delta\eta_{\ell\ell}}{2}\right)\right|, \tag{2.1}$$

where the pseudorapidity is defined as $\eta = -\ln\tan(\theta/2)$ with θ being the polar angle.[2] These variables are correlated with the rapidity and the boost of the WW system along

_____

[2]The ATLAS experiment uses a right-handed coordinate system with its origin at the nominal pp interaction point at the centre of the detector. The positive x-axis is defined by the direction from the interaction point to the centre of the LHC ring, with the positive y-axis pointing upwards, while the beam direction defines the z-axis. The azimuthal angle ϕ is measured around the beam axis and the polar angle θ is the angle from the z-axis. The distance in $\eta-\phi$ space between two objects is defined as $\Delta R = \sqrt{(\Delta\eta)^2 + (\Delta\phi)^2}$. Transverse energy is computed as $E_{\mathrm{T}} = E \cdot \sin\theta$.

the z-axis. The $|\cos(\theta^*)|$ variable has been suggested for searches for new physics in WW production in the low-p_T regime [15].

3 The ATLAS detector

The ATLAS detector is a general-purpose detector that is used to study collisions at the Large Hadron Collider (LHC). A detailed description can be found in ref. [16].

The inner detector (ID) is used to measure trajectories and momenta of charged particles within the central region of the ATLAS detector with pseudorapidities of $|\eta| < 2.5$. The ID is located inside a solenoid that provides a 2 T axial magnetic field. The ID consists of three sub-detector systems: a three-layer silicon-pixel tracker, a four-layer silicon-strip detector built of modules with pairs of single-sided sensors glued back-to-back, and a transition radiation tracker consisting of straw tubes. In the central region these sub-detectors are constructed in the shape of cylinders, while in the forward and backward regions, they take the form of disks. The innermost pixel layer of the ID is located just outside the beam-pipe.

Electromagnetic (EM) energy deposits are measured using a liquid-argon calorimeter with accordion-shaped electrodes and lead absorbers. The EM calorimeter is divided into a barrel part ($|\eta| < 1.475$) and two end-cap components ($1.375 < |\eta| < 3.2$). The transition region between the barrel and the end-caps of the calorimeter, $1.37 < |\eta| < 1.52$, has a large amount of material in front of the first active calorimeter layer; therefore electromagnetic objects measured in this region suffer from worse energy resolution and are not considered in this analysis.

For hadronic calorimetry, three different technologies are used. In the barrel region ($|\eta| < 1.7$), scintillator tiles with steel absorbers are used. Liquid argon with copper absorber plates are used in the end-cap region ($1.5 < |\eta| < 3.2$). The forward calorimeter ($3.1 < |\eta| < 4.9$) consists of liquid argon with tungsten and copper absorbers and has separate electromagnetic and hadronic sections.

The muon spectrometer (MS) provides precise measurements of the momentum of muons within $|\eta| < 2.7$ using three layers of precision tracking stations, consisting of drift tubes and cathode strip chambers. Resistive plate and thin-gap chambers are used to trigger on muons in the region $|\eta| < 2.4$. The magnetic fields for the MS are produced by one barrel and two end-cap air-core toroid magnets surrounding the calorimeter. Each magnet consists of eight superconducting coils arranged symmetrically in ϕ.

The ATLAS trigger system uses three consecutive stages to decide whether an event is selected to be read out for permanent storage. The first level of the trigger is implemented using custom-made electronics and operates at a design rate of at most 75 kHz. It is complemented by two software-based high-level triggers (HLT). The second level consists of fast online algorithms to inspect regions of interest flagged by the first trigger level. At the third level, the full event is reconstructed using algorithms similar to those in the offline event selection.

4 Data and Monte Carlo samples

The analysis is based on data collected by the ATLAS experiment during the 2012 data-taking period. Only runs with stable proton-proton (pp) beam collisions at $\sqrt{s} = 8$ TeV in which all relevant detector components were operating normally are used. This data sample corresponds to an integrated luminosity of $\mathcal{L} = 20.3\,\text{fb}^{-1}$, determined with an uncertainty of $\pm 1.9\%$ and derived from beam-separation scans performed in November 2012 [17].

The kinematic distributions of both the signal and background processes are modelled using Monte Carlo (MC) samples. The additional pp collisions accompanying the hard-scatter interactions (pile-up) are modelled by overlaying minimum-bias events generated using PYTHIA 8 [18]. To simulate the detector response, the MC events are passed through a detailed simulation of the ATLAS detector [19] based on GEANT4 [20].

For the WW signal events, three different MC samples are generated. The $q\bar{q} \to W^+W^-$ events are generated using the POWHEG-BOX 1.0 generator (referred to as POWHEG below) [21–24]. It is interfaced to PYTHIA 8.170 for the simulation of parton shower and hadronisation processes. The non-resonant gg-induced WW signal events are generated using the GG2WW program (version 3.1.3) [25] interfaced to HERWIG 6.5 and JIMMY 4.31 [26, 27] for parton showering, hadronisation and underlying event simulation. The resonant WW production via a Higgs boson with a mass of $m_H = 125$ GeV is modelled using POWHEG+PYTHIA 8.170. For these three samples, the CT10 NLO [28] parton distribution function (PDF) is employed in the event generation. PHOTOS [29] is used to model the radiation of photons, and AU2 [30] and AUET2 [31] are used as the parameter tunes for the underlying event in the POWHEG+PYTHIA and the HERWIG+JIMMY samples, respectively. To calculate acceptances (see section 8.2) or make differential predictions for the WW signal process, these samples are combined according to their respective cross sections as listed in table 1. Next-to-leading-order electroweak (EW) contributions of $\mathcal{O}(\alpha_{\text{EW}}^3)$ are described in refs. [32–35] and the corrections derived in ref. [36] are applied as scale factors to $q\bar{q} \to W^+W^-$ production in the acceptance calculation and in the setting of limits on anomalous triple-gauge-couplings (see section 10), but not for any other purpose or distribution shown in this paper.

The $t\bar{t}$ background is modelled with MC@NLO 4.03 [37] using the CT10 NLO PDF interfaced with HERWIG 6.5+JIMMY 4.31 with the AUET2 tune. The same generators and settings are used to simulate s-channel single-top production and the associated production of a top quark with a W boson, while the ACERMC 3.7 [38] MC generator interfaced to PYTHIA 6 [39] with the AUET2B tune [40] and the CTEQ6L1 PDF [41] is employed for the single-top-t-channel process. Alternative samples employing POWHEG+PYTHIA 8 and POWHEG+HERWIG 6.5+JIMMY 4.31 are used to determine systematic uncertainties in the data-driven estimate.

Drell-Yan and W+jets events are modelled using ALPGEN 2.14 [42] which is either interfaced to PYTHIA 6 (W+jets and $Z \to ee/\mu\mu$ samples with $m_{\ell\ell} > 60$ GeV) or to HERWIG 6.5 [26] and JIMMY 4.31 ($Z \to \tau\tau$ and remaining $Z \to ee/\mu\mu$ samples) for the simulation of parton showering, hadronisation and the underlying event modelling. The AUET2 tune is used for the underlying event. The CTEQ6L1 PDF is employed in the

event generation and for the parton shower. The MLM [43] matching scheme is used to remove overlaps between events with the same parton multiplicity generated by the matrix element and the parton shower.

The ZZ and $WZ(\gamma^*)$ diboson background processes are generated with Powheg interfaced to Pythia 8 using the AU2CT10 tune with the CT10 NLO PDF. The lower limit on the invariant mass of the decay leptons of the $Z(\gamma^*)$ in the ZZ sample is set to $m_{\ell\ell} > 4$ GeV, while for the $WZ(\gamma^*)$ it is $m_{\ell\ell} > 7$ GeV. For γ^* masses below 7 GeV, dedicated $W\gamma^*$ samples are produced using the Sherpa 1.4.2 generator [44] with its built-in parton shower and hadronisation using the CT10 NLO PDF. Events from $W\gamma$ production can also mimic the WW signature when the photon is misidentified as an electron. These events are generated using Alpgen interfaced to Herwig+Jimmy. The CTEQ6L1 PDF and the AUET2 tune are used for this sample.

The MC samples used in this analysis are summarised in table 1, where the total cross sections, σ_{total}, times the branching fractions, $\mathcal{B}$, into leptons are reported. The total cross sections are taken from theoretical calculations and the perturbative order of each calculation is also given in the table. The total cross sections are used to normalize the MC samples, which are essential for the modelling of kinematic distributions.

5 Object reconstruction and event selection

5.1 Pre-selection of events

Fast selection algorithms based on the detection of electrons or muons are used to trigger the readout of the events [52, 53]. The trigger selection algorithms are based on the transverse momentum of the leptons and use certain object quality criteria. These object quality criteria vary for the different triggers and are generally looser and more efficient for dilepton triggers as opposed to single-lepton triggers, which are designed to yield larger rate reductions. Another important consideration is the coverage of the first-level muon trigger, which is only about 80% in the central region ($|\eta| < 1.05$) of the detector [53]. In the ee and $\mu\mu$ final states, highly efficient dilepton triggers are used, which impose loose identification criteria on both electrons for the dielectron trigger and for the dimuon trigger only a single muon in the first trigger level. In the $e\mu$ final state the optimal signal yield is achieved by combining single-lepton triggers with the $e\mu$ dilepton trigger, as the latter is affected by the limited coverage for muons at the first trigger level and, due also to the trigger requirements on the electrons, yields a low efficiency.

For the single-electron trigger, the HLT criterion for the transverse momentum is either $p_{\text{T}}^e > 24\,\text{GeV}$, accompanied by track-based isolation requirements, or $p_{\text{T}}^e > 60\,\text{GeV}$. The single-muon trigger has a transverse momentum threshold of $p_{\text{T}}^\mu = 24\,\text{GeV}$ when a loose track-based isolation requirement is satisfied, or a transverse momentum threshold of $p_{\text{T}}^\mu = 36\,\text{GeV}$. The combined electron-muon trigger requires $p_{\text{T}}^\mu > 8\,\text{GeV}$ for the muon and $p_{\text{T}}^e > 12\,\text{GeV}$ for the electron. The dielectron trigger requires two electrons with a transverse momentum of $p_{\text{T}}^e > 12$ GeV while the dimuon trigger applies a transverse momentum requirement of $p_{\text{T}}^\mu > 18\,\text{GeV}$ for one and $p_{\text{T}}^\mu > 8\,\text{GeV}$ for the second muon.

Process		MC generator +parton shower +hadronisation	Calculation	$\sigma_{\text{total}} \cdot \mathcal{B}$ [pb]
WW Signal				
$q\bar{q} \to W^+W^-$		Powheg+Pythia 8	NLO [45]	5.58
$gg \to W^+W^-$ (non-resonant)		gg2ww +Herwig	LO† [25]	0.153
$gg \to H \to W^+W^-$		Powheg+Pythia 8	NNLO [46]	0.435
Top quark				
$t\bar{t}$		MC@NLO+Herwig	NNLO+NNLL [47]	26.6
Wt		MC@NLO+Herwig	NNLO+NNLL [48]	2.35
Single top t-channel		AcerMC+Pythia 6	NNLO+NNLL [49]	28.4
Single top s-channel		MC@NLO+Herwig	NNLO+NNLL [50]	1.82
Drell-Yan				
$Z \to ee/\mu\mu$	($m_{\ell\ell} > 60$ GeV)	Alpgen +Pythia 6		
$Z \to \tau\tau$	($m_{\ell\ell} > 60$ GeV)	Alpgen +Herwig	NNLO [51]	16500
$Z \to \ell\ell$	(10 GeV $< m_{\ell\ell} < 60$ GeV)	Alpgen +Herwig		
Other dibosons (VV)				
$W^{\pm}\gamma$	($p_{\mathrm{T}}^{\gamma} > 8$ GeV)	Alpgen +Herwig	NLO [45]	369.0
$W^{\pm}Z(/\gamma^*)$	($m_{\ell\ell} > 7$ GeV)	Powheg+Pythia 8	NLO [45]	12.7
$W^{\pm}Z(/\gamma^*)$	($m_{\ell\ell} < 7$ GeV)	Sherpa	NLO [45]	12.9
$ZZ \to 4\ell$	($m_{\ell\ell} > 4$ GeV)	Powheg+Pythia 8	NLO [45]	0.733
$ZZ \to \ell\ell\nu\nu$	($m_{\ell\ell} > 4$ GeV)	Powheg+Pythia 8	NLO [45]	0.504

Table 1. Monte Carlo samples used to model the signal and background processes. The total cross sections times branching fractions, $\sigma_{\text{total}} \cdot \mathcal{B}$, are quoted at $\sqrt{s} = 8$ TeV using higher-order calculations. The branching fractions $\mathcal{B}$ include the decays $t \to Wq$, $W \to \ell\nu$, and $Z \to \ell\ell$, while the decay of one Z boson to neutrinos is considered for the process $ZZ \to \ell\ell\nu\nu$. Here, ℓ refers to e, μ, or τ for signal and background processes, and all three lepton flavors are considered in $\mathcal{B}$. The $q\bar{q} \to W^+W^-$ process also includes qg initial states contributing to t-channel and s-channel WW production. The Higgs mass is taken to be $m_H = 125$ GeV.
† The process itself is calculated at LO, however it contributes only at NNLO to the total WW cross section.

With the chosen trigger scheme, the trigger efficiency defined with respect to the offline selection criteria is 99-100% for all three channels.

5.2 Lepton selection

Electrons are reconstructed from energy deposits in the EM calorimeter with an associated track. Electrons must satisfy $|\eta^e| < 2.47$, excluding the calorimeter transition region $1.37 < |\eta^e| < 1.52$. To efficiently reject multijet background, they are required to pass a very tight likelihood-based identification criterion [54] that uses discriminating variables based on calorimetric shower shapes and track parameters of the electron candidates. Electrons are required to be unaffected by known instrumental problems such as coherent noise in the calorimeters. Stringent requirements are placed on track impact parameters and electron

isolation to reject electrons from multijet background events. These isolation and tracking requirements are the same as those utilised in ref. [55]. To reject electrons reconstructed from a bremsstrahlung photon emitted by a muon traversing the calorimeter, any electron candidate reconstructed at a distance $\Delta R < 0.1$ from a selected muon is removed.

Muons are reconstructed by combining tracks reconstructed separately in the ID and the MS. Muons are required to be within the pseudorapidity region $|\eta^\mu| < 2.4$. To reject backgrounds, quality criteria are applied to the muon candidates as described in detail in ref. [56]. As in the case of electrons, the track parameter and isolation selection criteria applied to muons follow that in ref. [55]. For the rejection of muons from heavy-flavour decays, muons are removed if they are found within a cone of $\Delta R = 0.3$ to a selected jet.

5.3 Jet selection

Jets are reconstructed using the anti-k_t algorithm [57] with radius parameter $R = 0.4$ implemented in the FastJet package [58]. The inputs to the jet-finding algorithm are calibrated topological clusters [59]. The calibration of topological clusters to the hadronic energy scale depends on their local energy density and total energy [60]. A jet-area-dependent correction is applied to correct the jet energy for contributions from additional pp collisions based on an estimate of the pile-up activity in a given event using the method proposed in ref. [61]. The reconstructed jets are further calibrated using jet-energy-scale corrections from simulation. Their calibration is refined using data-driven corrections to account for residual differences between data and MC simulation [62, 63].

Jets are required to have a transverse momentum of $p_T^{\text{jet}} > 25$ GeV and pseudorapidity $|\eta^{\text{jet}}| < 4.5$. Jets are removed if they are found within a cone of $\Delta R = 0.3$ around a selected electron. For jets with $p_T^{\text{jet}} < 50$ GeV and $|\eta^{\text{jet}}| < 2.4$, an additional requirement is applied to reject jets from pile-up interactions in the event. The scalar sum of the transverse momenta of the tracks associated with both the primary vertex and the jet must be larger than one-half of the scalar sum of the momenta of all the tracks associated with the jet; jets with no associated tracks are also removed [64]. This selection criteria is henceforth denoted as requirement on the jet vertex fraction (JVF).

Selected b-jets are used in the estimation of the top-quark background described in section 6.1. Jets containing b-hadrons are identified within the central region of the detector, $|\eta^{\text{jet}}| < 2.5$, using a multivariate approach based on track impact-parameter significance, secondary vertex reconstruction and other tracking variables described in refs. [65, 66]. In this analysis the requirement on the multivariate discriminant is chosen to have a b-jet identification efficiency of 85%, which has been verified using a $t\bar{t}$ data sample. This corresponds to a rejection factor of 10 for light-flavour jets [66].

5.4 Reconstruction of missing transverse momentum

The reconstruction of missing transverse momentum is optimised to reject backgrounds without neutrinos in the final state.

Calorimeter-based missing transverse momentum, E_T^{miss}, is reconstructed as the magnitude of the negative vectorial sum of all measured and identified physics objects, denoted as $\mathbf{E}_T^{\text{miss}}$, where the bold notation indicates a vector throughout this paper. Additionally,

energy deposits in the calorimeter not associated with any high-p_T objects are also included as described in ref. [67].

The relative missing transverse momentum, $E_\mathrm{T,\,Rel}^\mathrm{miss}$, is defined as

$$E_\mathrm{T,\,Rel}^\mathrm{miss} = \begin{cases} E_\mathrm{T}^\mathrm{miss} \times \sin\left(\Delta\phi_\ell\right) & \text{if } \Delta\phi_\ell < \pi/2 \\ E_\mathrm{T}^\mathrm{miss} & \text{if } \Delta\phi_\ell \geq \pi/2, \end{cases} \tag{5.1}$$

where $\Delta\phi_\ell$ is the difference in azimuthal angle ϕ between $E_\mathrm{T}^\mathrm{miss}$ and the nearest lepton. With this definition, $E_\mathrm{T,\,Rel}^\mathrm{miss}$ is less affected by the mis-measurement of the energy of a lepton leading to spurious large calorimeter-based missing transverse momentum.

Additionally, track-based $p_\mathrm{T}^\mathrm{miss}$ is used, which is the magnitude of the negative vectorial sum ($p_\mathrm{T}^\mathrm{miss}$) of all identified and calibrated leptons and all tracks not associated with any lepton in the event. These tracks are required to have $p_\mathrm{T} > 0.5$ GeV and be associated to the reconstructed primary vertex, which makes $p_\mathrm{T}^\mathrm{miss}$ robust against additional pile-up interactions in the same bunch-crossing. A more detailed description of the $p_\mathrm{T}^\mathrm{miss}$ reconstruction can be found in ref. [68].

In events with genuine missing transverse momentum due to undetected neutrinos, $E_\mathrm{T}^\mathrm{miss}$ and $p_\mathrm{T}^\mathrm{miss}$ are complementary estimators of the total missing transverse momentum vector. A large difference between $E_\mathrm{T}^\mathrm{miss}$ and $p_\mathrm{T}^\mathrm{miss}$ indicates a mis-reconstruction of either of these two quantities in the context of this analysis.

5.5 *WW* selection

The *WW* candidate events are required to contain two oppositely charged leptons fulfilling the identification criteria, isolation and track impact-parameter requirements specified earlier. The leading and sub-leading leptons have to satisfy transverse momentum requirements of $p_\mathrm{T}^\ell > 25$ GeV and $p_\mathrm{T}^\ell > 20$ GeV, respectively. To suppress other diboson backgrounds, events are rejected if additional leptons with $p_\mathrm{T}^\ell > 7$ GeV fulfilling the above described selection criteria are present.

The event selection criteria are optimised to enhance the *WW* signal purity. The invariant mass of the dilepton pair is required to be greater than 15 GeV for $ee/\mu\mu$ final states to reject J/ψ, Υ and other low-mass resonances, while $e\mu$ final states are required to have an invariant mass above 10 GeV to remove multijet events. Figure 2 shows the invariant mass distributions of these selected dilepton events for the same-flavour and $e\mu$ final states. The backgrounds shown here are based purely on MC predictions, which are normalised to $\mathcal{L} = 20.3\,\mathrm{fb}^{-1}$ using the cross section times branching fractions shown in table 1. In figure 2, Drell-Yan production is the largest background for the ee and $\mu\mu$ final states, and it is therefore further suppressed by rejecting events that are reconstructed with an invariant mass closer than 15 GeV to the Z boson mass m_Z [69].

The Drell-Yan background in the same-flavour channel is still significant after this more restrictive invariant mass requirement, so stringent conditions are imposed using selection criteria related to missing transverse momentum. The requirements are less strict for $e\mu$ final states, where Drell-Yan production contributes only through $Z/\gamma^* \to \tau\tau$. The selection requirements are as follows. The relative missing transverse momentum, $E_\mathrm{T,\,Rel}^\mathrm{miss}$, is required to be larger than 15 GeV for the $e\mu$ and larger than 45 GeV for
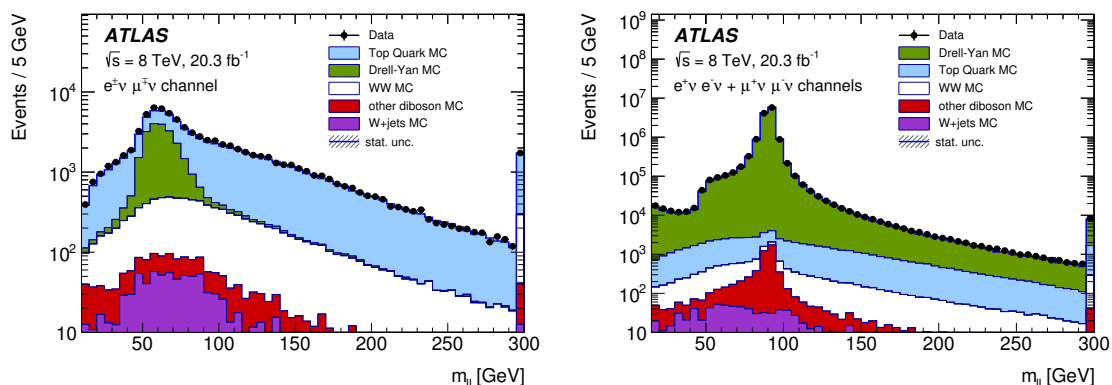
Figure 2. The invariant mass distributions are shown for dilepton pairs in selected events for $e\mu$ (left) and $ee + \mu\mu$ (right) final states after the dilepton selection and the $m_{\ell\ell}$ requirements described in the text. The points represent data and the stacked histograms are the MC predictions, which are normalised to $\mathcal{L} = 20.3\,\text{fb}^{-1}$ using the cross section times branching fractions shown in table 1. The last bin is an overflow bin. Only statistical uncertainties are shown.

the ee and $\mu\mu$ final states. Track-based missing transverse momentum, p_T^{miss}, is further required to be larger than 20 GeV for the $e\mu$ and larger than 45 GeV for the ee and $\mu\mu$ final states. The azimuthal angle between E_T^{miss} and p_T^{miss} is calculated and the condition $\Delta\phi(E_T^{\text{miss}}, p_T^{\text{miss}}) < 0.6$ must be met in the $e\mu$ final state, while $\Delta\phi(E_T^{\text{miss}}, p_T^{\text{miss}}) < 0.3$ must be satisfied for the ee and $\mu\mu$ final states.

The jet multiplicity distributions for data, the signal MC simulation and the different background contributions after applying these requirements are shown in figure 3. In order to suppress the dominant top-quark background, events are required to contain no selected jets. This requirement is referred to as the jet-veto requirement. The visible excess of events without selected jets at this stage is still subject to changes from data-driven refinements in the background estimate as discussed in section 6. Furthermore, there is a significant uncertainty in WW signal predictions as discussed in section 9.

A summary of all applied selection criteria is given in table 2.

6 Determination of backgrounds

After applying all selection requirements, the resulting WW candidate sample has significant background contributions from top-quark ($t\bar{t}$ and single top) production, which is the dominant background. In the $e\mu$ final state, W+jets production and Drell-Yan production of τ-leptons have similar contributions. Drell-Yan production is much larger than W+jets for the same-flavour final states. Diboson ($WZ(\gamma^*)$, ZZ, $W\gamma$) production constitutes a smaller background contribution for all final states.

6.1 Background from top-quark production

The dominant background contribution to the selected WW candidate events originates from top-quark ($t\bar{t}$ and single top) production. Top quarks decay into a real W boson and a b quark, such that top-quark events contain a pair of W-bosons accompanied by typically
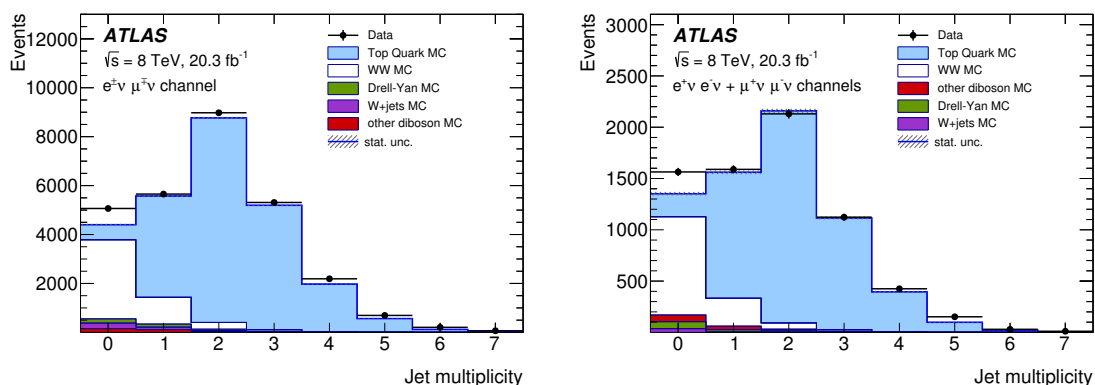
Figure 3. Jet multiplicity distributions for $e\mu$ (left) and $ee + \mu\mu$ (right) events before the jet-veto requirement is applied. The points represent data and the stacked histograms are the MC predictions, which are normalised to $\mathcal{L} = 20.3\,\text{fb}^{-1}$ using the cross section times branching fractions shown in table 1. For the $t\bar{t}$ production process the NNLO+NNLL theoretical calculation from ref. [47] is used. Only statistical uncertainties are shown.

	$e\mu$	$ee/\mu\mu$
p_T^ℓ (leading/sub-leading)	$> 25\,/\,20$ GeV	
$\|\eta^\ell\|$	$\|\eta^\mu\| < 2.4$ and $\|\eta^e\| < 2.47$, excluding $1.37 < \|\eta^e\| < 1.52$	
Number of additional leptons with $p_T > 7$ GeV	0	0
$m_{\ell\ell}$	> 10 GeV	> 15 GeV
$\|m_Z - m_{\ell\ell}\|$	—	> 15 GeV
$E_{T,\,\text{Rel}}^{\text{miss}}$	> 15 GeV	> 45 GeV
p_T^{miss}	> 20 GeV	> 45 GeV
$\Delta\phi(\mathbf{E}_T^{\text{miss}}, \mathbf{p}_T^{\text{miss}})$	< 0.6	< 0.3
Number of jets with $p_T > 25$ GeV, $\|\eta\| < 4.5$	0	0

Table 2. Criteria used to select WW candidate events in data.

two jets. Even after rejecting events with reconstructed jets with $p_T > 25$ GeV, a small fraction of top-quark events remains if the jets fall outside the acceptance. This small fraction however still constitutes the largest background to the selected WW candidate events. Background from top-quark production is estimated using a data-driven method first suggested in ref. [70], in which the top-quark contribution is extrapolated from a control region (CR) to the signal region (SR). The method does not rely on the possibly imperfect theoretical modelling of the low-p_T spectrum of jets in top-quark production, reducing significantly the uncertainty in the top-quark background estimate compared to MC-driven estimates.

The CR is selected by applying the WW signal selection with the sole exception of the jet-veto requirement, hence the SR is a subsample of the CR. The majority of events in the CR stem from top-quark production, while the dominant non-top-quark contribution originates from the WW signal process. In order to reduce the signal contamination and to reduce the overlap between the SR and CR, an additional control region, CR+H_{T} is selected by requiring the scalar sum of the transverse momenta of leptons and jets, $H_{\mathrm{T}} > 130$ GeV. In the resulting sample, the signal contamination is only about 9%, while top-quark events contribute about 90%. The number of top-quark events in the CR, $N_{\mathrm{CR}}^{\mathrm{top}}$, is calculated as the number of data events in the CR $+ H_{\mathrm{T}}$ region from which the non-top-quark contribution, estimated using MC, is subtracted, $N_{\mathrm{CR}+H_{\mathrm{T}}}^{\mathrm{data}} - N_{\mathrm{CR}+H_{\mathrm{T}}}^{\mathrm{non-top}}$. Then $(N_{\mathrm{CR}+H_{\mathrm{T}}}^{\mathrm{data}} - N_{\mathrm{CR}+H_{\mathrm{T}}}^{\mathrm{non-top}})$ is corrected for the H_{T} cut efficiency $\epsilon_{H_{\mathrm{T}}}$ estimated from top-quark MC samples. With the efficiency $\epsilon_{\mathrm{jet\text{-}veto}}$ for top-quark events to pass the jet-veto requirement, the top-quark background contribution in the SR can be calculated as:

$$N_{\mathrm{SR}}^{\mathrm{top}} = \frac{\left(N_{\mathrm{CR}+H_{\mathrm{T}}}^{\mathrm{data}} - N_{\mathrm{CR}+H_{\mathrm{T}}}^{\mathrm{non-top}} \right)}{\epsilon_{H_{\mathrm{T}}}} \times \epsilon_{\mathrm{jet\text{-}veto}}. \tag{6.1}$$

The jet-veto efficiency $\epsilon_{\mathrm{jet\text{-}veto}}$ is calculated as the MC efficiency $\epsilon_{\mathrm{jet\text{-}veto}}^{\mathrm{MC}}$ multiplied by a correction factor defined in eq. (6.2) and obtained from events with two leptons, the same requirements on missing transverse momentum, $E_{\mathrm{T, Rel}}^{\mathrm{miss}}$ and $p_{\mathrm{T}}^{\mathrm{miss}}$, as for the signal selection, and at least one b-tagged jet in the central region of the detector, $|\eta^{\mathrm{jet}}| < 2.5$. This b-tagged sample has a high purity of top-quark events and the small contribution from non-top-quark processes is subtracted. The probability p that a jet in a top-quark event fails the jet-selection requirements can be evaluated as the fraction of top-quark events that contain no jets other than the b-tagged jet. The correction factor takes into account the difference between p^{data} and p^{MC}, and the square of the ratio of data to MC probabilities accounts for the presence of on average two b-jets within the acceptance for the selected top-quark events. The jet-veto efficiency can be calculated as

$$\epsilon_{\mathrm{jet\text{-}veto}} = \epsilon_{\mathrm{jet\text{-}veto}}^{\mathrm{MC}} \times \left(\frac{p^{\mathrm{data}}}{p^{\mathrm{MC}}} \right)^2. \tag{6.2}$$

The systematic uncertainty in $N_{\mathrm{SR}}^{\mathrm{top}}$ in eq. (6.1) is studied using MC simulation. The largest contribution to the total uncertainty in the top-quark background estimate arises from the MC ratio $\epsilon_{\mathrm{jet\text{-}veto}}^{\mathrm{MC}}/(p^{\mathrm{MC}})^2$. The uncertainty from the reconstruction of objects and events for the MC ratio is about $\pm 5\%$, dominated by the systematic uncertainties in the determination of jet energy scale, jet energy resolution and b-tagging efficiency. The modelling uncertainty for the MC ratio is around $\pm 7\%$ and the dominant contribution comes from comparing the estimates from different parton shower and hadronisation models and different generators, while the PDF uncertainty and QCD scale variations have smaller effects. Further effects have been studied, but were found to be negligible. Among these effects is the uncertainty on the fraction due to single-top production which accounts for almost 40% of the total top-quark background contribution after the jet-veto requirement. To account for potential differences between the single-top and $t\bar{t}$ processes, additional

uncertainties are assigned by scaling the single-top cross section by a conservative 30% (measurements of this cross-section at the LHC have uncertainties just below 20% [71]). However, the resulting effect on the MC ratio and consequently on the top-quark background estimate are very small. Interference effects between Wt and $t\bar{t}$ have also been considered and similarly to the variations of the single-top cross section, the impact is found to be minor. An additional cross-check is performed by changing the exponent in the correction factor $\left(p^{\mathrm{data}}/p^{\mathrm{MC}}\right)^2$ to be 1.5 or 2.5, which reflects the average jet multiplicity in top-quark background events (see figure 3). The resulting change in the estimated yield of top-quark background is found to be less than 1%. This indicates that the result does not strongly depend on how one assumes the correction factor should account for the two jets in the final state. The value of $\left(p^{\mathrm{data}}/p^{\mathrm{MC}}\right)$ ranges between 0.982 and 1.009 with an uncertainty of 1.5–5% for the different final states, thus indicating good modelling of top-quark events in MC simulation. The uncertainty on this ratio is propagated to the total uncertainty on the top-quark background estimate. Apart from the MC ratio, further terms play a role in eq. (6.1) and need to be studied: the H_{T} cut efficiency $\epsilon_{H_{\mathrm{T}}}$ is 95% with about $\pm 1\%$ uncertainty taken as the difference between the efficiencies determined in data and MC simulation. Uncertainties that range from $\pm 15\%$ (diboson production) to $\pm 50\%$ (Z/W+jets) are assigned to the subtracted non-top-quark contributions in the CR, $N_{\mathrm{CR}+H_{\mathrm{T}}}^{\mathrm{non-top}}$. The systematic effect on $N_{\mathrm{SR}}^{\mathrm{top}}$ resulting from $N_{\mathrm{CR}+H_{\mathrm{T}}}^{\mathrm{non-top}}$ and $\epsilon_{H_{\mathrm{T}}}$ is found to be about 2%, and the statistical uncertainties of $N_{\mathrm{CR}+H_{\mathrm{T}}}^{\mathrm{data}}$ and p^{data} are negligible.

While the normalisation of the top-quark background is determined from data, the shape information used in the differential measurements relies on MC modelling. The bin-by-bin uncertainties in the differential distributions are evaluated by propagating (1) the uncertainties of the jet energy scale and resolution, (2) the uncertainties determining by taking the difference in the differential distributions found with different MC generators and parton shower models and (3) the uncertainties due to the QCD scale and parton distribution functions. All these uncertainties are added in quadrature and are treated as uncorrelated with the uncertainties for the top-quark background normalisation.

6.2 Background from W+jets production

In this paper, the W+jets background contribution also includes backgrounds from multi-jet production since they are determined together as explained below. The determination of background from W+jets production relies on comparing in data the number of events with leptons satisfying either of two alternative sets of selection requirements, namely the so-called *loose* (L) and *tight* (T) selection criteria, where the tight sample is a subset of the loose sample. The tight selection criteria are the same as those used for the signal selection. Loose electrons are selected by relaxing some of the particle identification criteria placed on tracking variables and calorimetric shower shapes and also by removing the requirements made on the electron isolation and impact parameters in the tight selection. For loose muons, the requirements on isolation and impact parameters are removed. Leptons satisfying the tight selection criteria can originate from *real* prompt leptons or *fake* background leptons, which are either due to non-prompt leptons from semileptonic decays of heavy-flavour hadrons, hadrons misidentified as electrons, or photon conversions

producing electrons. The same applies to leptons satisfying the loose selection criteria. The total number of events with two leptons satisfying different combinations of loose and tight criteria is the sum of four terms:

$$N^{\mathrm{LL}} = N^{\mathrm{LL}}_{\mathrm{fake,fake}} + N^{\mathrm{LL}}_{\mathrm{real,fake}} + N^{\mathrm{LL}}_{\mathrm{fake,real}} + N^{\mathrm{LL}}_{\mathrm{real,real}}$$
$$N^{\mathrm{LT}} = \epsilon_{\mathrm{fake}} N^{\mathrm{LL}}_{\mathrm{fake,fake}} + \epsilon_{\mathrm{fake}} N^{\mathrm{LL}}_{\mathrm{real,fake}} + \epsilon_{\mathrm{real}} N^{\mathrm{LL}}_{\mathrm{fake,real}} + \epsilon_{\mathrm{real}} N^{\mathrm{LL}}_{\mathrm{real,real}}$$
$$N^{\mathrm{TL}} = \epsilon_{\mathrm{fake}} N^{\mathrm{LL}}_{\mathrm{fake,fake}} + \epsilon_{\mathrm{real}} N^{\mathrm{LL}}_{\mathrm{real,fake}} + \epsilon_{\mathrm{fake}} N^{\mathrm{LL}}_{\mathrm{fake,real}} + \epsilon_{\mathrm{real}} N^{\mathrm{LL}}_{\mathrm{real,real}}$$
$$N^{\mathrm{TT}} = \epsilon_{\mathrm{fake}}^2 N^{\mathrm{LL}}_{\mathrm{fake,fake}} + \epsilon_{\mathrm{real}} \epsilon_{\mathrm{fake}} N^{\mathrm{LL}}_{\mathrm{real,fake}} + \epsilon_{\mathrm{fake}} \epsilon_{\mathrm{real}} N^{\mathrm{LL}}_{\mathrm{fake,real}} + \epsilon_{\mathrm{real}}^2 N^{\mathrm{LL}}_{\mathrm{real,real}}. \quad (6.3)$$

Here, the number of events that have exactly one loose lepton and one tight lepton (N^{LT} and N^{TL}), two loose leptons (N^{LL}), or two tight leptons (N^{TT}) are used. The first and second indices correspond to the qualities of the highest-p_{T} lepton and the lepton sub-leading in p_{T} respectively; ϵ_{real} and ϵ_{fake} in the above formulae are the probabilities for prompt and fake background leptons selected with the loose criteria to satisfy the tight selection criteria. The sample with two tight leptons, described by eq. (6.3), consists of contributions from multijet events with two fake leptons, W+jets events with one fake and one prompt lepton and finally events with two prompt leptons including the WW signal events. If the numbers of events with loose and tight leptons as well as the efficiencies ϵ_{real} and ϵ_{fake} are known, the numbers of events with one prompt and one fake lepton ($N^{\mathrm{LL}}_{\mathrm{real,fake}} + N^{\mathrm{LL}}_{\mathrm{fake,real}}$) and two fake leptons ($N^{\mathrm{LL}}_{\mathrm{fake,fake}}$) for the loose selection criteria can be obtained by solving the above system of equations. The numbers of W+jets and multijet events in the signal region, which are selected using the tight criteria, can then be extracted using the following relations:

$$N_{W+\mathrm{jets}} = \epsilon_{\mathrm{real}} \epsilon_{\mathrm{fake}} N^{\mathrm{LL}}_{\mathrm{real,fake}} + \epsilon_{\mathrm{fake}} \epsilon_{\mathrm{real}} N^{\mathrm{LL}}_{\mathrm{fake,real}} \quad (6.4)$$
$$N_{\mathrm{multijet}} = \epsilon_{\mathrm{fake}}^2 N^{\mathrm{LL}}_{\mathrm{fake,fake}} \quad (6.5)$$

The efficiency for real prompt leptons, ϵ_{real}, is evaluated using MC simulation, where data-to-MC correction factors extracted from $Z \rightarrow \ell\ell$ events [54, 56] are applied. The efficiency for fake leptons, ϵ_{fake}, is measured using a data control region enriched with fake leptons from multijet production. This control sample is selected using a lepton trigger which does not bias the loose selection. The sample must contain a jet that is opposite in azimuthal angle ($\Delta\phi > 2.0$) to a lepton satisfying the loose selection criteria to enhance the contribution of multijet events. The fraction of these selected loose leptons that satisfy the tight selection criteria is ϵ_{fake}. Prompt leptons from W and Z decay contaminate this multijet sample. To remove these prompt leptons, which would bias the determination of ϵ_{fake}, it is required that the missing transverse momentum is small, $E_{\mathrm{T}}^{\mathrm{miss}} < 25$ GeV, and that the transverse mass of the lepton and $E_{\mathrm{T}}^{\mathrm{miss}}$ is below 40 GeV, $m_{\mathrm{T}}^W < 40$ GeV. Only one lepton is allowed in the event. Up to 35% of the selected multijet control sample consists of prompt leptons from W+jets and Drell-Yan events, which are subtracted using MC simulation.

Both ϵ_{real} and ϵ_{fake} are determined separately for muons and electrons and also differentially as functions of p_{T} and η of the lepton. The main uncertainty in the fake-lepton efficiency comes from the fact that the composition of the various sources of fake leptons, e.g. heavy flavour decays, charged hadrons or conversions, might not be the same in the

sample used to measure the fake-lepton efficiency as in the sample these fake-lepton efficiencies are applied to. The effect is estimated using a comparison between the fake-lepton efficiency predicted using the above described W+jets MC sample and a simulated multijet MC sample, generated and showered using PYTHIA 8. The sample-dependence uncertainty is determined to be $\sim$30–50%, depending on the lepton flavour and the event kinematics. Furthermore, systematic uncertainties from the prompt lepton subtraction and statistical uncertainties are propagated to the W+jets background estimate. The total W+jets and multijet contribution to the final selected WW candidate sample is summarised in table 3. A qualitative check of the estimated W+jets background and multijet yield is performed using events with two leptons of the same charge, as described in section 6.3 below.

The differential W+jets distributions needed for a differential cross-section measurement are also determined in a fully data-driven way, by evaluating the system of linear equations eqs. (6.3) in each bin of the differential distributions.

6.3 Other diboson processes and validation of diboson and W+jets backgrounds

All backgrounds from diboson production are estimated using MC simulation. The main systematic uncertainties are due to the theoretical uncertainties of predicted cross sections used for normalisation and the description of the jet-veto requirement.

The predicted contributions for backgrounds from diboson production, W+jets and multijets are validated using a data control sample in which the two selected leptons are required to have the same electric charge (same-sign) and satisfy all the other selection requirements. The electron pseudorapidity is restricted to lie within $|\eta^e| < 2.1$ to suppress contributions from WW signal events where the electron is reconstructed with a wrong charge assignment, which become significant for the high-$|\eta^e|$ region due to the increase in material in the inner tracking detector. Since the rate of charge-misidentification is negligible for muons, they are accepted if $|\eta^\mu| < 2.4$. This selection only yields a sufficient number of events for comparisons in the $e\mu$ channel. Figure 4 shows the $E_{\mathrm{T}}^{\mathrm{miss}}$ and $m_{\ell\ell}$ distributions for this same-sign control sample, which is dominated by $WZ(\gamma^*)$ production, that is estimated using the simulated MC samples described above, and W+jets events that are estimated from data, as described in section 6.2. Both statistical and systematic uncertainties are shown for the W+jets estimate. For the diboson samples the theoretical uncertainty in the cross-section predictions are included but their experimental uncertainties have not been evaluated in this control region. The predictions and the data agree well.

6.4 Background from Drell-Yan production

The Drell-Yan background normalisation is constrained by an auxiliary fit. It is based on a profile likelihood approach where the numbers of signal and background events in signal and control regions are described by a Poisson probability density function. For the W+jets and multijet backgrounds, the normalisation and shape from the data-driven estimates described above are used. Similarly, the top-quark and diboson contributions are obtained as described above. The input template shapes for signal and Drell-Yan events are obtained from MC simulation. The different sources of experimental and theoretical
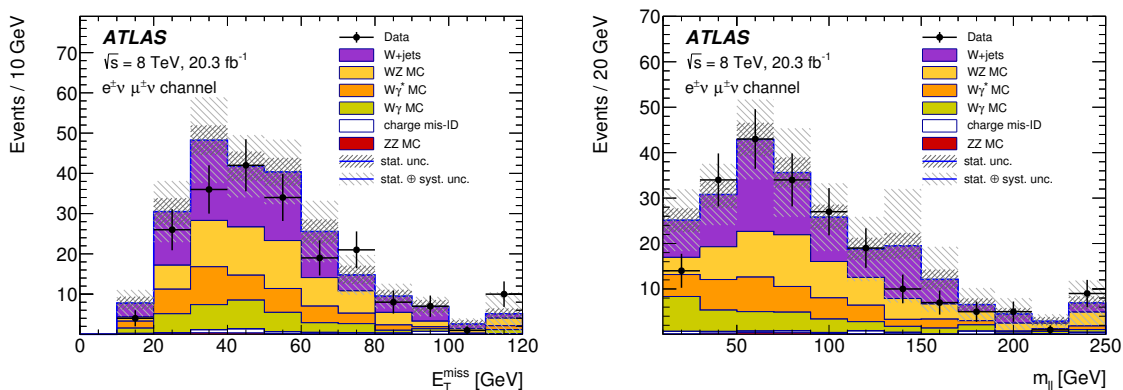
Figure 4. Distributions of E_T^{miss} and $m_{\ell\ell}$ for the same-sign control sample in the $e\mu$ channel. The last bin is an overflow bin. The selected leptons are required to have the same electric charge. The uncertainties shown include statistical and systematic uncertainties in the W+jets estimate as well as statistical uncertainties in all MC predictions. For the diboson contributions, the theoretical uncertainties in the cross-section predictions are also included. The experimental systematic uncertainties for the diboson production processes are not included. Contributions from processes with two opposite-sign final-state leptons, where one of them is reconstructed with a wrong charge assignment, are denoted by "charge mis-ID".

systematic uncertainties are included as nuisance parameters in the fit. Both the WW signal and Drell-Yan normalisation factors are fitted, but only the Drell-Yan background normalisation is used further for the cross-section determination. The WW cross section measured in section 9 is fully compatible with the WW normalisation factor extracted here.

For the fit, a control region dominated by Drell-Yan events is defined by inverting the p_T^{miss} requirement of $5 < p_T^{miss} < 20(45)$ GeV for the $e\mu$ ($ee+\mu\mu$) final states, where the minimum requirement of 5 GeV ensures that there is a well-defined p_T^{miss} direction, and removing the $\Delta\phi(\mathbf{E}_T^{miss}, \mathbf{p}_T^{miss})$ requirement. The fit is performed on the $\Delta\phi(\mathbf{E}_T^{miss}, \mathbf{p}_T^{miss})$ distribution in five bins of equal size for both the control region and the signal region simultaneously. In addition, a validation region dominated by Drell-Yan events is defined by inverting both the calorimetric and the track-based missing transverse momentum requirements but keeping the requirement on $\Delta\phi(\mathbf{E}_T^{miss}, \mathbf{p}_T^{miss})$. The result of the fit is extrapolated to this validation region where good data-MC agreement is observed.

In addition to the experimental uncertainties, theoretical uncertainties (QCD scale, PDF, parton-shower modelling in the simulation) are considered. For the uncertainties in the differential distributions of background events from Drell-Yan production, the constraints on the nuisance parameters from the likelihood fit are used. This information is propagated to the MC simulation, and predictions for Drell-Yan events are extracted for each bin with their uncertainties.

The largest uncertainties arise from the description of the jet and E_T^{miss} energy scale and resolution in the MC simulation and from the MC parton shower modelling. The latter is estimated by the difference between using the HERWIG/JIMMY and PYTHIA approaches in the MC simulation.
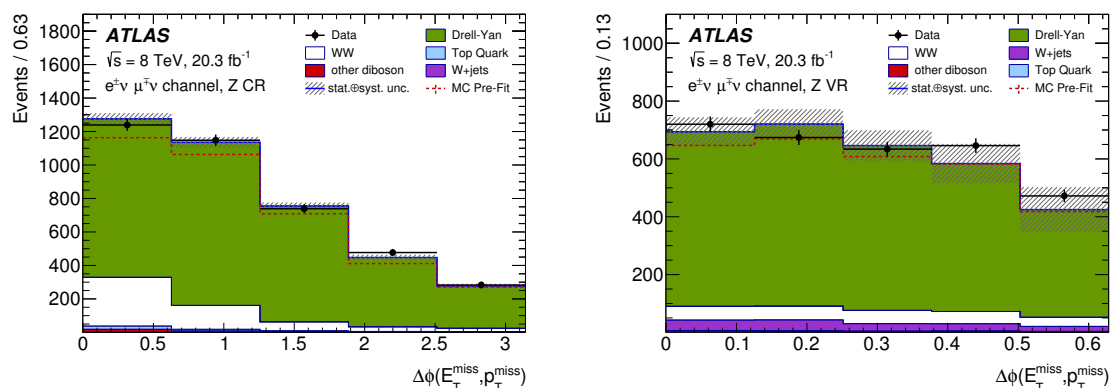
Figure 5. Distributions of $\Delta\phi(\mathbf{E}_T^{miss}, \mathbf{p}_T^{miss})$ are shown for data and MC predictions for the Drell-Yan control region (left) and the validation region (right). The MC predictions for Drell-Yan and WW signal have been scaled from the pre-fit predictions to reflect the results of the fit. The fit improves the description of the data by the simulated Drell-Yan events as compared to the MC pre-fit prediction.

Figure 5 shows the $\Delta\phi(\mathbf{E}_T^{miss}, \mathbf{p}_T^{miss})$ distributions for $e\mu$ final states in the control and validation regions before and after the profile likelihood fit of the Drell-Yan background. Good agreement between the data and the post-fit prediction is seen.

6.5 Other background contributions

The background contributed by WW pairs from vector-boson scattering, Higgs boson production via vector-boson fusion, as well as WH and ZH associated production with $H \to WW$ is evaluated using MC simulation. The sum of these processes contributes typically 0.3–0.6% to each final state at detector level for the selection considered in this analysis and is therefore neglected. The contributions from these processes are neither subtracted as backgrounds nor included explicitly as signal in the calculation of the cross section.

The background contributed by W pair production in double parton interactions is evaluated using a PYTHIA 8 MC sample scaled to a theoretical cross section obtained by combining the NNLO prediction for single W boson production and the measured effective-area parameter for double parton interactions [72]. The contribution in the signal region is found to be around 0.3%. To increase the impact of double parton interactions on the dominant $e\mu$ channel beyond the percent level would require an increase of the effective cross section by more than ten times its uncertainty. This background contribution is neglected.

6.6 WW candidate events and estimated background yields

The data event yields and the estimated background contributions are summarised in table 3. The MC predicts that 93% of all signal events selected in the sample are produced via the $q\bar{q} \to W^+W^-$ process, while 4% stem from non-resonant $gg \to W^+W^-$ and 3% from resonant $H \to WW$ production. Kinematic distributions comparing the selected data to the signal and backgrounds are shown in figures 6 and 7. The W+jets and multijet backgrounds are determined using fully data-driven methods, while for top-quark and Drell-

Final state	$e\mu$				ee				$\mu\mu$			
Observed events	5067				594				975			
Total expected events (Signal + background)	4420	±	30	±	320	507	±	9	±	39	817	±	12	±	65
WW signal (MC)	3240	±	10	±	280	346	±	3	±	33	613	±	5	±	60
Top quark (data-driven)	609	±	18	±	52	92	±	7	±	8	127	±	9	±	11
W+jets (data-driven)	250	±	20	±	140	14	±	5	±	14	6	±	5	±	12
Drell-Yan (data-driven)	175	±	3	±	18	28	±	0	±	13	33	±	0	±	17
Other dibosons (MC)	150	±	4	±	30	27	±	1	±	5	38	±	1	±	5
Total background	1180	±	30	±	150	161	±	9	±	21	205	±	11	±	24

Table 3. Summary of observed events and expected signal and background contributions in three dilepton channels. The first uncertainty is statistical, the second one corresponds to the systematic uncertainty and includes the uncertainty due to the integrated luminosity (where used in the normalisation). The systematic uncertainties in the total background and total expectation are calculated as the sum in quadrature of the uncertainties of the individual components. The MC simulation of the WW signal predicts that 93% of the events are produced via the $q\bar{q} \to W^+W^-$ process, while 4% stem from non-resonant $gg \to W^+W^-$ and 3% from resonant $H \to WW$ production.

Yan production the normalisation is determined from data, but their differential shapes are taken from MC predictions. The diboson background and the WW signal are taken from MC simulation.

The signal contribution is normalised to the integrated luminosity using the nNLO cross-section prediction, which is defined in section 9.1. The transverse momentum of the leading lepton, $p_{\mathrm{T}}^{\mathrm{lead}}$, invariant mass of the dilepton system, $m_{\ell\ell}$, and its transverse momentum, $p_{\mathrm{T}}(\ell\ell)$, the difference in azimuthal angle between the decay leptons, $\Delta\phi_{\ell\ell}$, their combined rapidity, $|y_{\ell\ell}|$, as well as the observable $|\cos(\theta^*)|$, defined in eq. (2.1), are shown. For the same-flavour final states in figure 7, a discontinuity in the distribution of the invariant mass of the dilepton system, $m_{\ell\ell}$, is visible due to the rejection of events that are reconstructed with an invariant mass close to the Z boson mass m_Z. For all distributions, an excess of the data over the signal and background is observed, and this is discussed in more detail in section 9.

7 Cross-section determination

7.1 Fiducial and total cross sections

After determining the background-subtracted number of signal candidate yields, $N_{\mathrm{data}} - N_{\mathrm{bkg}}$, the fiducial WW production cross section is extracted using a likelihood fit based on
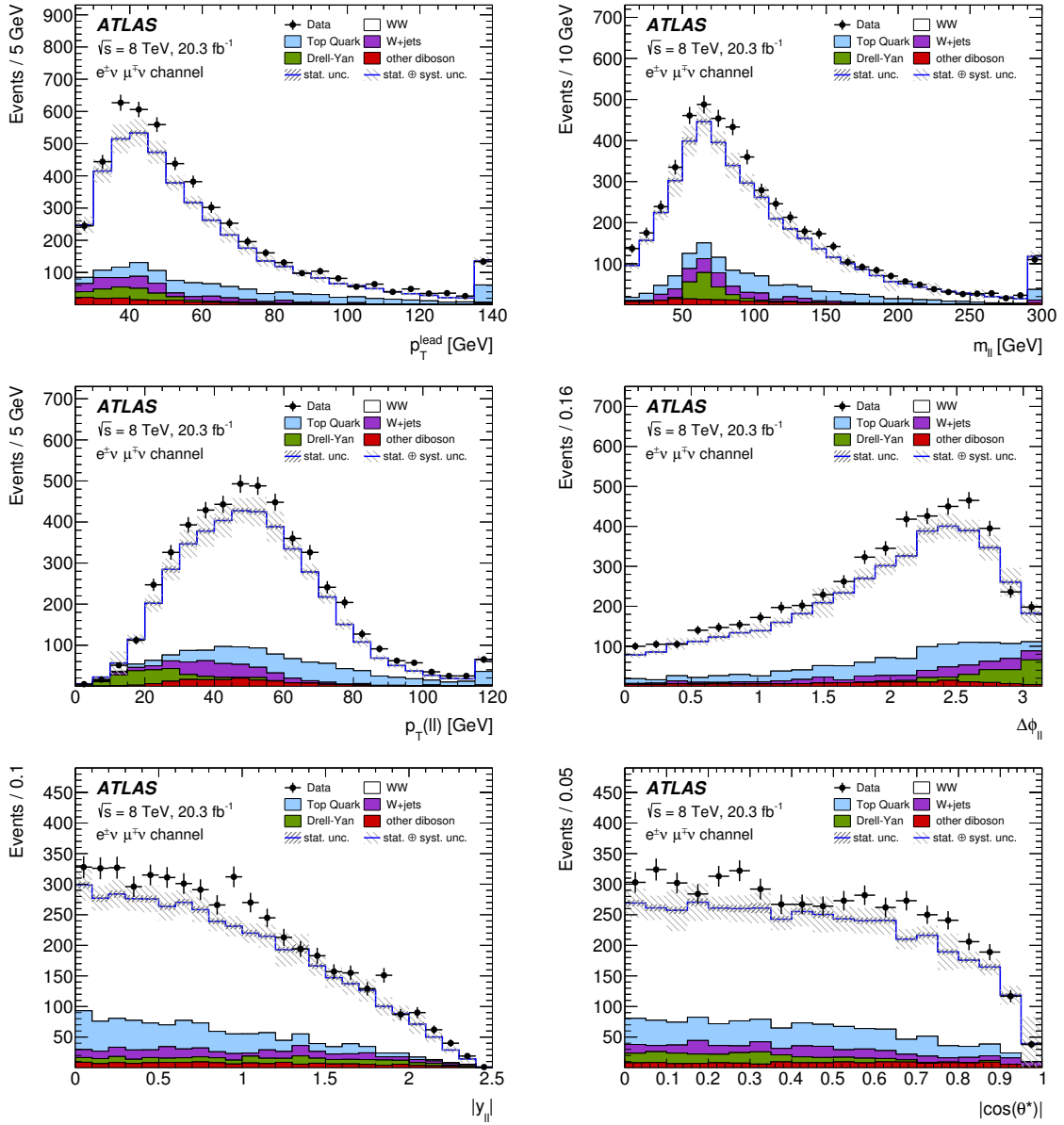
Figure 6. Kinematic distributions of the selected data events after the full event selection for the $e\mu$ final state. Data are shown together with the predictions of the signal and background production processes. The transverse momentum of the leading lepton, p_T^{lead}, the invariant mass, $m_{\ell\ell}$, and the transverse momentum of the dilepton system, $p_T(\ell\ell)$, as well as the difference in azimuthal angle between the decay leptons, $\Delta\phi_{\ell\ell}$, the dilepton rapidity, $|y_{\ell\ell}|$, and the observable $|\cos(\theta^*)|$ are shown (from left to right and top to bottom). The last bin of the p_T^{lead}, $m_{\ell\ell}$ and $p_T(\ell\ell)$ distributions is an overflow bin. Statistical and systematic uncertainties in the predictions are shown as bands in hatched style.
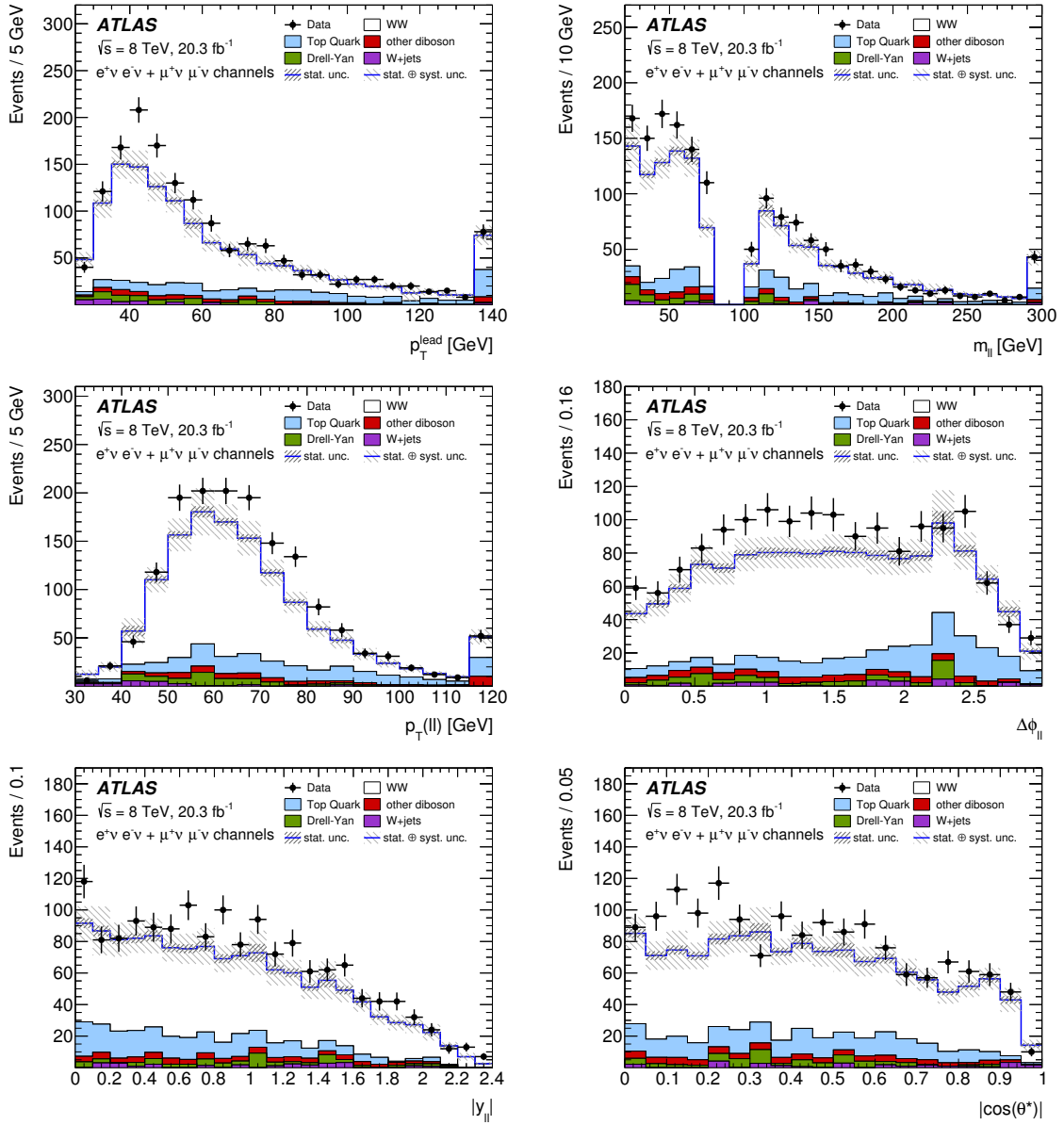
Figure 7. Kinematic distributions of the selected data events after the full event selection for the combined ee and $\mu\mu$ final states. Data are shown together with the predictions of the signal and background production processes. The transverse momentum of the leading lepton, p_T^{lead}, the invariant mass, $m_{\ell\ell}$, and the transverse momentum of the dilepton system, $p_T(\ell\ell)$, as well as the difference in azimuthal angle between the decay leptons, $\Delta\phi_{\ell\ell}$, their combined rapidity, $|y_{\ell\ell}|$, and the observable $|\cos(\theta^*)|$ are shown (from left to right and top to bottom). The last bin of the p_T^{lead}, $m_{\ell\ell}$ and $p_T(\ell\ell)$ distributions is an overflow bin. Statistical and systematic uncertainties in the predictions are shown as bands in hatched style.

|	$e\mu$	$ee/\mu\mu$
p_T^ℓ (leading/sub-leading)	$> 25\,/\,20$ GeV	
$|\eta^\ell|$	$|\eta^\mu| < 2.4$ and $|\eta^e| < 2.47$,	
	excluding $1.37 < |\eta^e| < 1.52$	
$m_{\ell\ell}$	> 10 GeV	> 15 GeV
$|m_Z - m_{\ell\ell}|$	—	> 15 GeV
Number of jets with $p_T > 25$ GeV, $|\eta| < 4.5$	0	0
$|\mathbf{\Sigma p}_T^{\nu_i}|$ if $\Delta\phi_\ell > \pi/2$ $|\mathbf{\Sigma p}_T^{\nu_i}| \times \sin(\Delta\phi_\ell)$ if $\Delta\phi_\ell < \pi/2$ ($E_{T,\,Rel}^{miss}$)	> 15 GeV	> 45 GeV
Transverse magnitude of the vectorial sum of all neutrinos, $|\mathbf{\Sigma p}_T^{\nu_i}|$ (p_T^{miss})	> 20 GeV	> 45 GeV

Table 4. Definitions of the respective fiducial regions used in the calculation of $\sigma_{\rm fid}^{e\mu}(WW)$, $\sigma_{\rm fid}^{ee}(WW)$ and $\sigma_{\rm fid}^{\mu\mu}(WW)$. In these definitions, ℓ is the charged lepton from the decays $W \to e\nu$ and $W \to \mu\nu$, and $\sin(\Delta\phi_\ell)$ is the minimum difference in azimuthal angle between the vector sum of the momenta of the neutrinos and any of the selected generator-level charged leptons.

the following equation:

$$\sigma_{\rm fid}^{\ell\ell'}(WW) = \frac{N_{\rm data} - N_{\rm bkg}}{C_{WW} \times \mathcal{L}}, \tag{7.1}$$

where $\mathcal{L}$ is the integrated luminosity. The correction factor C_{WW} is determined from MC simulation and accounts for detector efficiency, resolution effects and contributions from τ-lepton decays. It is defined as the ratio of the number of reconstructed WW events after the final selection with electrons or muons in the final state (including electrons or muons from τ decays) to the number of WW events generated in the fiducial region where only direct decays of W bosons to electrons and muons are allowed. The measured fiducial cross section $\sigma_{\rm fid}^{\ell\ell'}$ thus describes WW production with only prompt decays into $e\mu$, ee and $\mu\mu$ final states. The correction for contributions with intermediate $W \to \tau\nu$ decays only relies on the correct relative acceptance and the well-known relative branching fractions [69], not on the absolute normalization of the signal cross section.

The fiducial cross sections are measured separately in $e\mu$, ee and $\mu\mu$ final states in regions closely approximating the experimental selection. The fiducial regions are summarised in table 4.

To define the fiducial region, the following selection is applied to events from the MC generator before passing them through the detector simulation. Leptons are required to originate directly from W decays and be oppositely charged. They are recombined with any final-state photons from QED radiation that fall within $\Delta R = 0.1$ of the respective lepton to form so-called 'dressed-leptons'. The lepton kinematic requirements are imposed on these dressed leptons. Particle-level jets are constructed from stable particles with a lifetime of $\tau > 30$ ps, excluding muons and neutrinos, using the anti-k_t algorithm with a radius

parameter of 0.4. To remove jets reconstructed from signal electrons, jets lying a distance $\Delta R < 0.3$ from any signal electrons are removed. The four-momentum sum of the neutrinos stemming from the W boson decays is used for the calculation of both p_T^miss and $E_\text{T, Rel}^\text{miss}$.

The total cross section of WW production is defined to include all decay modes of the W bosons and all jet multiplicities. It is obtained by extrapolating the fiducial cross section for the effects of all acceptance cuts listed in table 4 with an additional acceptance factor, A_{WW}, and correcting for the leptonic branching fraction of W bosons $\mathcal{B}(W \to \ell\nu) = 0.108$ [69]:

$$\sigma_\text{tot}(pp \to WW) = \frac{\sigma_\text{fid}^{\ell\ell'}(pp \to WW)}{A_{WW} \times \mathcal{B}^2(W \to \ell\nu)} = \frac{N_\text{data} - N_\text{bkg}}{C_{WW} \times A_{WW} \times \mathcal{B}^2(W \to \ell\nu) \times \mathcal{L}}, \quad (7.2)$$

where A_{WW} is defined as the ratio of the MC signal event yield within the fiducial region to the total number of generated signal MC events. The numerical values for the different final states are given in table 5. For the $e\mu$ final state, the right-hand side of eq. (7.2) contains an additional combinatorial factor of $1/2$.

The total cross sections for the individual final states, $e\mu$, ee and $\mu\mu$, are then combined. The combination procedure is based on a likelihood fit where the systematic uncertainties, including the uncertainties due to backgrounds, are included as nuisance parameters. The minimisation of the negative log-likelihood function and the error calculation are performed using the Minuit package [73]. Several independent sources of systematic uncertainty are treated as correlated among the different final states, while the statistical uncertainties in the background estimates are treated as uncorrelated.

The numerical values of the correction factors C_{WW} and A_{WW} are shown in table 5, while the uncertainties are listed in table 7. These values are derived by adding the samples for all the WW production processes according to their cross sections as detailed in section 4. The same holds for the determination of their uncertainties. Table 5 also gives the values of the correction factors for the different WW production processes. The value for C_{WW} is largest for the $e\mu$ final state because events with W decays to τ-leptons, which only contribute to the numerator, make up a larger fraction of events in the $e\mu$ channel. This is due to less stringent requirements on E_T^miss. The difference in the C_{WW} values between ee and $\mu\mu$ is due to the different lepton identification efficiencies.

7.2 Measurement of the differential cross sections

Differential cross sections are defined in the fiducial regions and are measured as a function of the kinematic variables described in section 2. The measurement is carried out in the $e\mu$ final state, which has a larger signal acceptance and lower relative background contamination compared to the same-flavour channels. The reconstructed spectra are corrected for background contributions and then unfolded to the fiducial phase space by correcting for detector resolution and reconstruction efficiencies. The iterative Bayesian approach [74, 75] with three iterations is employed in this analysis. The choice of three iterations is optimised to minimise the statistical uncertainties and the dependence on the prior Monte Carlo distribution in the unfolded spectra.

	C_{WW} [%]			A_{WW} [%]			$C_{WW} \times A_{WW}$ [%]		
	$e\mu$	ee	$\mu\mu$	$e\mu$	ee	$\mu\mu$	$e\mu$	ee	$\mu\mu$
Total	51.2	29.1	47.4	22.8	8.6	9.3	11.7	2.5	4.4
$q\bar{q} \to W^+W^-$	51.4	29.2	47.7	23.5	8.7	9.5	12.1	2.6	4.5
$gg \to W^+W^-$ (non-resonant)	53.6	33.4	48.2	30.6	14.7	16.3	16.4	4.9	7.8
$gg \to H \to W^+W^-$	43.5	21.8	39.3	10.4	4.1	4.6	4.5	0.9	1.8

Table 5. Central values of C_{WW}, A_{WW} and $C_{WW} \times A_{WW}$ used in the calculation of the cross section. The numbers are derived using the weighted average of the numbers for the different WW production processes which are weighted according to their cross sections as detailed in section 4.

The measured differential cross sections are calculated from the unfolded signal spectra divided by the integrated luminosity and the corresponding bin widths. For the measurement, statistical uncertainties and the same systematic uncertainties as for the fiducial cross-section measurements are considered. In addition, the uncertainty due to the theoretical modelling is evaluated using a data-driven method that was introduced in ref. [76], in which the kinematic distributions of the MC signal events are corrected to match those from data and the uncertainty is considered as the difference between the unfolded data spectra derived with the modified MC distributions and those using the original MC simulation. The modelling uncertainty is found to be small ($\pm 1\%$) for most variables.

8 Systematic uncertainties

Systematic uncertainties in the measured WW cross section arise from the object reconstruction, the background determination, the procedures used to correct for detector effects, and the usage of theory predictions in correction and extrapolation procedures.

8.1 Experimental uncertainties

The relative systematic uncertainties from the reconstruction of the events in the detector and the background subtraction are summarised in table 6 for the fiducial and total cross-section measurements. The dominant systematic uncertainties in the combined measurement are the uncertainties due to the jet energy scale ($\sim 4\%$), the W+jets background ($\sim 3\%$) and the luminosity ($\sim 2\%$).

The uncertainties due to pile-up are estimated by varying the reweighting procedure for the MC samples used to reproduce the distributions of the number of primary vertices in data. The uncertainties in the correction factors to match the simulated efficiencies to the measured ones for the electron and muon trigger requirements [52, 53] as well as for the reconstruction, identification and isolation requirements [54, 56, 77, 78] are propagated to the measurement. A similar procedure is used to assess the uncertainty due to the lepton momentum scale and resolution [56, 79].

Uncertainties related to the selection and measurement of jets affect the measurement primarily via the definition of jets for the jet-veto requirement, but also via the $E_{\mathrm{T}}^{\mathrm{miss}}$

reconstruction. The impact on the cross-section measurements is evaluated by varying each of these in the simulation within their respective uncertainties as determined from data [62]. The main sources of uncertainty for jets are the jet energy scale (JES) and the jet energy resolution (JER). Uncertainties of the lepton and jet momentum scales and resolutions are propagated to the E_T^{miss} reconstruction. Additional uncertainties in the E_T^{miss} due to jets reconstructed with momenta below $p_T < 20\,\text{GeV}$ and calorimeter cells not associated with any reconstructed objects are accounted for separately and denoted "soft terms" in table 6. An uncertainty in the p_T^{miss} scale and resolution is estimated from a comparison between data and MC simulation in Z boson events with muonic decays.

Backgrounds are determined as discussed in section 6, and the uncertainties from the background subtraction are also given in table 6. For each of the top-quark and Drell-Yan background estimates, and the W+jets and the multijet background estimate, the total systematic uncertainty is given. The statistical uncertainties stem from the limited size of the MC samples used for the background estimates of the diboson production processes and from the limited size of the data samples used for data-driven estimations. The uncertainty in the integrated luminosity is $\pm 1.9\%$ and affects the cross-section determination through eqs. (7.1) and (7.2) and the normalisation of background from other diboson processes.

8.2 Modelling uncertainties

The modelling uncertainty in the WW signal enters the cross-section determination through the calculation of the correction factor C_{WW} and the acceptance correction factor A_{WW}. The dominant uncertainties in A_{WW} stem from the jet-veto requirement (3.4%), the parton shower model and the choice of generators ($\sim 2.5\%$), while the uncertainties due to other sources (PDF choice, NLO electroweak correction, residual QCD scale dependence) are found to be small ($<1\%$). In contrast to A_{WW}, which has a sizeable theory dependence, C_{WW} is mainly affected by the detector resolution and only has a small theoretical uncertainty ($\sim 1\%$). The product of $C_{WW} \times A_{WW}$ and its corresponding uncertainties are evaluated taking into account correlations between the uncertainties in C_{WW} and A_{WW}. Table 7 gives an overview of the theoretical uncertainties used in the cross-section calculation. They are determined independently for the different WW signal processes as detailed below and added according to the respective contribution of $q\bar{q} \to W^+W^-$ and resonant and non-resonant gg-induced W^+W^- production.

The PDF uncertainty is estimated as the envelope of the CT10 [28] prediction and the predictions obtained using MSTW2008 [80] and NNPDF2.3 [81] and their respective PDF uncertainties at 68% confidence level following ref. [82]. The PDF uncertainties for $q\bar{q}$ and gg-induced WW production are combined assuming full correlation.

The effect of the next-to-leading-order EWK contributions of $\mathcal{O}(\alpha_{EW}^3)$ is considered for the $q\bar{q} \to W^+W^-$ process only, but the resulting uncertainty in C_{WW} and A_{WW} is minor.

The uncertainties of the perturbative calculations can be estimated by varying the choice of renormalisation and factorisation scales and quoting the maximum difference between results from the central value and the alternative scale choices. However, it is suggested in ref. [83] that this approach may underestimate the uncertainty in the case a jet-veto requirement is applied and therefore a more conservative approach is proposed. In

Sources of uncertainty	$e\mu$	ee	$\mu\mu$	Combined
Experimental uncertainties in fiducial and total cross sections [%]				
Integrated luminosity	±2.0	±2.0	±2.0	±2.0
Pile-up	±1.4	±2.0	±2.0	±1.5
Trigger	±0.4	±2.8	±3.0	±0.8
Electron energy scale	±0.4	±1.5	—	±0.4
Electron energy resolution	±0.0	±0.2	—	±0.1
Electron identification and reconstruction	±1.0	±2.2	—	±0.9
Electron isolation	±0.2	±0.5	—	±0.2
Muon momentum scale	±0.1	—	±0.4	±0.1
Muon momentum resolution (ID)	±0.6	—	±1.7	±0.7
Muon momentum resolution (MS)	±0.1	—	±0.2	±0.1
Muon identification and reconstruction	±0.4	—	±0.8	±0.4
Muon isolation	±0.6	—	±1.2	±0.6
Jet vertex fraction (JVF)	±0.2	±0.3	±0.2	±0.2
Jet energy scale	±4.1	±3.9	±4.4	±4.1
Jet energy resolution	±1.4	±1.3	±1.5	±1.4
$E_{\mathrm{T}}^{\mathrm{miss}}$ scale soft terms	±1.1	±2.1	±1.9	±1.3
$E_{\mathrm{T}}^{\mathrm{miss}}$ resolution soft terms	±0.3	±0.4	±0.5	±0.4
$p_{\mathrm{T}}^{\mathrm{miss}}$ scale soft terms	±0.2	±0.4	±0.4	±0.3
$p_{\mathrm{T}}^{\mathrm{miss}}$ resolution soft terms	±0.1	±0.2	±0.1	±0.1
Background uncertainties in fiducial and total cross sections [%]				
Top-quark background	±1.4	±1.8	±1.4	±1.4
W+jets & multijet background	±3.6	±3.1	±2.0	±2.8
Drell-Yan background	±0.5	±3.0	±2.3	±0.9
MC statistics (top-quark, W+jets, Drell-Yan)	±0.6	±2.0	±1.4	±0.5
Other diboson cross sections	±0.7	±1.0	±0.6	±0.7
MC statistics (other diboson)	±0.1	±0.3	±0.2	±0.1

Table 6. Uncertainty sources and associated relative systematic uncertainties for the reconstruction and background subtraction for the WW cross sections measured in the $e\mu$, ee and $\mu\mu$ final states as well as for the combined cross section. The uncertainties apply to both the fiducial and total cross sections. In cases where no uncertainties are quoted they do not affect the specific final state (e.g. electron energy scale uncertainties for muon final states).

this approach, the scale variation uncertainties are treated as uncorrelated between cross sections for different inclusive jet multiplicities and predictions for exclusive jet multiplicities are obtained from the difference between the inclusive predictions. The uncertainty in the difference is then used to estimate the perturbative uncertainty due to the jet-veto requirement. This uncertainty is found to be about $\pm2.9\%$ for the $q\bar{q} \to W^+W^-$ process when using the NNLO predictions [3]. The uncertainty due to the jet-veto requirement for the $H \to W^+W^-$ production process has been determined to be $\pm11\%$ [55] and the same uncertainty is assumed for the non-resonant $gg \to W^+W^-$ process. The combined uncertainty due to the jet-veto requirement for the WW signal is about $\pm3.4\%$, assuming

	$\sigma(C_{WW})$ [%]			$\sigma(A_{WW})$ [%]			$\sigma(C_{WW} \times A_{WW})$ [%]		
	$e\mu$	ee	$\mu\mu$	$e\mu$	ee	$\mu\mu$	$e\mu$	ee	$\mu\mu$
PDF	0.10	0.34	0.13	0.81	0.94	0.93	0.85	1.3	0.98
EWK corrections (SF_{EW})	0.01	0.06	0.04	0.46	0.41	0.43	0.47	0.34	0.40
Jet veto	—	—	—	3.4	3.4	3.4	3.4	3.4	3.4
Scale	0.62	0.62	0.62	0.22	0.22	0.22	0.66	0.66	0.66
Soft QCD	0.35	0.92	0.80	2.5	2.6	2.7	2.5	3.0	2.9
Total	0.70	1.2	1.0	4.3	4.4	4.5	4.4	4.8	4.6

Table 7. Relative uncertainties of C_{WW}, A_{WW} and $C_{WW} \times A_{WW}$, due to the theoretical modelling of the WW signal processes, which include $q\bar{q} \to W^+W^-$ and non-resonant and resonant $gg \to W^+W^-$ production. The total uncertainties are calculated as the quadratic sum of the uncertainties from each source. The combined $C_{WW} \times A_{WW}$ uncertainties take into account the correlation between C_{WW} and A_{WW}.

full correlation of the $q\bar{q}$- and gg-induced processes. Without the jet-veto requirement, the residual perturbative uncertainty in A_{WW} due to the scale choice for the perturbative calculations is estimated using an approach in which the renormalisation (μ_R) and factorisation (μ_F) scales are varied independently by a factor of two or one-half. The uncertainty in A_{WW} due to the scale choice is calculated when not applying the jet-veto requirement to avoid double counting with the above described perturbative uncertainty due to the jet-veto requirement. It is found to be $\pm 0.2\%$. The uncertainty in C_{WW} due to the perturbative calculations, including the jet-veto requirement, is found to be about $\pm 0.6\%$.

Parton shower, hadronisation and underlying-event uncertainties (collectively called "soft QCD" in the following), and generator uncertainties, have effects that are estimated by comparing various MC signal samples. For $q\bar{q} \to W^+W^-$ production, the generator uncertainty is evaluated by comparing samples generated using POWHEG and MC@NLO both interfaced with HERWIG+JIMMY, whilst the soft QCD uncertainties are calculated using two samples generated with POWHEG and interfaced with HERWIG+JIMMY and PYTHIA 8, respectively. This yields an uncertainty of 1.3% dominated by the uncertainty in A_{WW} due to the choice of generator. The C_{WW} uncertainties are estimated to be 0.4–0.9% for the $q\bar{q} \to W^+W^-$ process and are applied to all production channels. The uncertainties in A_{WW} for non-resonant $gg \to W^+W^-$ production due to soft QCD effects and the choice of the generator are evaluated by comparing the results obtained from samples generated with GG2WW and MCFM both interfaced to HERWIG+JIMMY, and two samples generated with MCFM interfaced either to HERWIG+JIMMY or PYTHIA 8. This gives an uncertainty of about 30% in A_{WW}, which is dominated by a 28–29% uncertainty coming from the parton shower. Uncertainties in the modelling of resonant $H \to W^+W^-$ production are taken from ref. [55] and amount to 6.9% for A_{WW}.

9 Cross-section results

9.1 Theoretical predictions

Various calculations for WW diboson production, involving higher loop QCD corrections, electroweak corrections, or involving resummation of soft gluon terms are available, with different approaches taken to approximate these effects [3, 5, 7]. Hence, when comparing experimental results with theoretical predictions, these corrections play a relevant role.

Figure 1 illustrates the diagrams of the leading processes for WW production. The cross section of the $q\bar{q} \to W^+W^-$ process is known to $\mathcal{O}(\alpha_s^2)$ [3]. The loop-induced gg processes that include the non-resonant gg and resonant Higgs boson production processes start contributing at $\mathcal{O}(\alpha_s^2)$. The non-resonant gg process is only predicted at lowest order, $\mathcal{O}(\alpha_s^2)$, while the Higgs boson production cross section has been calculated to $\mathcal{O}(\alpha_s^4)$ [46].[3] Neither of the loop processes interferes at $\mathcal{O}(\alpha_s^2)$ with the $q\bar{q} \to W^+W^-$ process and the interference between the gg-induced processes is small and can be neglected. The resonant Higgs boson production process makes up 6.6% of the total cross section, while non-resonant gg production contributes 2.2%.

The combination of the above processes calculated to $\mathcal{O}(\alpha_s^2)$ for the $q\bar{q}$ and non-resonant gg processes and to $\mathcal{O}(\alpha_s^4)$ for the resonant gg contribution yields a prediction for the total WW production that is valid to NNLO accuracy in perturbative QCD.

These theoretical calculations are available only for the total production cross section; the kinematic distributions for the $q\bar{q} \to W^+W^-$ process are predicted only at order $\mathcal{O}(\alpha_s)$ [45]. Therefore, fiducial cross sections are estimated by applying the acceptance correction A_{WW} as calculated from the MC samples described in section 4 to the total cross sections. The first prediction for the fiducial cross section is that for WW production predicted partially at NNLO in α_s (nNLO) neglecting $\mathcal{O}(\alpha_s^2)$ contributions to the $q\bar{q}$ process. The nNLO prediction for the total cross section is about 8% lower than the NNLO prediction, and as a consequence, the nNLO fiducial cross section, $\sigma(\mathrm{nNLO_{fid}})$, is also lowered by the same amount.

An approximate NNLO fiducial cross section, $\sigma(\mathrm{approx.\ NNLO_{fid}})$, can be derived by using the total NNLO prediction [3, 46] and multiplying it by the fiducial acceptance and the branching fractions, $\sigma_{\mathrm{tot}}^{\mathrm{NNLO}} \times A_{WW} \times \mathcal{B}^2$.

These calculations can be refined by considering further effects. Logarithmic contributions from soft gluon emission from the initial state can be resummed at next-to-next-to-leading logarithmic (NNLL) accuracy, yielding a theoretical prediction with reduced scale uncertainties and a more accurate description of the transverse momentum of the WW system, p_{T}^{WW}, and the jet multiplicity.

An approximate NNLO+NNLL prediction of fiducial cross sections, $\sigma(\mathrm{approx.\ NNLO + NNLL_{fid}})$, is provided in ref. [7], and is about 15–18% higher than the nNLO prediction and around 7–10% higher than the approximate NNLO prediction.

---

[3]A more recent 3-loop calculation of the theoretical prediction for the resonant gg process to $\mathcal{O}(\alpha_s^5)$ [84] yields a 0.15% increase of the total WW production cross section with respect to the calculation to $\mathcal{O}(\alpha_s^4)$ but it is not considered here.

The use of resummation calculations also affects the calculation of the acceptance A_{WW} and this effect was investigated in ref. [5]. Based on ref. [5] an alternative approximation for the fiducial cross section including NNLL effects, $\sigma(\text{NNLO } p_{\text{T}}\text{-Resum}_{\text{fid}})$, is calculated as the product of $\sigma(\text{NNLO}_{\text{tot}})$, the branching fraction, and a corrected fiducial acceptance factor $A_{p_{\text{T}}-\text{Resum}_{WW}}$. The corrected $A_{p_{\text{T}}-\text{Resum}_{WW}}$ is derived by reweighting the shape of the p_{T}^{WW} distribution in the MC samples described in section 4 to the predicted NLO+NNLL shape given in ref. [5].

The uncertainty in the NNLO calculation of the total cross section accounts for the effects of QCD scale and PDF uncertainties, which are added linearly, while the theoretical uncertainties of the fiducial cross sections include the parton shower uncertainty in addition to the QCD scale and PDF uncertainties, the effects of which are again added linearly.

9.2 Cross-section measurements and comparisons with theoretical predictions

The measured fiducial and total cross sections are compared to theoretical calculations evaluated at different orders in α_{s}, as summarised in tables 8 and 9, respectively.

The cross-section measurements in their fiducial phase spaces, defined in table 4, are minimally dependent on theory corrections, since the fiducial volumes correspond closely to the detector-level selection. The measured fiducial cross sections are summarised in table 8, including statistical and systematic uncertainties. They are about two standard deviations higher than the nNLO prediction, and about 1.4 standard deviations larger than $\sigma(\text{approx. NNLO}_{\text{fid}})$, while they are found to be compatible with the predictions that consider resummation corrections. A graphical comparison between the fiducial cross-section measurements and various theoretical predictions is shown in figure 8.

The total cross sections are measured separately in the three different final states and then combined. The results for the individual measurements and the combined cross section are summarised in table 9. The combined cross section is found to be compatible with the NNLO prediction within about 1.4 standard deviations. A graphical comparison between the individual measurements and their combination is shown in figure 9. The result is fully compatible with the recently published measurement by the CMS Collaboration [14].

The measured unfolded differential cross sections are shown in figure 10. They are compared to predictions obtained using POWHEG+PYTHIA for the $q\bar{q} \to W^+W^-$ and $gg \to H \to W^+W^-$ production processes and GG2WW+HERWIG+JIMMY for non-resonant gg-induced WW production. These predictions are added as described in section 4. The data are also compared to an alternative prediction, where the $q\bar{q} \to W^+W^-$ contribution is reweighted using the approximated resummed calculation from ref. [5] described above. For a third prediction, the $q\bar{q} \to W^+W^-$ contribution is replaced using MC@NLO+HERWIG+JIMMY. All three predictions are normalised to the NNLO theoretical prediction for the total cross section.

The predictions generally undershoot the data, except for high p_{T} of the leading lepton, at high $m_{\ell\ell}$ and for high values of $\Delta\phi_{\ell\ell}$, where there is a small deficit in data compared to the expectation from either MC prediction. A small discrepancy between the MC predictions and the data is visible for the unfolded differential distribution of the transverse momentum of the leading lepton, $p_{\text{T}}^{\text{lead}}$, which differs between POWHEG and MC@NLO.

Prediction		Fiducial cross section $pp \to WW \to \ell\ell\nu\nu$ [fb]
Measured $\sigma_{\text{fid}}^{e\mu}(WW)$		$374 \pm 7(\text{stat}) ^{+25}_{-23}(\text{syst}) ^{+8}_{-7}(\text{lumi})$
$\sigma(\text{nNLO}_{\text{fid},e\mu})$	$= (\sigma_{\text{tot}}^{\text{nNLO}} \times A_{WW} \times \mathcal{B}^2)$ [45]+[46]	311 ± 15
$\sigma(\text{approx. NNLO}_{\text{fid},e\mu})$	$= (\sigma_{\text{tot}}^{\text{NNLO}} \times A_{WW} \times \mathcal{B}^2)$ [3]+[46]	335 ± 18
$\sigma(\text{approx. (NNLO + NNLL)}_{\text{fid},e\mu})$ [7]		358 ± 14
$\sigma(\text{NNLO } p_{\text{T}}\text{-Resum}_{\text{fid},e\mu})$	$= (\sigma_{\text{tot}}^{\text{NNLO}} \times A_{\text{p}_{\text{T}}-\text{Resum}_{WW}} \times \mathcal{B}^2)$ [5]	349 ± 19
Measured $\sigma_{\text{fid}}^{ee}(WW)$		$73.4^{+4.2}_{-4.1}(\text{stat}) ^{+6.5}_{-5.6}(\text{syst}) \pm 1.5(\text{lumi})$
$\sigma(\text{nNLO}_{\text{fid},ee})$	[45]+[46]	58.5 ± 2.8
$\sigma(\text{approx. NNLO}_{\text{fid},ee})$	[3]+[46]	63.0 ± 3.4
$\sigma(\text{approx. (NNLO + NNLL)}_{\text{fid},ee})$ [7]		69.0 ± 2.7
$\sigma(\text{NNLO } p_{\text{T}}\text{-Resum}_{\text{fid},ee})$	[5]	65.5 ± 3.6
Measured $\sigma_{\text{fid}}^{\mu\mu}(WW)$		$80.2^{+3.3}_{-3.2}(\text{stat}) ^{+6.4}_{-5.5}(\text{syst}) \pm 1.6(\text{lumi})$
$\sigma(\text{nNLO}_{\text{fid},\mu\mu})$	[45]+[46]	63.7 ± 3.1
$\sigma(\text{approx. NNLO}_{\text{fid},\mu\mu})$	[3]+[46]	68.6 ± 3.7
$\sigma(\text{approx. (NNLO + NNLL)}_{\text{fid},\mu\mu})$[7]		75.1 ± 3.0
$\sigma(\text{NNLO } p_{\text{T}}\text{-Resum}_{\text{fid},\mu\mu})$	[5]	71.2 ± 4.0

Table 8. Measured cross sections in the fiducial region for each channel as defined in table 4, compared with various theoretical predictions described in the text of section 9.1.

Final state	Total cross section $pp \to WW$ [pb]
$e\mu$	$70.6 \pm 1.3(\text{stat}) ^{+5.8}_{-5.1}(\text{syst}) \pm 1.4(\text{lumi})$
ee	$73.6^{+4.2}_{-4.1}(\text{stat}) ^{+7.5}_{-6.4}(\text{syst}) \pm 1.5(\text{lumi})$
$\mu\mu$	$74.0 \pm 3.0(\text{stat}) ^{+7.1}_{-5.9}(\text{syst}) \pm 1.5(\text{lumi})$
Combined	$71.1 \pm 1.1(\text{stat}) ^{+5.7}_{-5.0}(\text{syst}) \pm 1.4(\text{lumi})$
$\sigma(\text{NNLO}_{\text{tot}})$ theory prediction [3]+[46]	$63.2^{+1.6}_{-1.4}(\text{scale}) \pm 1.2(\text{PDF})$

Table 9. Measured total WW production cross sections in each final state together with the combined value, compared to the $\sigma(\text{NNLO}_{\text{tot}})$ theory prediction.

The full difference between the two MC predictions is accounted for in section 10, when limits on anomalous couplings are extracted. The differences between data and MC simulation for the unfolded differential distributions in $|y_{\ell\ell}|$ and $|\cos(\theta^*)|$ are mostly constant as a function of these variables.

In general, the shapes of the unfolded data distributions agree with either prediction at the level of $\pm 15\%$. The $H \to W^+W^-$ contribution to the differential predictions is typically 2% to at most 8.5% per bin, and therefore has a small impact on the comparison.
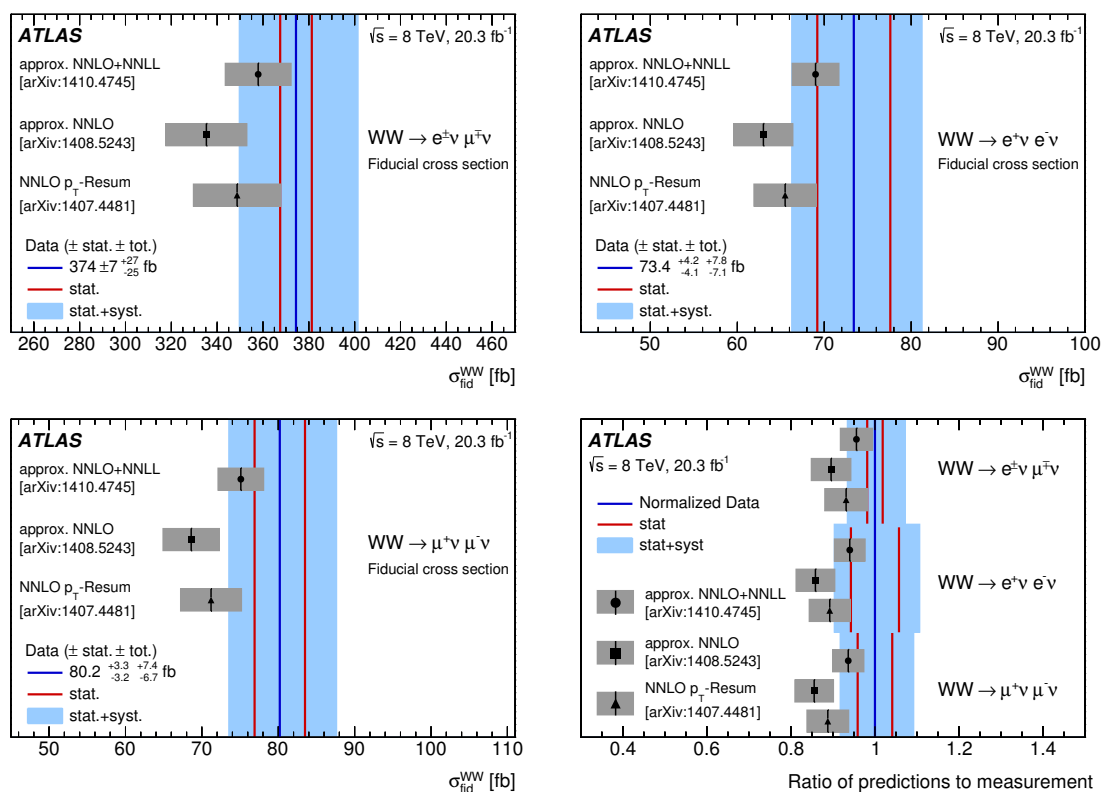
Figure 8. Comparison of the measured fiducial cross sections with various theoretical predictions. The comparison is made for all final states, $e\mu$ (top left), ee (top right) and $\mu\mu$ (bottom left). The bottom right figure shows the measured and predicted fiducial cross sections normalised to the respective measured values for all final states. Theoretical predictions are indicated as black markers with grey error bands, while the central value of the measured cross sections is indicated by a blue line with red lines showing the statistical uncertainty and blue bands for the total uncertainty including statistical and systematic uncertainties.

Tables 13 to 18 in the appendix give an overview of the measured unfolded differential cross sections and the statistical, experimental and background uncertainties in the measurement. The bin-to-bin correlations are preserved for each source of systematic uncertainty and the correlation matrices are made available in the appendix. The systematic uncertainties are treated as fully correlated. This includes the background uncertainties, except the uncertainties due to the limited statistics of the MC simulation and the uncertainties related to the W+jets estimate, specifically the uncertainties on the measured fake lepton efficiencies and the sample dependence, since both these uncertainties have a large statistical component. The background uncertainties are added in quadrature to the statistical and experimental uncertainties to obtain the total uncertainty in each bin. The total uncertainties range from 10% to 30%. Normalised unfolded differential cross-section distributions are also measured, as these are more suited to analysis of the shapes of differential distributions. Results and tables are made available in the appendix.
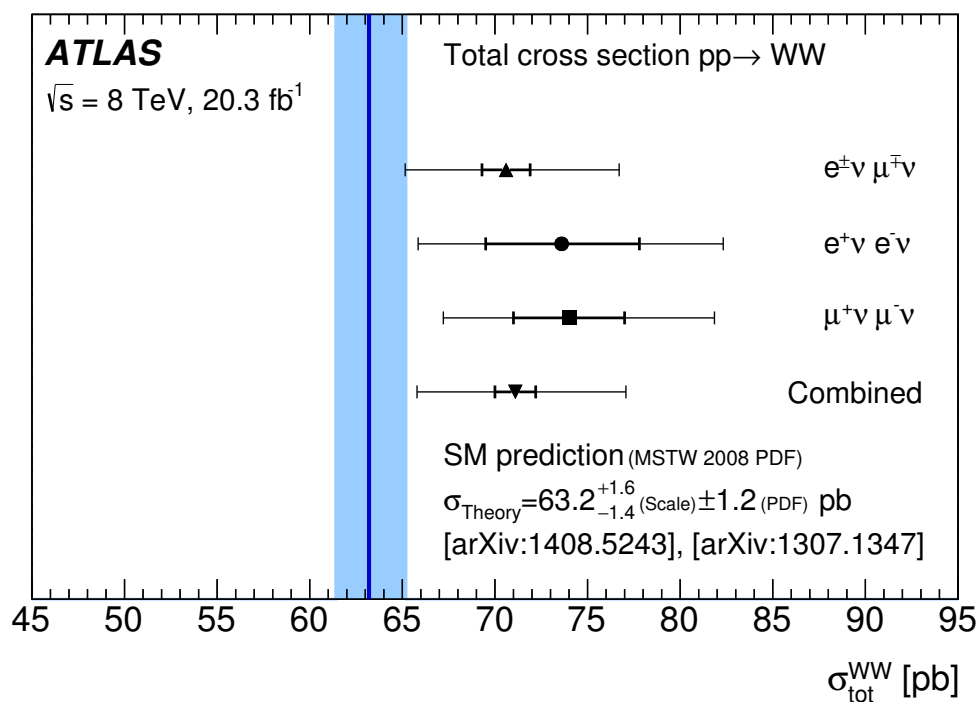
Figure 9. The *WW* cross sections measured at $\sqrt{s} = 8$ TeV compared to the NNLO prediction. The uncertainties in the measurement show the statistical as well as the total uncertainty including the luminosity uncertainty.
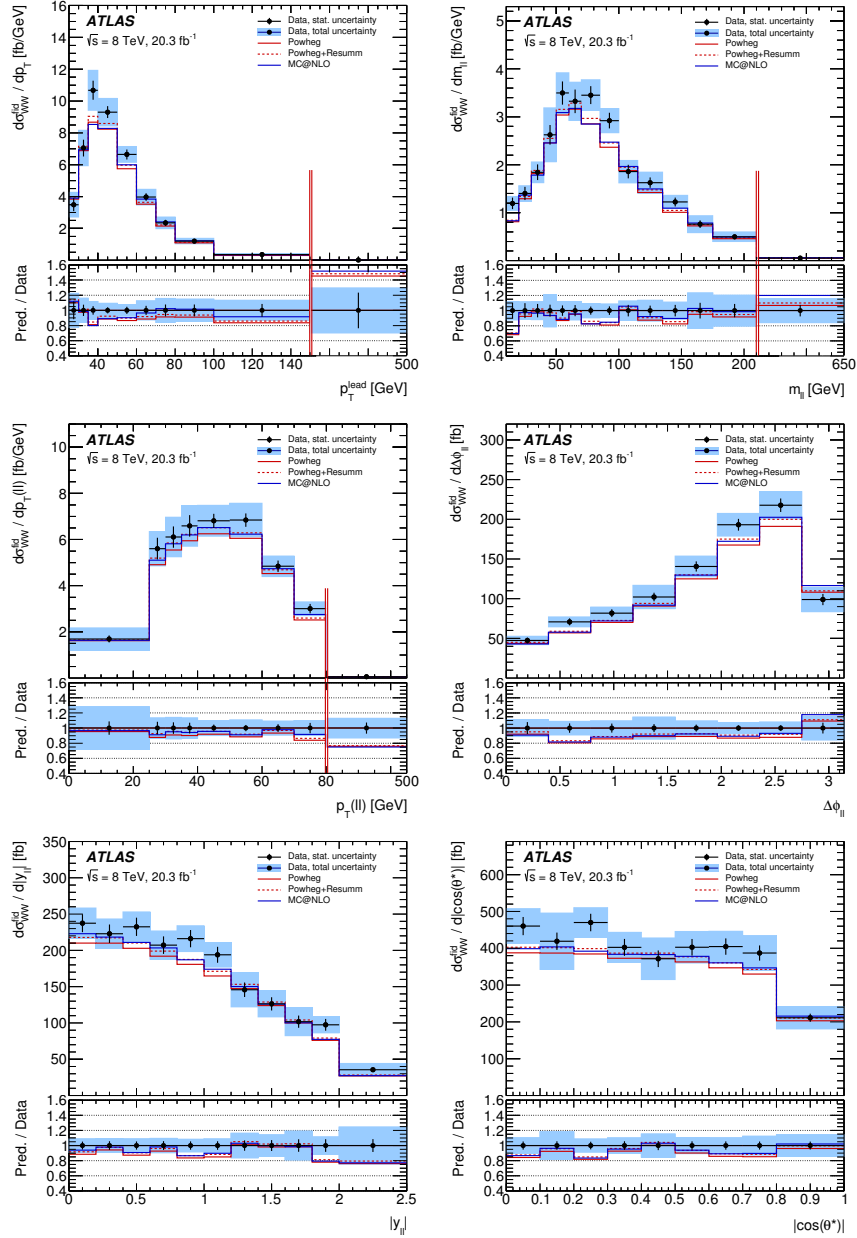
Figure 10. Measured unfolded differential cross sections of WW production in the $e\mu$ final state for the transverse momentum of the leading lepton, p_T^{lead}, the invariant mass, $m_{\ell\ell}$, and the transverse momentum of the dilepton system, $p_T(\ell\ell)$, as well as the difference in azimuthal angle between the decay leptons, $\Delta\phi_{\ell\ell}$, their combined rapidity, $|y_{\ell\ell}|$, and the observable $|\cos(\theta^*)|$. The measured cross-section values are shown as markers with error bars giving the statistical uncertainty and blue bands indicating the size of the total uncertainty. Three different MC predictions are compared to the measurement. The solid red line shows the nominal prediction, whilst the dashed red line shows the prediction in case the $q\bar{q} \rightarrow W^+W^-$ contribution is replaced by the POWHEG+PYTHIA prediction reweighted to the resummed calculation of ref. [5]. The blue line depicts a prediction obtained using MC@NLO+HERWIG+JIMMY for the $q\bar{q} \rightarrow W^+W^-$ contribution. All three predictions are normalised to the NNLO theoretical prediction for the total cross section. For the top three histograms, double red lines indicate changes in the x-axis scale.

10 Limits on anomalous triple-gauge-boson couplings

10.1 Theoretical parameterisation

The non-Abelian self-couplings of W and Z bosons and photons can be probed via the WWV vertex, where $V = Z$ or γ, present when the bosons are produced via the s-channel exchange of a Z or γ as shown in figure 1(b). The SM, with its SU(2) × U(1) structure, makes definite predictions for these triple-gauge-boson couplings [85]. The SM Lagrangian can be extended with additional degrees of freedom that modify the couplings. Considering only terms that conserve charge conjugation (C) and parity (P) separately, the modified Lagrangian can be written as:

$$\mathcal{L} = ig_{WWV} \left[g_1^V (W_{\mu\nu}^+ W^{-\mu} - W^{+\mu} W_{\mu\nu}^-) V^\nu + k^V W_\mu^+ W_\nu^- V^{\mu\nu} + \frac{\lambda^V}{m_W^2} W_\mu^{+\nu} W_\nu^{-\rho} V_\rho^\mu \right],$$

(10.1)

where $V = Z$ or γ; $W_{\mu\nu}^\pm = \partial_\mu W_\nu^\pm - \partial_\nu W_\mu^\pm$; $V_{\mu\nu} = \partial_\mu V_\nu - \partial_\nu V_\mu$. The overall coupling constants g_{WWV} are given by $g_{WW\gamma} = -e$ and $g_{WWZ} = -e \cot\theta_W$, where θ_W is the weak mixing angle.

Electromagnetic gauge invariance requires that $g_1^\gamma = 1$. The three other coupling parameters that are non-zero in the SM are $g_1^Z = 1$, $k^Z = 1$, and $k^\gamma = 1$. Deviations from the SM are introduced as

$$\Delta g_1^Z = 1 - g_1^Z; \qquad \Delta k^Z = 1 - k^Z; \qquad \Delta k^\gamma = 1 - k^\gamma.$$

(10.2)

The remaining couplings are zero in the SM, $\lambda^\gamma = \lambda^Z = 0$. A significant non-zero value for any of the parameters Δg_1^Z, Δk^Z, Δk^γ, λ^γ and λ^Z would be evidence of new interactions not included in the SM.

If anomalous couplings occur, these extra terms in the Lagrangian would contribute and would induce a violation of unitarity at sufficiently high energies. Therefore, form factors are introduced to dampen the rise of the WW production cross section so that it takes physical values even at the highest partonic centre-of-mass energies relevant for 8 TeV pp collisions:

$$\Delta g_1^V \to \frac{\Delta g_1^V}{\left(1 + \dfrac{\hat{s}}{\Lambda^2}\right)^2}, \qquad \Delta k^V \to \frac{\Delta k^V}{\left(1 + \dfrac{\hat{s}}{\Lambda^2}\right)^2}, \qquad \lambda^V \to \frac{\lambda^V}{\left(1 + \dfrac{\hat{s}}{\Lambda^2}\right)^2},$$

(10.3)

where $\hat{s}$ is the square of the invariant mass of the vector boson pair. The form-factor scale, Λ, is typically taken to be in the TeV range. Upper bounds on the size of the anomalous gauge boson couplings can be derived as a function of Λ based on unitarity considerations [86].

Several restrictions can be put on the couplings and are explored in this paper in addition to the scenario where none of the couplings is restricted per se: the *Equal Couplings* constraint assumes the coupling parameters for the WWZ and $WW\gamma$ vertices to be equal. Hence, $g_1^Z = g_1^\gamma = 1$, which leaves only two independent parameters: $\Delta k^\gamma = \Delta k^Z$ and

$\lambda^\gamma = \lambda^Z$. Imposing SU(2) × U(1) symmetry for the effective field operators [87] suggests the following constraint

$$\Delta g_1^Z = \Delta k^Z + \tan^2\theta_W \Delta k^\gamma,$$
$$\lambda^\gamma = \lambda^Z, \tag{10.4}$$

where θ_W is the weak mixing angle. This constraint is called the *LEP* constraint hereafter since it was introduced due to the limited statistics available at LEP for anomalous TGC studies. Assuming the absence of cancellations between tree-level and one-loop contributions, leads to the *Hagiwara-Ishihara-Szalapski-Zeppenfeld (HISZ)* constraint scenario [2] with two free parameters where the following relations hold:

$$\Delta g_1^Z = \frac{\Delta k^Z}{\cos^2\theta_W - \sin^2\theta_W},$$
$$\Delta k^\gamma = 2\Delta k^Z \frac{\cos^2\theta_W}{\cos^2\theta_W - \sin^2\theta_W},$$
$$\lambda^\gamma = \lambda^Z. \tag{10.5}$$

An alternative way to parameterise new physics in diboson production processes is based on *effective field theory (EFT)* [88]. It removes two complications of the generalised Lagrangian described above: it respects SU(2) × U(1) gauge invariance and does not introduce arbitrary form factors, though it assumes that higher-dimensional operators are suppressed by the mass scale of new physics. In the effective field theory approach, the effective Lagrangian is an expansion in operators that are SU(2) × U(1) gauge invariant and conserve charge conjugation and parity. The dimensionless coefficients, C_i, parameterise the strength of the coupling between new physics and SM particles:

$$\mathcal{L} = \mathcal{L}_{\mathrm{SM}} + \sum_i \frac{C_i}{\Lambda^2} \mathcal{O}_i. \tag{10.6}$$

There are five dimension-six operators, $\mathcal{O}_i$, but only three of those conserve C and P and are considered in the following:

$$\mathcal{O}_{WWW} = \mathrm{Tr}[W_{\mu\nu}W^{\nu\rho}W_\rho^\mu],$$
$$\mathcal{O}_W = (D_\mu\phi^0)^\dagger W^{\mu\nu} (D_\nu\phi^0),$$
$$\mathcal{O}_B = (D_\mu\phi^0)^\dagger B^{\mu\nu} (D_\nu\phi^0), \tag{10.7}$$

where ϕ^0 is the Higgs boson doublet field and

$$D_\mu = \partial_\mu + \frac{i}{2}g\tau^I W_\mu^I + \frac{i}{2}g' B_\mu,$$
$$W_{\mu\nu} = \frac{i}{2}g\tau^I \left(\partial_\mu W_\nu^I - \partial_\nu W_\mu^I + g\epsilon_{IJK} W_\mu^J W_\nu^K\right),$$
$$B_{\mu\nu} = \frac{i}{2}g' \left(\partial_\mu B_\nu - \partial_\nu B_\mu\right), \tag{10.8}$$

with $I = 1, 2, 3$ and similarly for J and K. The free parameters of the effective field theory approach used here are $C_{WWW}/\Lambda^2, C_W/\Lambda^2$ and C_B/Λ^2. The parameter C_W/Λ^2 also affects the Higgs production processes predicted to contribute at the 3% level in the SM. Possible enhancements of the Higgs production process are neglected in the subtraction of the resonant gg-induced $H \to WW$ production process as background and are fully attributed to the $q\bar{q} \to W^+W^-$ process in the limit setting.

10.2 Confidence intervals for the aTGC parameters

Anomalous triple-gauge-boson couplings (aTGCs) can modify the WW production cross section at large $\hat{s}$. A number of variables were investigated, and the transverse momentum of the leading lepton, p_T^{lead}, was found to be particularly sensitive to aTGCs and is therefore used to extract limits on the aTGC parameters. The extraction is based on detector-level distributions. A profile-likelihood-ratio test statistic [89] is used to check whether the data and predictions with aTGCs are compatible. Then a frequentist method [90] is used to determine the 95% confidence interval for the aTGC parameters. The $e\mu$ final state constitutes a major fraction of the selected data sample and has a higher signal-to-background ratio than the ee and $\mu\mu$ final states; therefore only the $e\mu$ events are used in the limit extraction.

The likelihood function used in the test statistic is the product of Poissonian probability density functions over the considered p_T^{lead} bins (150–250 GeV, 250–350 GeV and 350–1000 GeV) where the binning extends to large p_T^{lead} to maximise the sensitivity to anomalous couplings. However, the range shown in figure 10 is smaller as it has been optimised with respect to the uncertainties of the measured cross section based on the observed number of events. The binning for the aTGC analysis has been optimised using Asimov data [89]. Events with p_T^{lead} below 150 GeV are not considered because aTGC signals are not expected to contribute here significantly.

The number of observed data events and the prediction for the signal and background processes are used to construct the Poissonian probability density functions, in which systematic uncertainties are considered as nuisance parameters each constrained with a Gaussian distribution. A reweighting procedure implemented in MC@NLO [37] is used to obtain the signal predictions for arbitrary values of aTGCs; therefore in the study of aTGCs the SM $q\bar{q} \to W^+W^-$ events are modelled using MC@NLO interfaced to HERWIG+JIMMY. Only the $q\bar{q} \to W^+W^-$ process is considered as signal. The process $gg \to WW$, which includes resonant $H \to W^+W^-$ production, is considered as background, where the effects of possible anomalous couplings on the $H \to W^+W^-$ vertex are neglected.

Next-to-leading-order electroweak corrections to SM WW production are considered in the extraction of aTGC limits [32–35]. The correction is negative and becomes more significant in the high-p_T^{lead} region. Table 10 gives the relative size of the correction and its uncertainty. An additional systematic uncertainty in modelling the shape of the p_T^{lead} distribution for the $q\bar{q} \to W^+W^-$ process is estimated by comparing the predictions from MC@NLO and POWHEG+PYTHIA 8. The difference between these two MC predictions can be as large as 20% in the high p_T^{lead} bins. The shape of the p_T^{lead} distribution is found to be less dependent on other theoretical modelling uncertainties that are described in section 8. Experimental resolution and background uncertainties are fully accounted for.

Figure 11 compares the detector-level p_T^{lead} distribution with the SM prediction as well as the predictions for non-zero aTGC parameters, which are defined in the *no constraints* scenario that assumes no correlation between the parameters. In the left plot the predictions with arbitrarily large aTGC parameters are shown to demonstrate the effect of anomalous-triple-gauge-boson couplings on the distribution. In comparison, the right

p_T^{lead} [GeV]	25–75	75–150	150–250	250–350	350–1000
SF_{EW}	< 1%	−4%	−10%	−16%	−24%
$\delta\text{SF}_{\text{EW}}$	0.1%	<0.5%	2%	4%	7%

Table 10. Size of the next-to-leading-order EWK correction scale factor [36], SF_{EW}, and its systematic uncertainty ($\delta\text{SF}_{\text{EW}}$) in each bin of p_T^{lead}.
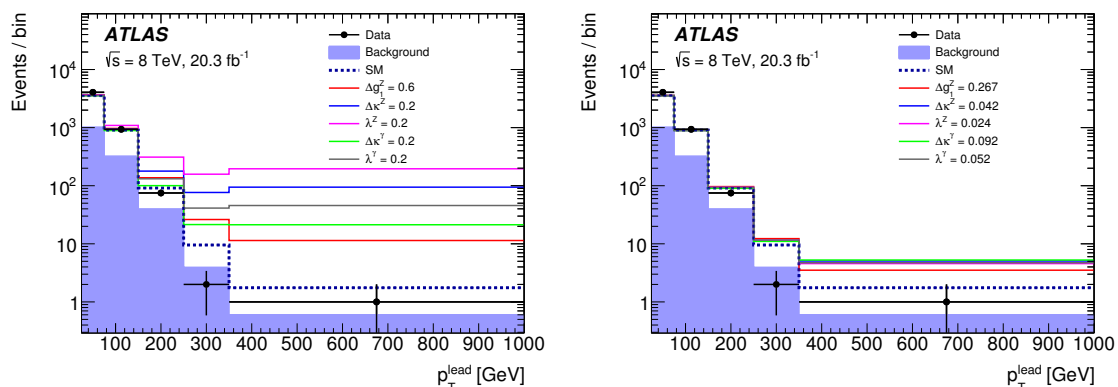
Figure 11. The leading lepton transverse momentum, p_T^{lead}, for $e\mu$ final states is compared for data and MC-generated events using different arbitrary values for aTGC parameters (left). The detector-level distributions are shown using values of aTGC parameters corresponding to the upper bounds of the observed 95% confidence interval (right). The aTGC parameters are defined in the *no constraints* scenario, and the form-factor scale is set to be infinity. The next-to-leading-order EWK correction scale factors from table 10 have been applied here. Except for the anomalous coupling parameter under study, all others are set to zero.

plot shows the predicted shapes with the values of aTGC parameters corresponding to the upper bounds of the observed 95% confidence interval.

To derive the confidence interval for some specific anomalous coupling parameters in any of the described scenarios, the other parameters are set to their SM values. Table 11 gives the expected and observed 95% confidence interval for each of the anomalous coupling parameters defined in the *no constraints*, *LEP*, *HISZ* and *Equal Couplings* scenarios. The limits are obtained with both $\Lambda = \infty$ and $\Lambda = 7$ TeV. A form-factor scale of 7 TeV is chosen as the largest value allowed by the unitarity requirement [86] for most aTGC parameters. The confidence intervals for the effective field theory approach are given in table 12. Figure 12 shows the expected and observed limits at 95% confidence level (C.L.), in red and black respectively, and the theoretical constraint due to the unitarity requirement (shown as blue dashed lines) as a function of form-factor scales from $\Lambda = 2$ TeV to $\Lambda = 10$ TeV. The largest value of form-factor scales that can preserve unitarity is ~7–9 TeV for most aTGC parameters, while it is only about 3 TeV for Δg_1^Z. All observed limits are more stringent than the expected limits because the data distribution falls more steeply than expected and a deficit of events is observed for the highest p_T^{lead} bins.

The limits in the plane of two coupling parameters are shown for the *no constraints* and *LEP* scenarios in figure 13 and figure 14, respectively. Further limits obtained for the
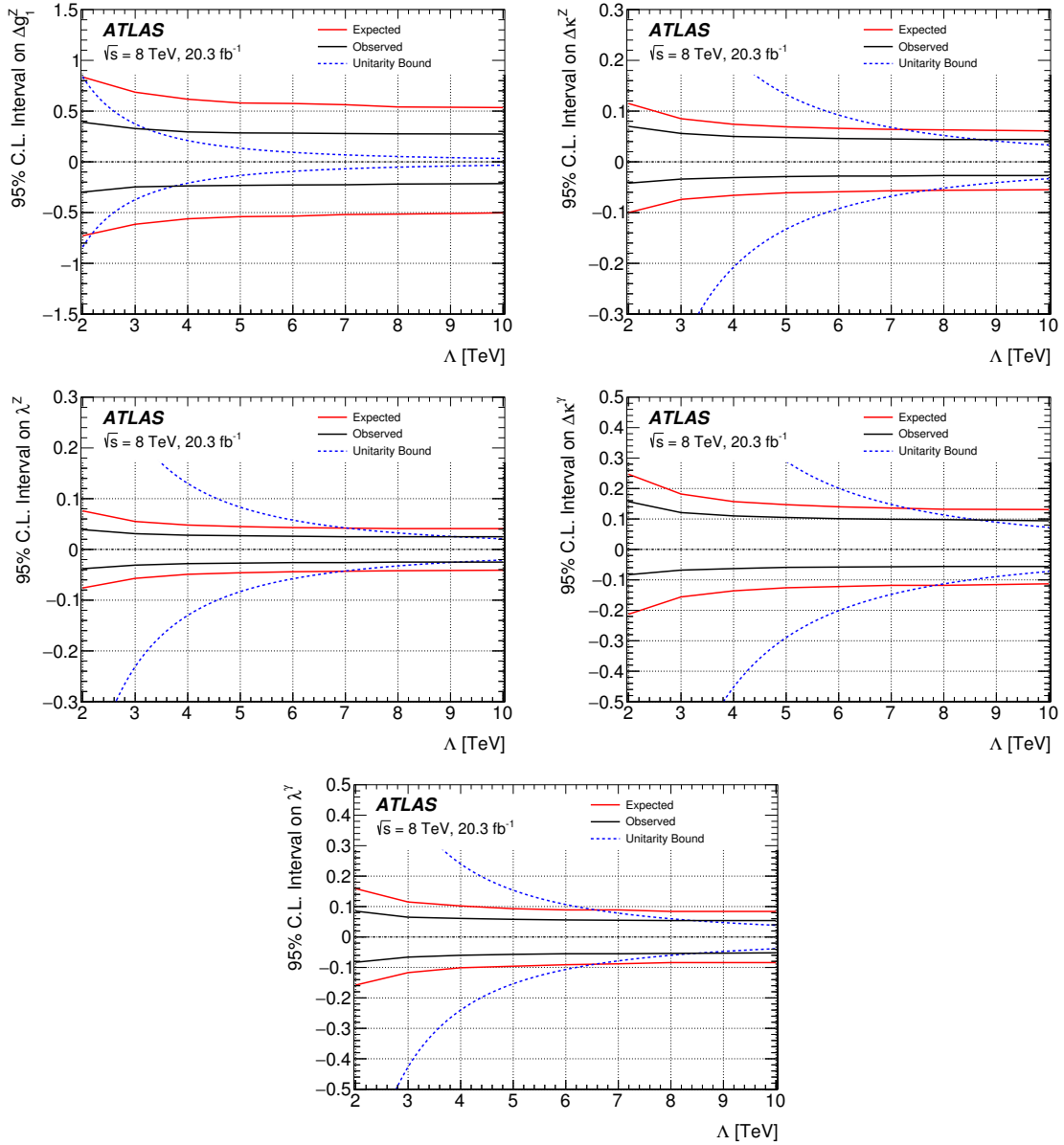
Figure 12. The expected and observed intervals at 95% confidence level (C.L.), in red and black respectively, and the theoretical constraint [86] due to the unitarity requirement (shown as blue dashed lines) as a function of form-factor scales from $\Lambda = 2$ TeV to $\Lambda = 10$ TeV. The plots are made for the aTGC parameters defined in the *no constraints* scenario. Except for the anomalous coupling parameter shown, all others are set to zero.

Scenario	Parameter	Expected	Observed	Expected	Observed
		$\Lambda = \infty$		$\Lambda = 7$ TeV	
	Δg_1^Z	$[-0.498, 0.524]$	$[-0.215, 0.267]$	$[-0.519, 0.563]$	$[-0.226, 0.279]$
	Δk^Z	$[-0.053, 0.059]$	$[-0.027, 0.042]$	$[-0.057, 0.064]$	$[-0.028, 0.045]$
No constraints scenario	λ^Z	$[-0.039, 0.038]$	$[-0.024, 0.024]$	$[-0.043, 0.042]$	$[-0.026, 0.025]$
	Δk^γ	$[-0.109, 0.124]$	$[-0.054, 0.092]$	$[-0.118, 0.136]$	$[-0.057, 0.099]$
	λ^γ	$[-0.081, 0.082]$	$[-0.051, 0.052]$	$[-0.088, 0.089]$	$[-0.055, 0.055]$
	Δg_1^Z	$[-0.033, 0.037]$	$[-0.016, 0.027]$	$[-0.035, 0.041]$	$[-0.017, 0.029]$
LEP	Δk^Z	$[-0.037, 0.035]$	$[-0.025, 0.020]$	$[-0.041, 0.038]$	$[-0.027, 0.021]$
	λ^Z	$[-0.031, 0.031]$	$[-0.019, 0.019]$	$[-0.033, 0.033]$	$[-0.020, 0.020]$
HISZ	Δk^Z	$[-0.026, 0.030]$	$[-0.012, 0.022]$	$[-0.028, 0.033]$	$[-0.013, 0.024]$
	λ^Z	$[-0.031, 0.031]$	$[-0.019, 0.019]$	$[-0.033, 0.034]$	$[-0.020, 0.020]$
Equal Couplings	Δk^Z	$[-0.041, 0.048]$	$[-0.020, 0.035]$	$[-0.045, 0.052]$	$[-0.021, 0.037]$
	λ^Z	$[-0.030, 0.030]$	$[-0.019, 0.019]$	$[-0.034, 0.033]$	$[-0.020, 0.020]$

Table 11. The expected and observed 95% confidence intervals for the anomalous coupling parameters defined in the *no constraints* scenario, *LEP*, *HISZ* and *Equal Couplings* scenarios. The results are shown with $\Lambda = \infty$ and $\Lambda = 7$ TeV.

Scenario	Parameter	Expected [TeV^{-2}]	Observed [TeV^{-2}]
	C_{WWW}/Λ^2	$[-7.62, 7.38]$	$[-4.61, 4.60]$
EFT	C_B/Λ^2	$[-35.8, 38.4]$	$[-20.9, 26.3]$
	C_W/Λ^2	$[-12.58, 14.32]$	$[-5.87, 10.54]$

Table 12. The expected and observed 95% confidence intervals for the *EFT* approach.

Equal Couplings and *HISZ* scenarios are shown in figure 15. Finally, the 95% confidence-level contours for linear combinations of aTGC parameters defined in the effective field theory approach are shown in figure 16.

Due to the increased integrated luminosity and the higher centre-of-mass energy, the new limits are more stringent by up to 50% than those previously published by the ATLAS Collaboration using data taken at $\sqrt{s} = 7$ TeV [12]. The constraints derived in the LEP scenario are similar to the combined results of the LEP experiments and in a few cases the derived limits exceed the bounds placed by LEP. The 95% confidence-level limits on Δg_1^Z obtained in this analysis range from -0.016 to 0.027 whilst the limits from LEP cover values from -0.021 to 0.054. The 95% confidence intervals on C_{WWW}/Λ^2 and C_B/Λ^2 derived in this analysis are similar, or up to 20-30% more restrictive than those obtained by the CMS Collaboration in ref. [14], which derives limits for the effective field theory approach only and uses the invariant dilepton mass distribution, $m_{\ell\ell}$. The limits derived on C_W/Λ^2 cover a complementary range around zero compared to the bounds from CMS, they have similar numerical values but opposite sign. Since the effects of EFT operators on distributions depend primarily on their absolute magnitude and not on their sign, these differences between the ATLAS and CMS constraints on C_W/Λ^2 can be considered insignificant.
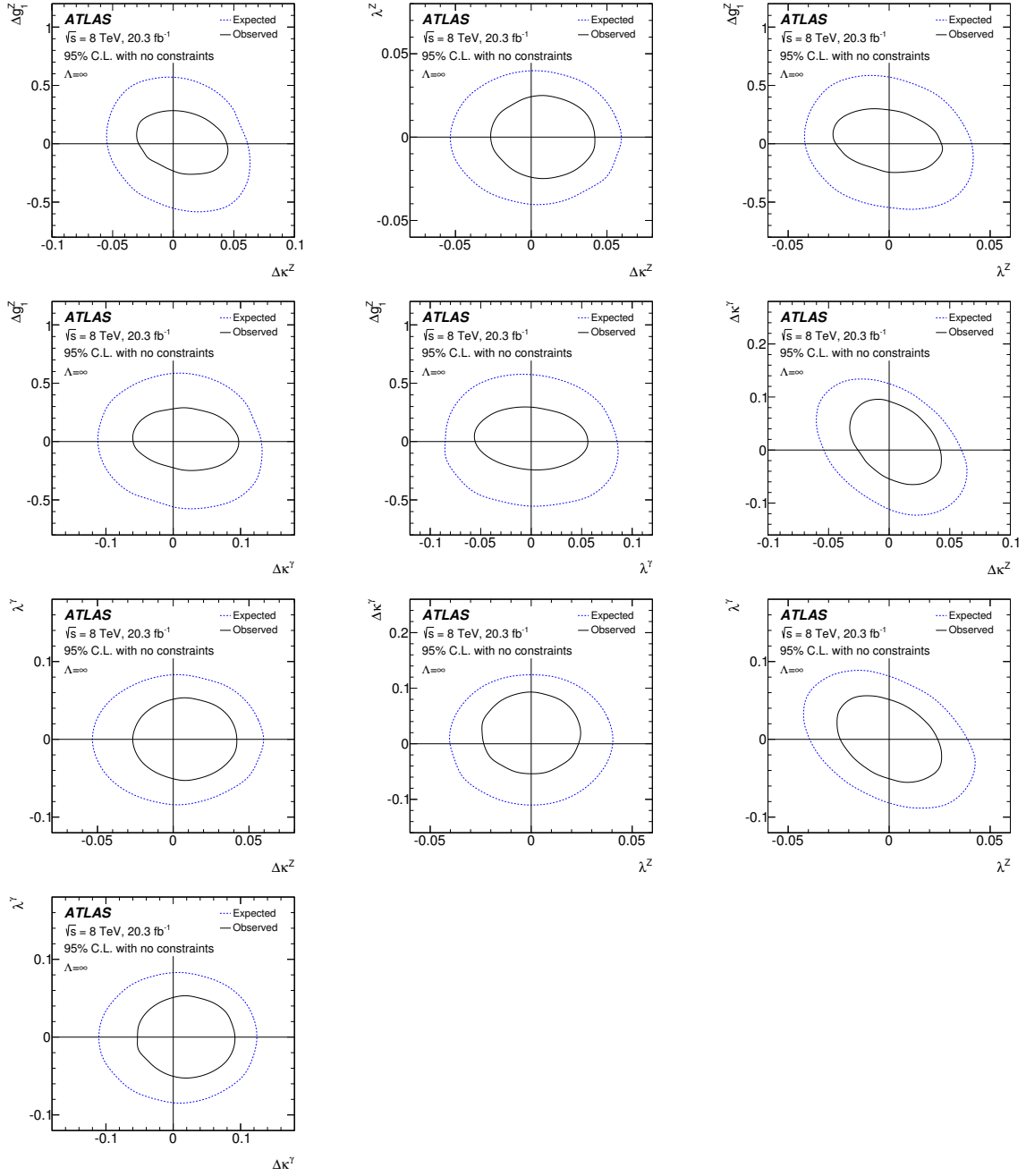
Figure 13. The expected and observed 95% confidence-level contours for limits in the plane of two simultaneously non-zero parameters in the *no constraints* scenario. Except for the two anomalous coupling parameters under study, all others are set to zero.
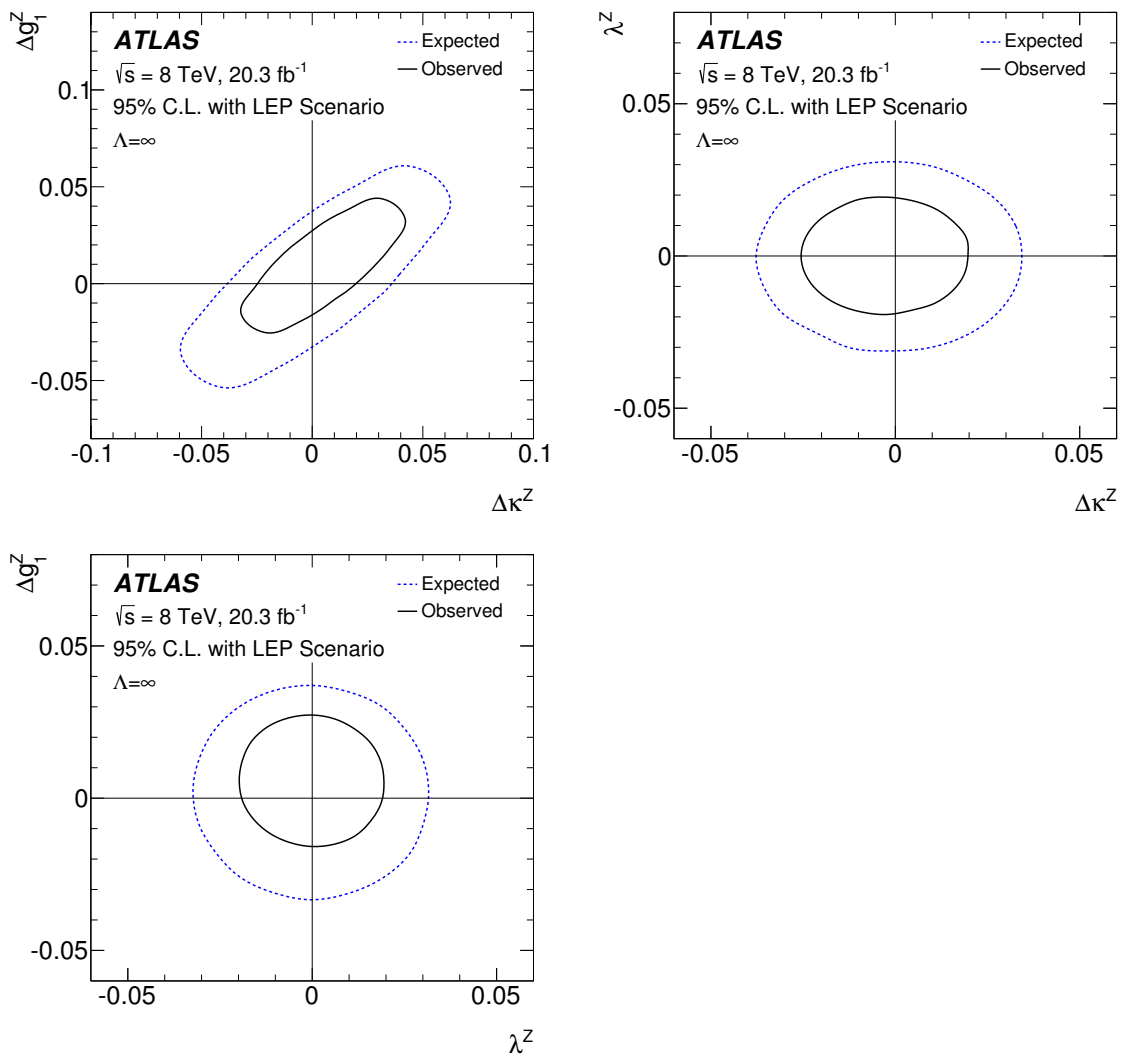
Figure 14. The expected and observed 95% confidence-level contours for limits in the plane of two simultaneously non-zero parameters in the *LEP* scenario. Except for the two anomalous coupling parameters under study, all others are set to zero.
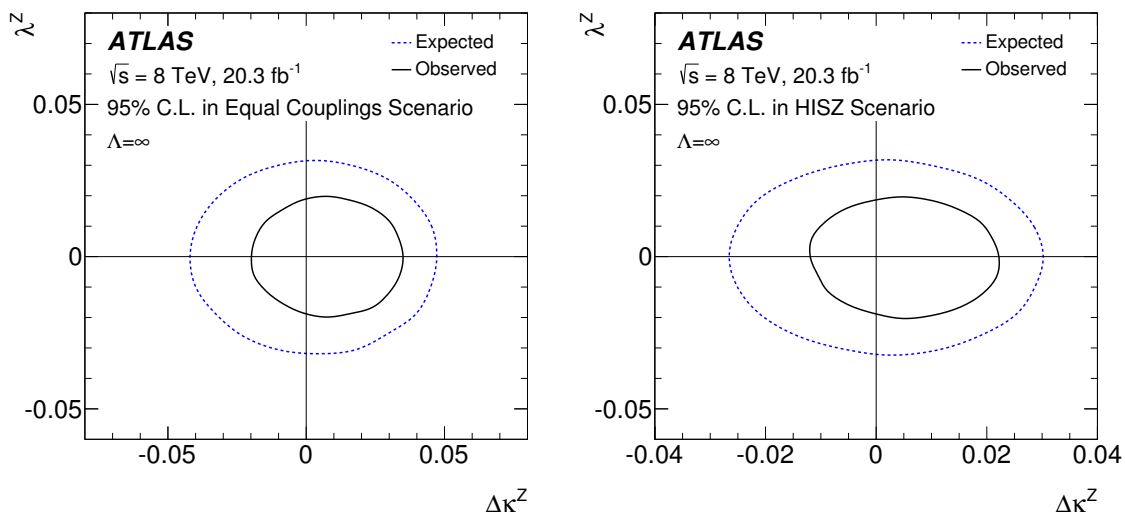
Figure 15. The expected and observed 95% confidence-level contours for limits in the plane of two simultaneously non-zero parameters in the *Equal Couplings* (left) and the *HISZ* scenario (right).
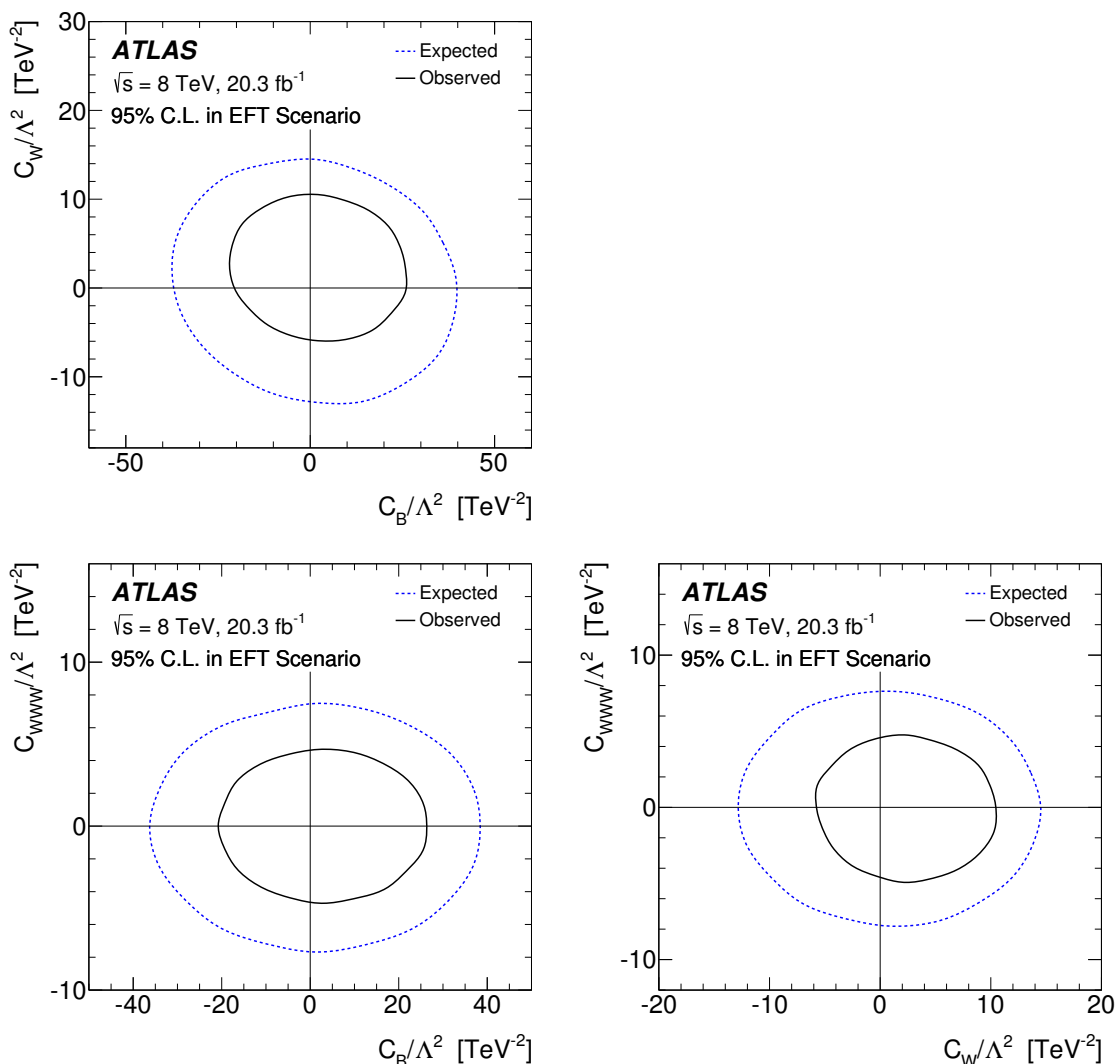
Figure 16. The expected and observed 95% confidence-level contours for limits in the plane of two simultaneously non-zero parameters in the effective field theory framework. In each case, only the two effective field theory couplings under study are allowed to differ from zero.

11 Conclusions

The WW production cross section in pp collisions at $\sqrt{s} = 8$ TeV is measured using data corresponding to an integrated luminosity of 20.3 fb^{-1} collected by the ATLAS detector at the LHC during 2012. The measurement is conducted in three dilepton final states ($e\mu$, ee and $\mu\mu$) that are all accompanied by missing transverse momentum due to the neutrinos produced in the leptonic W decays. Fiducial and total cross sections are measured and limits on anomalous triple gauge couplings are derived. The uncertainty of the fiducial cross-section measurement is dominated by systematic uncertainties due to reconstruction and background estimation, while the total cross-section uncertainty is subject to significant contributions from the modelling of the extrapolation from the fiducial to the full phase space.

The measured total WW production cross section is measured to be 71.1 ± 1.1(stat) $^{+5.7}_{-5.0}$(syst) ±1.4(lumi) pb, from the combination of the three analysed final states extrapolated to the full phase space. This is about 1.4 standard deviations higher than the NNLO prediction of 63.2 $^{+1.6}_{-1.4}$(scale) ±1.2(PDF) pb.

The fiducial cross sections for the three final states are about two standard deviations higher than the partial NLO predictions. However, the difference is reduced by taking into account higher-order effects that increase the cross-section prediction by 5–10%. The measured fiducial cross sections are found to be consistent with predictions that include both the NNLO and resummed QCD corrections up to NNLL accuracy. Differential cross sections are measured in the fiducial region using events in the $e\mu$ final state. The shapes of the measured unfolded differential cross section distributions agree with the predictions at the level of 15%, and the discrepancy is mainly caused by the overall normalization offset. Larger deviations at the 20% level are observed in the unfolded distribution of the leading lepton p_{T} for large transverse momenta. All measured cross sections are consistent within 1.5-2 standard deviations with the predictions.

The distribution of the transverse momentum of the leading lepton, $p_{\mathrm{T}}^{\mathrm{lead}}$, is used to investigate anomalous triple-gauge-boson coupling parameters. The data show no indications of anomalous couplings and are fully compatible with the SM, hence limits on these parameters are set. The derived limits are better than expected due to a deficit in data for large momenta of the leading lepton. Due to the increased integrated luminosity and the higher centre-of-mass energy, the limits reported here are more stringent than those previously published by the ATLAS Collaboration using data taken at $\sqrt{s} = 7$ TeV. They are also competitive with the results obtained at the LEP collider [8]. The limits can also be compared with the limits observed by the CMS experiment [14], which computed limits based on the dilepton invariant mass distribution $m_{\ell\ell}$, and which also reported better observed limits than expected limits. The confidence interval on C_{WWW}/Λ^2 and C_B/Λ^2 derived in this analysis are similar, or up to 20-30% more restrictive than those observed by the CMS experiment [14]. The limits derived on C_W/Λ^2 cover a complementary range around zero compared to the bounds by the CMS experiment.

Acknowledgments

A Tables of differential cross sections

A.1 Differential cross section measurements

p_T^{lead} [GeV]	25–30	30–35	35–40	40–50	50–60	60–70	70–80	80–100	100–150	150–500
	Differential cross sections									
Results [fb/GeV]	3.49	7.05	10.7	9.30	6.65	3.97	2.35	1.20	0.363	0.00867
Total Unc.	23 %	16 %	12 %	9.4%	7.6%	13 %	16 %	15 %	13 %	30 %
Stat. Unc.	12 %	7.6%	5.7%	4.0%	4.8%	6.1%	8.0%	7.9%	8.6%	24 %
Syst. Unc.	6.7%	6.3%	5.3%	5.2%	5.4%	5.6%	5.5%	6.3%	6.0%	7.9%
Bkg. Unc.	18 %	13 %	9.2%	6.8%	2.4%	9.5%	13 %	11 %	8.4%	17 %

Table 13. Unfolded cross sections measured differentially in bins of the transverse momentum of the leading lepton, p_T^{lead}, and related uncertainties. The systematic uncertainty includes uncertainties from event reconstruction and theoretical uncertainties in the signal acceptance, including the luminosity. Uncertainties in the estimated background contributions are shown separately. Systematic, background and statistical uncertainties are added in quadrature to obtain the total uncertainty in each bin. The correlation matrix for the total uncertainty is made available separately.

$p_T(\ell\ell)$ [GeV]	0–25	25–30	30–35	35–40	40–50	50–60	60–70	70–80	80–500
	Differential cross sections								
Results [fb/GeV]	1.69	5.60	6.11	6.59	6.81	6.84	4.84	3.00	0.0601
Total Unc.	29 %	13 %	14 %	14 %	10 %	11 %	9.4%	10 %	13 %
Stat. Unc.	8.9%	8.5%	7.7%	7.2%	4.6%	4.3%	5.2%	7.0%	7.4%
Syst. Unc.	6.4%	5.6%	5.8%	5.3%	5.2%	5.1%	5.6%	5.5%	7.8%
Bkg. Unc.	27 %	8.9%	11 %	10 %	7.2%	8.5%	5.5%	4.8%	7.4%

Table 14. Unfolded cross sections measured differentially in bins of the transverse momentum of the dilepton system, $p_T(\ell\ell)$, and related uncertainties. The systematic uncertainty includes uncertainties from event reconstruction and theoretical uncertainties in the signal acceptance, including the luminosity. Uncertainties in the estimated background contributions are shown separately. Systematic, background and statistical uncertainties are added in quadrature to obtain the total uncertainty in each bin. The correlation matrix for the total uncertainty is made available separately.

$m_{\ell\ell}$ [GeV]	10–20	20–30	30–40	40–50	50–60	60–70	70–85	85–100	100–115	115–135	135–155	155–175	175–210	210–650
						Differential cross sections								
Results [fb/GeV]	1.19	1.40	1.84	2.62	3.50	3.32	3.45	2.92	1.86	1.63	1.22	0.761	0.498	0.0501
Total Unc.	12 %	12 %	12 %	22 %	12 %	12 %	9.4%	8.8%	13 %	14 %	11 %	24 %	21 %	16 %
Stat. Unc.	10 %	10.0%	8.9%	7.8%	7 %	7.5%	5.5%	5.6%	7.8%	6.8%	7.6%	10 %	8.8%	7.6%
Syst. Unc.	5.8%	5.8%	5.7%	5.5%	5.6%	5.5%	5.6%	5.5%	5.8%	5.3%	5.4%	5.7%	5.6%	6.1%
Bkg. Unc.	3.7%	2.2%	5.5%	19 %	8.3%	8.1%	5.3%	3.9%	8.7%	11 %	6.5%	20 %	18 %	13 %

Table 15. Unfolded cross sections measured differentially in bins of the invariant mass of the dilepton system, $m_{\ell\ell}$, and related uncertainties. The systematic uncertainty includes uncertainties from event reconstruction and theoretical uncertainties in the signal acceptance, including the luminosity. Uncertainties in the estimated background contributions are shown separately. Systematic, background and statistical uncertainties are added in quadrature to obtain the total uncertainty in each bin. The correlation matrix for the total uncertainty is made available separately.

$\Delta\phi_{\ell\ell}$	0–$\pi/8$	$\pi/8$–$\pi/4$	$\pi/4$–$3\pi/8$	$3\pi/8$–$\pi/2$	$\pi/2$–$5\pi/8$	$5\pi/8$–$3\pi/4$	$3\pi/4$–$7\pi/8$	$7\pi/8$–π
				Differential cross sections				
Results [fb]	47.3	70.7	81.6	102	140	193	217	98.8
Total Unc.	11 %	9.0%	9.5%	15 %	9.5%	7.5%	8.0%	16 %
Stat. Unc.	8.0%	6.3%	6.1%	5.4%	4.6%	3.9%	4.0%	7.3%
Syst. Unc.	6.0%	5.5%	5.3%	5.3%	5.1%	5.4%	5.2%	5.9%
Bkg. Unc.	5.2%	3.3%	5.1%	13 %	6.5%	3.5%	4.5%	13 %

Table 16. Unfolded cross sections measured differentially in bins of the difference in azimuth angle between the decay leptons, $\Delta\phi_{\ell\ell}$, and related uncertainties. The systematic uncertainty includes uncertainties from event reconstruction and theoretical uncertainties in the signal acceptance, including the luminosity. Uncertainties in the estimated background contributions are shown separately. Systematic, background and statistical uncertainties are added in quadrature to obtain the total uncertainty in each bin. The correlation matrix for the total uncertainty is made available separately.

$|y_{\ell\ell}|$	0–0.2	0.2–0.4	0.4–0.6	0.6–0.8	0.8–1	1–1.2	1.2–1.4	1.4–1.6	1.6–1.8	1.8–2	2–2.5
					Differential cross sections						
Results [fb]	237	223	232	207	216	194	146	126	102	97.4	35.5
Total Unc.	8.9%	9.2%	8.9%	9.5%	8.3%	8.8%	16 %	14 %	19 %	11 %	25 %
Stat. Unc.	5.2%	5.8%	5.4%	5.9%	5.5%	5.7%	6.9%	7.3%	8.3%	8.4%	8.5%
Syst. Unc.	5.4%	5.5%	5.5%	5.5%	5.1%	5.3%	5.3%	5.4%	5.5%	5.6%	5.4%
Bkg. Unc.	4.8%	4.6%	4.4%	5.1%	3.4%	4.1%	14 %	11 %	16 %	5.5%	22 %

Table 17. Unfolded cross sections measured differentially in bins of the absolute value of the rapidity of the dilepton system, $|y_{\ell\ell}|$, and related uncertainties. The systematic uncertainty includes uncertainties from event reconstruction and theoretical uncertainties in the signal acceptance, including the luminosity. Uncertainties in the estimated background contributions are shown separately. Systematic, background and statistical uncertainties are added in quadrature to obtain the total uncertainty in each bin. The correlation matrix for the total uncertainty is made available separately.

$|\cos(\theta^*)|$	0–0.1	0.1–0.2	0.2–0.3	0.3–0.4	0.4–0.5	0.5–0.6	0.6–0.7	0.7–0.8	0.8–1
				Differential cross sections					
Results [fb]	460	419	470	402	371	403	405	387	211
Total Unc.	10 %	18 %	8.4%	10 %	15 %	10 %	10 %	12 %	14 %
Stat. Unc.	5.4%	5.7%	5.1%	5.8%	6.1%	5.6%	5.5%	5.4%	5.3%
Syst. Unc.	5.4%	5.3%	5.6%	5.5%	5.2%	5.5%	5.2%	5.1%	5.4%
Bkg. Unc.	6.7%	17 %	3.6%	6.0%	13 %	7.0%	6.8%	9.6%	12 %

Table 18. Unfolded cross sections measured differentially in bins of the observable $|\cos(\theta^*)|$ and related uncertainties. The systematic uncertainty includes uncertainties from event reconstruction and theoretical uncertainties in the signal acceptance, including the luminosity. Uncertainties in the estimated background contributions are shown separately. Systematic, background and statistical uncertainties are added in quadrature to obtain the total uncertainty in each bin. The correlation matrix for the total uncertainty is made available separately.

A.2 Normalised differential cross sections

p_T^{lead} [GeV]	25–30	30–35	35–40	40–50	50–60	60–70	70–80	80–100	100–150	150–500
	Normalised differential cross sections									
Results [GeV⁻¹]	0.00933	0.0188	0.0285	0.0249	0.0178	0.0106	0.00628	0.00322	0.000971	0.0000232
Total Unc.	25 %	19 %	8.3 %	5.0 %	5.1 %	8.4 %	13 %	11 %	11 %	28 %
Stat. Unc.	12 %	7.2%	5.4%	3.6%	4.5 %	5.9%	7.8%	7.7%	8.5%	24 %
Syst. Unc.	3.3%	3.2%	2.2%	0.67%	0.79%	1.3%	1.4%	1.8%	2.1%	5.0%
Bkg. Unc.	22 %	17 %	6.0%	3.4%	2.3%	6.0%	10 %	7.1%	6.6%	13 %

Table 19. Unfolded cross sections measured differentially, normalised to unity and scaled with the inverse bin width in bins of the transverse momentum of the leading lepton, p_T^{lead}, and related uncertainties. The systematic uncertainty includes uncertainties from event reconstruction and theoretical uncertainties in the signal acceptance, including the luminosity. Uncertainties in the estimated background contributions are shown separately. Systematic, background and statistical uncertainties are added in quadrature to obtain the total uncertainty in each bin. The correlation matrix for the total uncertainty is made available separately.

$p_T(\ell\ell)$ [GeV]	0–25	25–30	30–35	35–40	40–50	50–60	60–70	70–80	80–500
	Normalised differential cross sections								
Results [GeV⁻¹]	0.00453	0.0150	0.0163	0.0176	0.0182	0.0183	0.0129	0.00803	0.000161
Total Unc.	31 %	12 %	12 %	11 %	6.6 %	7.5 %	6.5 %	7.5%	9.6%
Stat. Unc.	8.2%	8.3%	7.5%	7.0%	4.2 %	4.1 %	5.0%	6.8%	7.2%
Syst. Unc.	2.9%	2.2%	2.0%	1.5%	0.85%	0.90%	1.6%	1.6%	3.6%
Bkg. Unc.	29 %	7.9%	9.3%	8.3%	5.0 %	6.2 %	3.8%	2.8%	5.2%

Table 20. Unfolded cross sections measured differentially, normalised to unity and scaled with the inverse bin width in bins of the transverse momentum of the dilepton system, $p_T(\ell\ell)$, and related uncertainties. The systematic uncertainty includes uncertainties from event reconstruction and theoretical uncertainties in the signal acceptance, including the luminosity. Uncertainties in the estimated background contributions are shown separately. Systematic, background and statistical uncertainties are added in quadrature to obtain the total uncertainty in each bin. The correlation matrix for the total uncertainty is made available separately.

Table 21. Unfolded cross sections measured differentially, normalised to unity and scaled with the inverse bin width in bins of the invariant mass of the dilepton system, $m_{\ell\ell}$, and related uncertainties. The systematic uncertainty includes uncertainties from event reconstruction and theoretical uncertainties in the signal acceptance, including the luminosity. Uncertainties in the estimated background contributions are shown separately. Systematic, background and statistical uncertainties are added in quadrature to obtain the total uncertainty in each bin. The correlation matrix for the total uncertainty is made available separately.

$m_{\ell\ell}$ [GeV]	10–20	20–30	30–40	40–50	50–60	60–70	70–85	85–100	100–115	115–135	135–155	155–175	175–210	210–650
	Normalised differential cross sections													
Results [GeV^{-1}]	0.00319	0.00374	0.00493	0.00702	0.00935	0.00889	0.00923	0.00781	0.00497	0.00435	0.00327	0.00203	0.00133	0.000134
Total Unc.	10 %	11 %	9.0%	18 %	8.1%	8.5%	5.5 %	5.7%	11 %	9.9%	9.1%	23 %	24 %	19 %
Stat. Unc.	10 %	9.8%	8.7%	7.6%	6.7%	7.1%	5.2 %	5.3%	7.6%	6.5%	7.4%	10 %	8.7%	7.5%
Syst. Unc.	2.0%	1.7%	1.4%	1.1%	1.5%	2.1%	0.94%	1.8%	2.6%	1 %	2.1%	1.8%	1.3%	1.6%
Bkg. Unc.	2.1%	5.3%	1.7%	16 %	4.2%	4.0%	1.6 %	1 %	7.2%	7.4%	4.9%	20 %	22 %	17 %

Table 22. Unfolded cross sections measured differentially, normalised to unity and scaled with the inverse bin width in bins of the difference in azimuth angle between the decay leptons, $\Delta\phi_{\ell\ell}$, and related uncertainties. The systematic uncertainty includes uncertainties from event reconstruction and theoretical uncertainties in the signal acceptance, including the luminosity. Uncertainties in the estimated background contributions are shown separately. Systematic, background and statistical uncertainties are added in quadrature to obtain the total uncertainty in each bin. The correlation matrix for the total uncertainty is made available separately.

$\Delta\phi_{\ell\ell}$	0–$\pi/8$	$\pi/8$–$\pi/4$	$\pi/4$–$3\pi/8$	$3\pi/8$–$\pi/2$	$\pi/2$–$5\pi/8$	$5\pi/8$–$3\pi/4$	$3\pi/4$–$7\pi/8$	$7\pi/8$–π
	Normalised differential cross sections							
Results	0.127	0.189	0.219	0.273	0.376	0.516	0.582	0.265
Total Unc.	8.0%	6.8%	11 %	9.9 %	4.9 %	4.1 %	3.9 %	12 %
Stat. Unc.	7.8%	6.1%	5.9 %	5.1 %	4.3 %	3.5 %	3.5 %	6.8%
Syst. Unc.	1.4%	1.1%	0.97%	0.77%	0.58%	0.60%	0.84%	1.6%
Bkg. Unc.	1.1%	2.7%	9.5 %	8.4 %	2.3 %	2.2 %	1.7 %	9.7%

$|y_{\ell\ell}|$	0–0.2	0.2–0.4	0.4–0.6	0.6–0.8	0.8–1	1–1.2	1.2–1.4	1.4–1.6	1.6–1.8	1.8–2	2–2.5
					Normalised differential cross sections						
Results	0.635	0.596	0.622	0.554	0.578	0.518	0.390	0.338	0.272	0.261	0.0950
Total Unc.	9.3 %	5.8 %	9.2 %	6.2 %	5.5 %	5.5 %	13 %	10 %	15 %	9.3%	21 %
Stat. Unc.	4.9 %	5.4 %	5.1 %	5.5 %	5.2 %	5.4 %	6.7 %	7.1 %	8.1 %	8.2%	8.4%
Syst. Unc.	0.73%	1.0 %	0.76%	0.83%	0.69%	0.68%	0.84%	0.95%	1.0 %	1.2%	1.4%
Bkg. Unc.	7.9 %	1.9 %	7.6 %	2.7 %	1.6 %	1.1 %	11 %	7.5 %	13 %	4.2%	19 %

Table 23. Unfolded cross sections measured differentially, normalised to unity and scaled with the inverse bin width in bins of the rapidity of the dilepton system, $|y_{\ell\ell}|$, and related uncertainties. The systematic uncertainty includes uncertainties from event reconstruction and theoretical uncertainties in the signal acceptance, including the luminosity. Uncertainties in the estimated background contributions are shown separately. Systematic, background and statistical uncertainties are added in quadrature to obtain the total uncertainty in each bin. The correlation matrix for the total uncertainty is made available separately.

$|\cos(\theta^*)|$	0–0.1	0.1–0.2	0.2–0.3	0.3–0.4	0.4–0.5	0.5–0.6	0.6–0.7	0.7–0.8	0.8–1
				Normalised differential cross sections					
Results	1.24	1.12	1.25	1.08	0.993	1.07	1.08	1.03	0.565
Total Unc.	6.0 %	14 %	5.1 %	5.9 %	11 %	6.1 %	6.9 %	14 %	17 %
Stat. Unc.	5.1 %	5.3 %	4.8 %	5.4 %	5.7 %	5.4 %	5.3 %	5.2 %	5.0 %
Syst. Unc.	0.72%	0.49%	0.70%	0.75%	0.66%	0.72%	0.87%	0.71%	0.83%
Bkg. Unc.	2.9 %	13 %	1.8 %	2.2 %	9.1 %	2.9 %	4.4 %	13 %	17 %

Table 24. Unfolded cross sections measured differentially, normalised to unity and scaled with the inverse bin width in bins of the observable, $|\cos(\theta^*)|$, and related uncertainties. The systematic uncertainty includes uncertainties from event reconstruction and theoretical uncertainties in the signal acceptance, including the luminosity. Uncertainties in the estimated background contributions are shown separately. Systematic, background and statistical uncertainties are added in quadrature to obtain the total uncertainty in each bin. The correlation matrix for the total uncertainty is made available separately.

A.3 Bin-to-bin correlation matrices for the differential measurements

$p_{\mathrm{T}}^{\mathrm{lead}}$ [GeV]	25–30	30–35	35–40	40–50	50–60	60–70	70–80	80–100	100–150	150–500
25– 30	1	0.13	0.091	0.14	0.20	0.11	0.094	0.13	0.12	0.092
30– 35	0.13	1	0.060	0.17	0.24	0.12	0.091	0.14	0.15	0.078
35– 40	0.091	0.060	1	0.22	0.32	0.20	0.15	0.19	0.22	0.088
40– 50	0.14	0.17	0.22	1	0.39	0.27	0.22	0.28	0.30	0.15
50– 60	0.20	0.24	0.32	0.39	1	0.33	0.28	0.39	0.43	0.21
60– 70	0.11	0.12	0.20	0.27	0.33	1	0.16	0.25	0.29	0.17
70– 80	0.094	0.091	0.15	0.22	0.28	0.16	1	0.19	0.25	0.14
80–100	0.13	0.14	0.19	0.28	0.39	0.25	0.19	1	0.33	0.21
100–150	0.12	0.15	0.22	0.30	0.43	0.29	0.25	0.33	1	0.21
150–500	0.092	0.078	0.088	0.15	0.21	0.17	0.14	0.21	0.21	1

Table 25. Correlation matrix for the total uncertainties for the unnormalised unfolded distribution of the leading lepton p_{T}, including all sources of systematic and statistical uncertainties.

$p_{\mathrm{T}}(\ell\ell)$ [GeV]	0–25	25–30	30–35	35–40	40–50	50–60	60–70	70–80	80–500
0– 25	1	0.084	0.082	0.085	0.12	0.10	0.13	0.12	0.14
25– 30	0.084	1	0.14	0.16	0.24	0.20	0.23	0.23	0.24
30– 35	0.082	0.14	1	0.13	0.24	0.21	0.24	0.22	0.24
35– 40	0.086	0.16	0.13	1	0.19	0.20	0.23	0.22	0.22
40– 50	0.12	0.24	0.24	0.19	1	0.26	0.34	0.33	0.37
50– 60	0.10	0.20	0.21	0.20	0.26	1	0.29	0.29	0.35
60– 70	0.13	0.22	0.24	0.22	0.34	0.28	1	0.33	0.45
70– 80	0.12	0.23	0.22	0.22	0.33	0.29	0.34	1	0.43
80–500	0.14	0.24	0.25	0.22	0.38	0.35	0.46	0.43	1

Table 26. Correlation matrix for the total uncertainties for the unnormalised unfolded $p_{\mathrm{T}}(\ell\ell)$ distribution, including all sources of systematic and statistical uncertainties.

$m_{\ell\ell}$ [GeV]	10 −20	20 −30	30 −40	40 −50	50 −60	60 −70	70 −85	85 −100	100 −115	115 −135	135 −155	155 −175	175 −210	210 −650
10– 20	1	0.19	0.23	0.12	0.23	0.19	0.26	0.32	0.15	0.18	0.24	0.10	0.14	0.17
20– 30	0.19	1	0.20	0.13	0.23	0.21	0.33	0.33	0.23	0.20	0.24	0.13	0.15	0.20
30– 40	0.23	0.20	1	0.11	0.25	0.23	0.31	0.31	0.23	0.19	0.24	0.13	0.12	0.17
40– 50	0.12	0.13	0.10	1	0.10	0.13	0.17	0.18	0.13	0.11	0.13	0.071	0.081	0.093
50– 60	0.22	0.23	0.25	0.10	1	0.19	0.31	0.33	0.22	0.20	0.24	0.12	0.15	0.17
60– 70	0.17	0.19	0.22	0.13	0.18	1	0.27	0.26	0.26	0.20	0.21	0.13	0.13	0.16
70– 85	0.26	0.33	0.31	0.17	0.31	0.27	1	0.38	0.31	0.26	0.31	0.15	0.18	0.22
85–100	0.30	0.31	0.30	0.18	0.32	0.26	0.38	1	0.23	0.25	0.34	0.16	0.20	0.25
100–115	0.13	0.20	0.22	0.13	0.21	0.26	0.30	0.22	1	0.18	0.18	0.12	0.14	0.16
115–135	0.18	0.20	0.19	0.11	0.20	0.20	0.26	0.26	0.18	1	0.17	0.13	0.13	0.17
135–155	0.23	0.23	0.23	0.13	0.24	0.22	0.31	0.35	0.19	0.17	1	0.085	0.16	0.19
155–175	0.10	0.13	0.13	0.071	0.12	0.13	0.15	0.17	0.12	0.13	0.085	1	0.070	0.10
175–210	0.14	0.15	0.12	0.082	0.15	0.14	0.19	0.20	0.15	0.13	0.16	0.070	1	0.12
210–650	0.17	0.20	0.17	0.093	0.17	0.16	0.22	0.25	0.17	0.16	0.19	0.10	0.12	1

Table 27. Correlation matrix for the total uncertainties for the unnormalised unfolded $m_{\ell\ell}$ distribution, including all sources of systematic and statistical uncertainties.

$\Delta\phi_{\ell\ell}$	$0–\pi/8$	$\pi/8–\pi/4$	$\pi/4–3\pi/8$	$3\pi/8–\pi/2$	$\pi/2–5\pi/8$	$5\pi/8–3\pi/4$	$3\pi/4–7\pi/8$	$7\pi/8–\pi$
$0–\ \pi/8$	1	0.35	0.34	0.23	0.33	0.43	0.38	0.24
$\pi/8–\ \pi/4$	0.35	1	0.38	0.25	0.36	0.48	0.42	0.25
$\pi/4–3\pi/8$	0.34	0.38	1	0.23	0.32	0.45	0.40	0.22
$3\pi/8–\ \pi/2$	0.23	0.25	0.23	1	0.22	0.30	0.28	0.16
$\pi/2–5\pi/8$	0.33	0.36	0.32	0.22	1	0.45	0.43	0.24
$5\pi/8–3\pi/4$	0.43	0.47	0.45	0.30	0.45	1	0.57	0.33
$3\pi/4–7\pi/8$	0.38	0.42	0.40	0.28	0.43	0.57	1	0.32
$7\pi/8–\ \pi$	0.24	0.25	0.22	0.16	0.24	0.33	0.32	1

Table 28. Correlation matrix for the total uncertainties for the unnormalised unfolded $\Delta\phi_{\ell\ell}$ distribution, including all sources of systematic and statistical uncertainties.

$|y_{\ell\ell}|$	0–0.2	0.2–0.4	0.4–0.6	0.6–0.8	0.8–1	1–1.2	1.2–1.4	1.4–1.6	1.6–1.8	1.8–2	2–2.5
0 –0.2	1	0.46	0.49	0.46	0.46	0.44	0.22	0.26	0.21	0.35	0.15
0.2–0.4	0.46	1	0.44	0.48	0.44	0.43	0.24	0.25	0.22	0.34	0.14
0.4–0.6	0.49	0.44	1	0.43	0.45	0.44	0.23	0.25	0.21	0.34	0.14
0.6–0.8	0.46	0.48	0.43	1	0.42	0.42	0.22	0.26	0.20	0.33	0.14
0.8–1.0	0.46	0.45	0.45	0.42	1	0.41	0.23	0.26	0.21	0.34	0.14
1.0–1.2	0.44	0.43	0.44	0.42	0.41	1	0.20	0.25	0.22	0.33	0.14
1.2–1.4	0.22	0.24	0.23	0.22	0.23	0.20	1	0.13	0.11	0.18	0.075
1.4–1.6	0.26	0.25	0.25	0.26	0.26	0.25	0.13	1	0.12	0.19	0.098
1.6–1.8	0.21	0.22	0.21	0.20	0.21	0.22	0.11	0.12	1	0.16	0.081
1.8–2.0	0.35	0.35	0.34	0.34	0.34	0.33	0.19	0.19	0.16	1	0.13
2.0–2.5	0.15	0.14	0.14	0.14	0.14	0.14	0.075	0.098	0.081	0.13	1

Table 29. Correlation matrix for the total uncertainties for the unnormalised unfolded $|y_{\ell\ell}|$ distribution, including all sources of systematic and statistical uncertainties.

$|\cos(\theta^*)|$	0–0.1	0.1–0.2	0.2–0.3	0.3–0.4	0.4–0.5	0.5–0.6	0.6–0.7	0.7–0.8	0.8–1
0 –0.1	1	0.20	0.44	0.36	0.23	0.33	0.33	0.26	0.22
0.1–0.2	0.20	1	0.24	0.21	0.14	0.19	0.18	0.14	0.12
0.2–0.3	0.44	0.24	1	0.44	0.29	0.42	0.40	0.32	0.29
0.3–0.4	0.36	0.21	0.44	1	0.25	0.34	0.33	0.28	0.23
0.4–0.5	0.23	0.14	0.29	0.25	1	0.23	0.21	0.18	0.15
0.5–0.6	0.33	0.19	0.42	0.34	0.23	1	0.32	0.26	0.22
0.6–0.7	0.33	0.18	0.40	0.33	0.21	0.32	1	0.25	0.21
0.7–0.8	0.26	0.14	0.32	0.28	0.18	0.26	0.25	1	0.17
0.8–1.0	0.22	0.12	0.29	0.23	0.15	0.22	0.21	0.17	1

Table 30. Correlation matrix for the total uncertainties for the unnormalised unfolded $|\cos(\theta^*)|$ distribution, including all sources of systematic and statistical uncertainties.

A.4 Bin-to-bin correlation matrices for the normalised differential measurements

$p_\mathrm{T}^\mathrm{lead}$ [GeV]	25–30	30–35	35–40	40–50	50–60	60–70	70–80	80–100	100–150	150–500
25– 30	1	0.74	−0.66	−0.59	0.35	−0.63	−0.47	−0.54	0.12	−0.25
30– 35	0.74	1	−0.71	−0.60	0.35	−0.65	−0.49	−0.57	0.11	−0.29
35– 40	−0.66	−0.71	1	0.35	−0.39	0.45	0.31	0.33	−0.23	0.16
40– 50	−0.59	−0.60	0.35	1	−0.50	0.39	0.14	0.22	−0.18	0.15
50– 60	0.35	0.35	−0.39	−0.50	1	−0.45	−0.21	−0.30	−0.049	−0.22
60– 70	−0.63	−0.65	0.45	0.39	−0.45	1	0.19	0.34	−0.080	0.27
70– 80	−0.47	−0.49	0.31	0.14	−0.21	0.19	1	0.35	−0.26	0.020
80–100	−0.54	−0.57	0.33	0.22	−0.30	0.34	0.35	1	−0.12	0.21
100–150	0.12	0.11	−0.23	−0.18	−0.049	−0.080	−0.26	−0.12	1	0.087
150–500	−0.26	−0.30	0.17	0.15	−0.22	0.27	0.020	0.21	0.087	1

Table 31. Correlation matrix for the total uncertainties for the normalised unfolded leading lepton p_T distribution, including all sources of systematic and statistical uncertainties.

$p_\mathrm{T}(\ell\ell)$ [GeV]	0–25	25–30	30–35	35–40	40–50	50–60	60–70	70–80	80–500
0– 25	1	−0.20	−0.42	−0.72	−0.63	−0.82	−0.23	−0.078	0.016
25– 30	−0.20	1	0.41	0.12	−0.19	0.12	−0.37	−0.26	−0.21
30– 35	−0.42	0.41	1	0.25	−0.048	0.35	−0.31	−0.25	−0.16
35– 40	−0.72	0.12	0.25	1	0.37	0.60	0.096	−0.0072	−0.15
40– 50	−0.63	−0.19	−0.048	0.37	1	0.43	0.30	0.12	−0.050
50– 60	−0.82	0.12	0.35	0.60	0.43	1	0.072	−0.030	−0.11
60– 70	−0.23	−0.37	−0.31	0.096	0.30	0.072	1	0.080	0.048
70– 80	−0.078	−0.26	−0.25	−0.0072	0.12	−0.030	0.080	1	−0.021
80–500	0.016	−0.21	−0.16	−0.15	−0.050	−0.11	0.048	−0.021	1

Table 32. Correlation matrix for the total uncertainties for the normalised unfolded $p_\mathrm{T}(\ell\ell)$ distribution, including all sources of systematic and statistical uncertainties.

$m_{\ell\ell}$ [GeV]	10	20	30	40	50	60	70	85	100	115	135	155	175	210
	−20	−30	−40	−50	−60	−70	−85	−100	−115	−135	−155	−175	−210	−650
10– 20	1	−0.025	−0.011	−0.074	−0.069	−0.093	−0.10	0.0042	−0.13	−0.052	−0.041	0.016	0.063	0.049
20– 30	−0.025	1	−0.15	−0.43	−0.28	−0.27	−0.060	0.042	0.018	−0.32	0.021	−0.026	0.39	0.40
30– 40	−0.011	−0.15	1	0.063	0.065	0.0067	−0.048	−0.059	−0.013	0.0089	−0.00094	−0.075	−0.17	−0.14
40– 50	−0.074	−0.43	0.063	1	0.37	0.37	0.039	−0.14	−0.079	0.49	−0.078	−0.053	−0.80	−0.79
50– 60	−0.069	−0.28	0.065	0.37	1	0.11	−0.012	−0.16	0.014	0.18	−0.046	−0.15	−0.49	−0.46
60– 70	−0.093	−0.27	0.0067	0.37	0.11	1	−0.094	−0.17	0.048	0.14	0.020	−0.18	−0.44	−0.41
70– 85	−0.10	−0.060	−0.049	0.039	−0.012	−0.094	1	−0.20	0.067	−0.11	0.046	−0.22	−0.15	−0.11
85–100	0.0042	0.042	−0.059	−0.14	−0.16	−0.17	−0.20	1	−0.10	−0.20	−0.0095	−0.060	0.098	0.12
100–115	−0.13	0.018	−0.013	−0.079	0.014	0.048	0.067	−0.10	1	−0.41	0.30	−0.59	−0.054	0.12
115–135	−0.052	−0.32	0.0089	0.49	0.18	0.14	−0.11	−0.20	−0.41	1	−0.39	0.38	−0.45	−0.58
135–155	−0.041	0.021	−0.00094	−0.078	−0.046	0.020	0.046	−0.0095	0.30	−0.39	1	−0.52	−0.034	0.12
155–175	0.016	−0.026	−0.075	−0.053	−0.15	−0.18	−0.22	−0.060	−0.59	0.38	−0.52	1	0.15	−0.088
175–210	0.063	0.39	−0.17	−0.80	−0.49	−0.44	−0.15	0.098	−0.054	−0.45	−0.034	0.15	1	0.75
210–650	0.049	0.40	−0.14	−0.79	−0.46	−0.41	−0.11	0.12	0.12	−0.58	0.12	−0.088	0.75	1

Table 33. Correlation matrix for the total uncertainties for the normalised unfolded $m_{\ell\ell}$ distribution, including all sources of systematic and statistical uncertainties.

$\Delta\phi_{\ell\ell}$	0–$\pi/8$	$\pi/8$–$\pi/4$	$\pi/4$–$3\pi/8$	$3\pi/8$–$\pi/2$	$\pi/2$–$5\pi/8$	$5\pi/8$–$3\pi/4$	$3\pi/4$–$7\pi/8$	$7\pi/8$–π
0– $\pi/8$	1	−0.071	−0.052	0.024	−0.034	−0.11	−0.16	−0.055
$\pi/8$– $\pi/4$	−0.071	1	0.24	−0.27	−0.13	0.065	−0.076	−0.25
$\pi/4$–$3\pi/8$	−0.052	0.24	1	−0.70	−0.32	0.36	0.14	−0.41
$3\pi/8$– $\pi/2$	0.024	−0.27	−0.70	1	0.23	−0.45	−0.27	0.16
$\pi/2$–$5\pi/8$	−0.034	−0.13	−0.32	0.23	1	−0.24	−0.13	−0.21
$5\pi/8$–$3\pi/4$	−0.11	0.065	0.36	−0.45	−0.24	1	−0.0077	−0.41
$3\pi/4$–$7\pi/8$	−0.16	−0.076	0.14	−0.27	−0.13	−0.0077	1	−0.42
$7\pi/8$– π	−0.055	−0.25	−0.41	0.16	−0.21	−0.41	−0.42	1

Table 34. Correlation matrix for the total uncertainties for the normalised unfolded $\Delta\phi_{\ell\ell}$ distribution, including all sources of systematic and statistical uncertainties.

$|y_{\ell\ell}|$	0–0.2	0.2–0.4	0.4–0.6	0.6–0.8	0.8–1	1–1.2	1.2–1.4	1.4–1.6	1.6–1.8	1.8–2	2–2.5
0 –0.2	1	0.037	0.62	0.027	0.14	0.0066	−0.39	−0.60	−0.58	0.088	−0.75
0.2–0.4	0.037	1	0.087	0.069	−0.070	−0.078	−0.28	−0.13	−0.26	−0.12	−0.13
0.4–0.6	0.62	0.087	1	0.11	0.14	0.038	−0.57	−0.47	−0.69	0.00076	−0.61
0.6–0.8	0.027	0.069	0.11	1	−0.094	−0.063	−0.38	−0.026	−0.33	−0.16	−0.033
0.8–1.0	0.14	−0.070	0.14	−0.094	1	−0.11	−0.19	−0.19	−0.25	−0.055	−0.23
1.0–1.2	0.0066	−0.078	0.038	−0.063	−0.11	1	−0.20	−0.066	−0.13	−0.086	−0.064
1.2–1.4	−0.39	−0.28	−0.57	−0.38	−0.19	−0.20	1	0.054	0.64	0.089	0.17
1.4–1.6	−0.60	−0.13	−0.47	−0.026	−0.19	−0.066	0.054	1	0.28	−0.23	0.63
1.6–1.8	−0.58	−0.26	−0.69	−0.33	−0.25	−0.13	0.64	0.28	1	−0.028	0.44
1.8–2.0	0.088	−0.12	0.00076	−0.16	−0.055	−0.086	0.089	−0.23	−0.028	1	−0.22
2.0–2.5	−0.75	−0.13	−0.61	−0.033	−0.23	−0.064	0.17	0.63	0.44	−0.22	1

Table 35. Correlation matrix for the total uncertainties for the normalised unfolded $|y_{\ell\ell}|$ distribution, including all sources of systematic and statistical uncertainties.

$|\cos(\theta^*)|$	0–0.1	0.1–0.2	0.2–0.3	0.3–0.4	0.4–0.5	0.5–0.6	0.6–0.7	0.7–0.8	0.8–1
0 –0.1	1	0.30	−0.25	0.047	0.27	0.065	−0.25	−0.47	−0.29
0.1–0.2	0.30	1	−0.35	0.23	0.74	0.38	0.0026	−0.79	−0.83
0.2–0.3	−0.25	−0.35	1	−0.27	−0.34	−0.26	−0.023	0.27	0.22
0.3–0.4	0.047	0.23	−0.27	1	0.20	0.014	−0.23	−0.35	−0.21
0.4–0.5	0.27	0.74	−0.34	0.20	1	0.33	−0.071	−0.75	−0.74
0.5–0.6	0.065	0.38	−0.26	0.014	0.33	1	−0.076	−0.44	−0.43
0.6–0.7	−0.25	0.0026	−0.023	−0.23	−0.071	−0.076	1	0.17	−0.26
0.7–0.8	−0.47	−0.79	0.27	−0.35	−0.75	−0.44	0.17	1	0.61
0.8–1.0	−0.29	−0.83	0.22	−0.21	−0.74	−0.43	−0.26	0.61	1

Table 36. Correlation matrix for the total uncertainties for the normalised unfolded $|\cos(\theta^*)|$ distribution, including all sources of systematic and statistical uncertainties.

References

[1] M. Baak et al., *Working group report: precision study of electroweak interactions*, in *Community Summer Study* 2013*: Snowmass on the Mississippi (CSS*2013*)*, Minneapolis MN U.S.A. July 29–August 6 2013 [`arXiv:1310.6708`] [InSPIRE].

[2] K. Hagiwara, S. Ishihara, R. Szalapski and D. Zeppenfeld, *Low-energy effects of new interactions in the electroweak boson sector*, *Phys. Rev.* **D 48** (1993) 2182 [InSPIRE].

[3] T. Gehrmann et al., *W^+W^- production at hadron colliders in next to next to leading order QCD*, *Phys. Rev. Lett.* **113** (2014) 212001 [`arXiv:1408.5243`] [InSPIRE].

[4] M. Grazzini, S. Kallweit, D. Rathlev and M. Wiesemann, *Transverse-momentum resummation for vector-boson pair production at NNLL+NNLO*, *JHEP* **08** (2015) 154 [`arXiv:1507.02565`] [InSPIRE].

[5] P. Meade, H. Ramani and M. Zeng, *Transverse momentum resummation effects in W^+W^- measurements*, *Phys. Rev.* **D 90** (2014) 114006 [`arXiv:1407.4481`] [InSPIRE].

[6] P. Jaiswal and T. Okui, *Explanation of the WW excess at the LHC by jet-veto resummation*, *Phys. Rev.* **D 90** (2014) 073009 [`arXiv:1407.4537`] [InSPIRE].

[7] P.F. Monni and G. Zanderighi, *On the excess in the inclusive $W^+W^- \to \ell^+\ell^-\nu\bar{\nu}$ cross section*, *JHEP* **05** (2015) 013 [`arXiv:1410.4745`] [InSPIRE].

[8] DELPHI, OPAL, LEP Electroweak, ALEPH and L3 collaborations, S. Schael et al., *Electroweak measurements in electron-positron collisions at W-boson-pair energies at LEP*, *Phys. Rept.* **532** (2013) 119 [`arXiv:1302.3415`] [InSPIRE].

[9] CDF collaboration, F. Abe et al., *Observation of W^+W^- production in $\bar{p}p$ collisions at $\sqrt{s} = 1.8\,TeV$*, *Phys. Rev. Lett.* **78** (1997) 4536 [InSPIRE].

[10] CDF collaboration, T. Aaltonen et al., *Measurement of the W^+W^- production cross section and search for anomalous $WW\gamma$ and WWZ couplings in $p\bar{p}$ collisions at $\sqrt{s} = 1.96$ TeV*, *Phys. Rev. Lett.* **104** (2010) 201801 [arXiv:0912.4500] [INSPIRE].

[11] D0 collaboration, V.M. Abazov et al., *Measurement of the WW production cross section with dilepton final states in $p\bar{p}$ collisions at $\sqrt{s} = 1.96$ TeV and limits on anomalous trilinear gauge couplings*, *Phys. Rev. Lett.* **103** (2009) 191801 [arXiv:0904.0673] [INSPIRE].

[12] ATLAS collaboration, *Measurement of W^+W^- production in pp collisions at $\sqrt{s} = 7$ TeV with the ATLAS detector and limits on anomalous WWZ and $WW\gamma$ couplings*, *Phys. Rev.* **D 87** (2013) 112001 [*Erratum ibid.* **D 88** (2013) 079906] [arXiv:1210.2979] [INSPIRE].

[13] CMS collaboration, *Measurement of the W^+W^- cross section in pp collisions at $\sqrt{s} = 7$ TeV and limits on anomalous $WW\gamma$ and WWZ couplings*, *Eur. Phys. J.* **C 73** (2013) 2610 [arXiv:1306.1126] [INSPIRE].

[14] CMS collaboration, *Measurement of the W^+W^- cross section in pp collisions at $\sqrt{s} = 8$ TeV and limits on anomalous gauge couplings*, *Eur. Phys. J.* **C 76** (2016) 401 [arXiv:1507.03268] [INSPIRE].

[15] J.S. Kim, K. Rolbiecki, K. Sakurai and J. Tattersall, *'Stop' that ambulance! New physics at the LHC?*, *JHEP* **12** (2014) 010 [arXiv:1406.0858] [INSPIRE].

[16] ATLAS collaboration, *The ATLAS experiment at the CERN Large Hadron Collider*, 2008 *JINST* **3** S08003 [INSPIRE].

[17] ATLAS collaboration, *Luminosity determination in pp collisions at $\sqrt{s} = 8$ TeV using the ATLAS detector at the LHC*, arXiv:1608.03953 [INSPIRE].

[18] T. Sjöstrand, S. Mrenna and P.Z. Skands, *A brief introduction to PYTHIA 8.1*, *Comput. Phys. Commun.* **178** (2008) 852 [arXiv:0710.3820] [INSPIRE].

[19] ATLAS collaboration, *The ATLAS simulation infrastructure*, *Eur. Phys. J.* **C 70** (2010) 823 [arXiv:1005.4568] [INSPIRE].

[20] GEANT4 collaboration, S. Agostinelli et al., *GEANT4: a simulation toolkit*, *Nucl. Instrum. Meth.* **A 506** (2003) 250 [INSPIRE].

[21] P. Nason, *A new method for combining NLO QCD with shower Monte Carlo algorithms*, *JHEP* **11** (2004) 040 [hep-ph/0409146] [INSPIRE].

[22] S. Frixione, P. Nason and C. Oleari, *Matching NLO QCD computations with parton shower simulations: the POWHEG method*, *JHEP* **11** (2007) 070 [arXiv:0709.2092] [INSPIRE].

[23] S. Alioli, P. Nason, C. Oleari and E. Re, *A general framework for implementing NLO calculations in shower Monte Carlo programs: the POWHEG BOX*, *JHEP* **06** (2010) 043 [arXiv:1002.2581] [INSPIRE].

[24] S. Alioli, P. Nason, C. Oleari and E. Re, *NLO vector-boson production matched with shower in POWHEG*, *JHEP* **07** (2008) 060 [arXiv:0805.4802] [INSPIRE].

[25] T. Binoth, M. Ciccolini, N. Kauer and M. Krämer, *Gluon-induced W-boson pair production at the LHC*, *JHEP* **12** (2006) 046 [hep-ph/0611170] [INSPIRE].

[26] G. Corcella et al., *HERWIG 6: an event generator for hadron emission reactions with interfering gluons (including supersymmetric processes)*, *JHEP* **01** (2001) 010 [hep-ph/0011363] [INSPIRE].

[27] J.M. Butterworth, J.R. Forshaw and M.H. Seymour, *Multiparton interactions in photoproduction at HERA*, *Z. Phys.* **C 72** (1996) 637 [hep-ph/9601371] [INSPIRE].

[28] H.-L. Lai et al., *New parton distributions for collider physics*, *Phys. Rev.* **D 82** (2010) 074024 [arXiv:1007.2241] [INSPIRE].

[29] P. Golonka and Z. Was, *PHOTOS Monte Carlo: a precision tool for QED corrections in Z and W decays*, *Eur. Phys. J.* **C 45** (2006) 97 [hep-ph/0506026] [INSPIRE].

[30] ATLAS collaboration, *Summary of ATLAS PYTHIA 8 tunes*, ATL-PHYS-PUB-2012-003, CERN, Geneva Switzerland (2012).

[31] ATLAS collaboration, *New ATLAS event generator tunes to* 2010 *data*, ATL-PHYS-PUB-2011-008, CERN, Geneva Switzerland (2011).

[32] A. Bierweiler, T. Kasprzik, J.H. Kühn and S. Uccirati, *Electroweak corrections to W-boson pair production at the LHC*, *JHEP* **11** (2012) 093 [arXiv:1208.3147] [INSPIRE].

[33] M. Billóni, S. Dittmaier, B. Jäger and C. Speckner, *Next-to-leading order electroweak corrections to $pp \to W^+W^- \to 4$ leptons at the LHC in double-pole approximation*, *JHEP* **12** (2013) 043 [arXiv:1310.1564] [INSPIRE].

[34] J. Baglio, L.D. Ninh and M.M. Weber, *Massive gauge boson pair production at the LHC: a next-to-leading order story*, *Phys. Rev.* **D 88** (2013) 113005 [arXiv:1307.4331] [INSPIRE].

[35] A. Bierweiler, T. Kasprzik and J.H. Kühn, *Vector-boson pair production at the LHC to $\mathcal{O}(\alpha^3)$ accuracy*, *JHEP* **12** (2013) 071 [arXiv:1305.5402] [INSPIRE].

[36] S. Gieseke, T. Kasprzik and J.H. Kühn, *Vector-boson pair production and electroweak corrections in HERWIG++*, *Eur. Phys. J.* **C 74** (2014) 2988 [arXiv:1401.3964] [INSPIRE].

[37] S. Frixione and B.R. Webber, *Matching NLO QCD computations and parton shower simulations*, *JHEP* **06** (2002) 029 [hep-ph/0204244] [INSPIRE].

[38] B.P. Kersevan and E. Richter-Was, *The Monte Carlo event generator AcerMC versions* 2.0 *to* 3.8 *with interfaces to PYTHIA* 6.4*, HERWIG* 6.5 *and ARIADNE* 4.1, *Comput. Phys. Commun.* **184** (2013) 919 [hep-ph/0405247] [INSPIRE].

[39] T. Sjöstrand et al., *High-energy physics event generation with PYTHIA* 6.1, *Comput. Phys. Commun.* **135** (2001) 238 [hep-ph/0010017] [INSPIRE].

[40] ATLAS collaboration, *ATLAS tunes of PYTHIA* 6 *and PYTHIA* 8 *for MC*11, ATL-PHYS-PUB-2011-009, CERN, Geneva Switzerland (2011).

[41] J. Pumplin, D.R. Stump, J. Huston, H.L. Lai, P.M. Nadolsky and W.K. Tung, *New generation of parton distributions with uncertainties from global QCD analysis*, *JHEP* **07** (2002) 012 [hep-ph/0201195] [INSPIRE].

[42] M.L. Mangano, M. Moretti, F. Piccinini, R. Pittau and A.D. Polosa, *ALPGEN, a generator for hard multiparton processes in hadronic collisions*, *JHEP* **07** (2003) 001 [hep-ph/0206293] [INSPIRE].

[43] M.L. Mangano, M. Moretti and R. Pittau, *Multijet matrix elements and shower evolution in hadronic collisions: $Wb\bar{b} + n$ jets as a case study*, *Nucl. Phys.* **B 632** (2002) 343 [hep-ph/0108069] [INSPIRE].

[44] T. Gleisberg et al., *Event generation with SHERPA* 1.1, *JHEP* **02** (2009) 007 [arXiv:0811.4622] [INSPIRE].

[45] J.M. Campbell, R.K. Ellis and C. Williams, *Vector boson pair production at the LHC*, *JHEP* **07** (2011) 018 [arXiv:1105.0020] [INSPIRE].

[46] LHC HIGGS CROSS SECTION WORKING GROUP collaboration, J.R. Andersen et al., *Handbook of LHC Higgs cross sections: 3. Higgs properties*, arXiv:1307.1347 [INSPIRE].

[47] M. Czakon and A. Mitov, *Top++: a program for the calculation of the top-pair cross-section at hadron colliders*, *Comput. Phys. Commun.* **185** (2014) 2930 [arXiv:1112.5675] [INSPIRE].

[48] N. Kidonakis, *Two-loop soft anomalous dimensions for single top quark associated production with a W^- or H^-*, *Phys. Rev.* **D 82** (2010) 054018 [arXiv:1005.4451] [INSPIRE].

[49] N. Kidonakis, *Next-to-next-to-leading-order collinear and soft gluon corrections for t-channel single top quark production*, *Phys. Rev.* **D 83** (2011) 091503 [arXiv:1103.2792] [INSPIRE].

[50] N. Kidonakis, *NNLL resummation for s-channel single top quark production*, *Phys. Rev.* **D 81** (2010) 054028 [arXiv:1001.5034] [INSPIRE].

[51] S. Catani and M. Grazzini, *An NNLO subtraction formalism in hadron collisions and its application to Higgs boson production at the LHC*, *Phys. Rev. Lett.* **98** (2007) 222002 [hep-ph/0703012] [INSPIRE].

[52] ATLAS collaboration, *Performance of the ATLAS electron and photon trigger in p-p collisions at $\sqrt{s} = 7\,TeV$ in 2011*, ATLAS-CONF-2012-048, CERN, Geneva Switzerland (2012).

[53] ATLAS collaboration, *Performance of the ATLAS muon trigger in pp collisions at $\sqrt{s} = 8\,TeV$*, *Eur. Phys. J.* **C 75** (2015) 120 [arXiv:1408.3179] [INSPIRE].

[54] ATLAS collaboration, *Electron efficiency measurements with the ATLAS detector using the 2012 LHC proton-proton collision data*, ATLAS-CONF-2014-032, CERN, Geneva Switzerland (2014).

[55] ATLAS collaboration, *Observation and measurement of Higgs boson decays to WW^* with the ATLAS detector*, *Phys. Rev.* **D 92** (2015) 012006 [arXiv:1412.2641] [INSPIRE].

[56] ATLAS collaboration, *Measurement of the muon reconstruction performance of the ATLAS detector using 2011 and 2012 LHC proton-proton collision data*, *Eur. Phys. J.* **C 74** (2014) 3130 [arXiv:1407.3935] [INSPIRE].

[57] M. Cacciari, G.P. Salam and G. Soyez, *The anti-k_t jet clustering algorithm*, *JHEP* **04** (2008) 063 [arXiv:0802.1189] [INSPIRE].

[58] M. Cacciari and G.P. Salam, *Dispelling the N^3 myth for the k_t jet-finder*, *Phys. Lett.* **B 641** (2006) 57 [hep-ph/0512210] [INSPIRE].

[59] ATLAS collaboration, *Calorimeter clustering algorithms: description and performance*, ATL-LARG-PUB-2008-002, CERN, Geneva Switzerland (2008).

[60] T. Barillari et al., *Local hadronic calibration*, ATL-COM-LARG-2008-006, CERN, Geneva Switzerland (2008) [ATL-LARG-PUB-2009-001-2] [ATL-LARG-PUB-2009-001].

[61] M. Cacciari and G.P. Salam, *Pileup subtraction using jet areas*, *Phys. Lett.* **B 659** (2008) 119 [arXiv:0707.1378] [INSPIRE].

[62] ATLAS collaboration, *Jet energy measurement and its systematic uncertainty in proton-proton collisions at $\sqrt{s} = 7\,TeV$ with the ATLAS detector*, *Eur. Phys. J.* **C 75** (2015) 17 [arXiv:1406.0076] [INSPIRE].

[63] ATLAS collaboration, *Monte Carlo calibration and combination of in-situ measurements of jet energy scale, jet energy resolution and jet mass in ATLAS*, ATLAS-CONF-2015-037, CERN, Geneva Switzerland (2015).

[64] ATLAS collaboration, *Pile-up subtraction and suppression for jets in ATLAS*, ATLAS-CONF-2013-083, CERN, Geneva Switzerland (2013).

[65] ATLAS collaboration, *Performance of b-jet identification in the ATLAS experiment*, 2016 *JINST* **11** P04008 [arXiv:1512.01094] [INSPIRE].

[66] ATLAS collaboration, *Calibration of the performance of b-tagging for c and light-flavour jets in the* 2012 *ATLAS data*, ATLAS-CONF-2014-046, CERN, Geneva Switzerland (2014).

[67] ATLAS collaboration, *Performance of missing transverse momentum reconstruction in ATLAS studied in proton-proton collisions recorded in* 2012 *at 8 TeV*, ATLAS-CONF-2013-082, CERN, Geneva Switzerland (2013).

[68] ATLAS collaboration, *Pile-up suppression in missing transverse momentum reconstruction in the ATLAS experiment in proton-proton collisions at* $\sqrt{s} = 8$ *TeV*, ATLAS-CONF-2014-019, CERN, Geneva Switzerland (2014).

[69] PARTICLE DATA GROUP collaboration, J. Beringer et al., *Review of particle physics (RPP)*, *Phys. Rev.* **D 86** (2012) 010001 [INSPIRE].

[70] B. Mellado, X. Ruan and Z. Zhang, *Extraction of top backgrounds in the Higgs boson search with the* $H \to WW^\star \to \ell\ell + E_{\mathrm{T}}^{\mathrm{miss}}$ *decay with a full-jet veto at the LHC*, *Phys. Rev.* **D 84** (2011) 096005 [arXiv:1101.1383] [INSPIRE].

[71] ATLAS collaboration, *Measurement of the production cross-section of a single top quark in association with a W boson at 8 TeV with the ATLAS experiment*, *JHEP* **01** (2016) 064 [arXiv:1510.03752] [INSPIRE].

[72] ATLAS collaboration, *Measurement of hard double-parton interactions in* $W(\to \ell\nu) + 2$ *jet events at* $\sqrt{s} = 7$ *TeV with the ATLAS detector*, *New J. Phys.* **15** (2013) 033038 [arXiv:1301.6872] [INSPIRE].

[73] F. James and M. Roos, *Minuit: a system for function minimization and analysis of the parameter errors and correlations*, *Comput. Phys. Commun.* **10** (1975) 343 [INSPIRE].

[74] T. Adye, *Unfolding algorithms and tests using RooUnfold*, arXiv:1105.1160 [INSPIRE].

[75] G. D'Agostini, *Improved iterative Bayesian unfolding*, arXiv:1010.0632.

[76] B. Malaescu, *An Iterative, Dynamically Stabilized (IDS) method of data unfolding*, CERN-PH-EP-2011-111, CERN, Geneva Switzerland (2011) [arXiv:1106.3107] [INSPIRE].

[77] ATLAS collaboration, *Muon reconstruction efficiency and momentum resolution of the ATLAS experiment in proton-proton collisions at* $\sqrt{s} = 7$ *TeV in* 2010, *Eur. Phys. J.* **C 74** (2014) 3034 [arXiv:1404.4562] [INSPIRE].

[78] ATLAS collaboration, *Electron reconstruction and identification efficiency measurements with the ATLAS detector using the* 2011 *LHC proton-proton collision data*, *Eur. Phys. J.* **C 74** (2014) 2941 [arXiv:1404.2240] [INSPIRE].

[79] ATLAS collaboration, *Electron performance measurements with the ATLAS detector using the* 2010 *LHC proton-proton collision data*, *Eur. Phys. J.* **C 72** (2012) 1909 [arXiv:1110.3174] [INSPIRE].

[80] A.D. Martin, W.J. Stirling, R.S. Thorne and G. Watt, *Parton distributions for the LHC*, *Eur. Phys. J.* **C 63** (2009) 189 [arXiv:0901.0002] [INSPIRE].

[81] R.D. Ball et al., *Parton distributions with LHC data*, *Nucl. Phys.* **B 867** (2013) 244 [arXiv:1207.1303] [INSPIRE].

[82] S. Alekhin et al., *The PDF4LHC working group interim report*, arXiv:1101.0536 [INSPIRE].

[83] I.W. Stewart and F.J. Tackmann, *Theory uncertainties for Higgs and other searches using jet bins*, *Phys. Rev.* **D 85** (2012) 034011 [arXiv:1107.2117] [INSPIRE].

[84] C. Anastasiou, C. Duhr, F. Dulat, F. Herzog and B. Mistlberger, *Higgs boson gluon-fusion production in QCD at three loops*, *Phys. Rev. Lett.* **114** (2015) 212001 [arXiv:1503.06056] [INSPIRE].

[85] K. Hagiwara, R.D. Peccei, D. Zeppenfeld and K. Hikasa, *Probing the weak boson sector in $e^+e^- \to W^+W^-$*, *Nucl. Phys.* **B 282** (1987) 253 [INSPIRE].

[86] H. Aihara et al., *Anomalous gauge boson interactions*, hep-ph/9503425 [INSPIRE].

[87] G. Gounaris et al., *Triple gauge boson couplings*, hep-ph/9601233 [INSPIRE].

[88] C. Degrande et al., *Effective field theory: a modern approach to anomalous couplings*, *Annals Phys.* **335** (2013) 21 [arXiv:1205.4231] [INSPIRE].

[89] G. Cowan, K. Cranmer, E. Gross and O. Vitells, *Asymptotic formulae for likelihood-based tests of new physics*, *Eur. Phys. J.* **C 71** (2011) 1554 [*Erratum ibid.* **C 73** (2013) 2501] [arXiv:1007.1727] [INSPIRE].

[90] G.J. Feldman and R.D. Cousins, *A unified approach to the classical statistical analysis of small signals*, *Phys. Rev.* **D 57** (1998) 3873 [physics/9711021] [INSPIRE].

The ATLAS collaboration

G. Aad[87], B. Abbott[115], J. Abdallah[153], O. Abdinov[11], R. Aben[109], M. Abolins[92],
O.S. AbouZeid[160], H. Abramowicz[155], H. Abreu[154], R. Abreu[118], Y. Abulaiti[148a,148b],
B.S. Acharya[164a,164b,a], L. Adamczyk[39a], D.L. Adams[26], J. Adelman[110], S. Adomeit[102],
T. Adye[133], A.A. Affolder[76], T. Agatonovic-Jovin[13], J. Agricola[55], J.A. Aguilar-Saavedra[128a,128f],
S.P. Ahlen[23], F. Ahmadov[67,b], G. Aielli[135a,135b], H. Akerstedt[148a,148b], T.P.A. Åkesson[83],
A.V. Akimov[98], G.L. Alberghi[21a,21b], J. Albert[169], S. Albrand[56], M.J. Alconada Verzini[73],
M. Aleksa[31], I.N. Aleksandrov[67], C. Alexa[27b], G. Alexander[155], T. Alexopoulos[10], M. Alhroob[115],
G. Alimonti[93a], L. Alio[87], J. Alison[32], S.P. Alkire[36], B.M.M. Allbrooke[151], P.P. Allport[18],
A. Aloisio[106a,106b], A. Alonso[37], F. Alonso[73], C. Alpigiani[140], B. Alvarez Gonzalez[31],
D. Álvarez Piqueras[167], M.G. Alviggi[106a,106b], B.T. Amadio[15], K. Amako[68],
Y. Amaral Coutinho[25a], C. Amelung[24], D. Amidei[91], S.P. Amor Dos Santos[128a,128c],
A. Amorim[128a,128b], S. Amoroso[49], N. Amram[155], G. Amundsen[24], C. Anastopoulos[141],
L.S. Ancu[50], N. Andari[110], T. Andeen[32], C.F. Anders[59b], G. Anders[31], J.K. Anders[76],
K.J. Anderson[32], A. Andreazza[93a,93b], V. Andrei[59a], S. Angelidakis[9], I. Angelozzi[109], P. Anger[45],
A. Angerami[36], F. Anghinolfi[31], A.V. Anisenkov[111,c], N. Anjos[12], A. Annovi[126a,126b],
M. Antonelli[48], A. Antonov[100], J. Antos[146b], F. Anulli[134a], M. Aoki[68], L. Aperio Bella[18],
G. Arabidze[92], Y. Arai[68], J.P. Araque[128a], A.T.H. Arce[46], F.A. Arduh[73], J-F. Arguin[97],
S. Argyropoulos[64], M. Arik[19a], A.J. Armbruster[31], O. Arnaez[31], H. Arnold[49], M. Arratia[29],
O. Arslan[22], A. Artamonov[99], G. Artoni[122], S. Artz[85], S. Asai[157], N. Asbah[43], A. Ashkenazi[155],
B. Åsman[148a,148b], L. Asquith[151], K. Assamagan[26], R. Astalos[146a], M. Atkinson[166], N.B. Atlay[143],
K. Augsten[130], M. Aurousseau[147b], G. Avolio[31], B. Axen[15], M.K. Ayoub[119], G. Azuelos[97,d],
M.A. Baak[31], A.E. Baas[59a], M.J. Baca[18], H. Bachacou[138], K. Bachas[156], M. Backes[31],
M. Backhaus[31], P. Bagiacchi[134a,134b], P. Bagnaia[134a,134b], Y. Bai[34a], J.T. Baines[133],
O.K. Baker[176], E.M. Baldin[111,c], P. Balek[131], T. Balestri[150], F. Balli[86], W.K. Balunas[124],
E. Banas[40], Sw. Banerjee[173,e], A.A.E. Bannoura[175], L. Barak[31], E.L. Barberio[90],
D. Barberis[51a,51b], M. Barbero[87], T. Barillari[103], M. Barisonzi[164a,164b], T. Barklow[145],
N. Barlow[29], S.L. Barnes[86], B.M. Barnett[133], R.M. Barnett[15], Z. Barnovska[5], A. Baroncelli[136a],
G. Barone[24], A.J. Barr[122], F. Barreiro[84], J. Barreiro Guimarães da Costa[34a], R. Bartoldus[145],
A.E. Barton[74], P. Bartos[146a], A. Basalaev[125], A. Bassalat[119], A. Basye[166], R.L. Bates[54],
S.J. Batista[160], J.R. Batley[29], M. Battaglia[139], M. Bauce[134a,134b], F. Bauer[138], H.S. Bawa[145,f],
J.B. Beacham[113], M.D. Beattie[74], T. Beau[82], P.H. Beauchemin[163], R. Beccherle[126a,126b],
P. Bechtle[22], H.P. Beck[17,g], K. Becker[122], M. Becker[85], M. Beckingham[170], C. Becot[119],
A.J. Beddall[19b], A. Beddall[19b], V.A. Bednyakov[67], C.P. Bee[150], L.J. Beemster[109],
T.A. Beermann[31], M. Begel[26], J.K. Behr[122], C. Belanger-Champagne[89], W.H. Bell[50], G. Bella[155],
L. Bellagamba[21a], A. Bellerive[30], M. Bellomo[88], K. Belotskiy[100], O. Beltramello[31], O. Benary[155],
D. Benchekroun[137a], M. Bender[102], K. Bendtz[148a,148b], N. Benekos[10], Y. Benhammou[155],
E. Benhar Noccioli[176], J.A. Benitez Garcia[161b], D.P. Benjamin[46], J.R. Bensinger[24],
S. Bentvelsen[109], L. Beresford[122], M. Beretta[48], D. Berge[109], E. Bergeaas Kuutmann[165],
N. Berger[5], F. Berghaus[169], J. Beringer[15], C. Bernard[23], N.R. Bernard[88], C. Bernius[112],
F.U. Bernlochner[22], T. Berry[79], P. Berta[131], C. Bertella[85], G. Bertoli[148a,148b],
F. Bertolucci[126a,126b], C. Bertsche[115], D. Bertsche[115], M.I. Besana[93a], G.J. Besjes[37],
O. Bessidskaia Bylund[148a,148b], M. Bessner[43], N. Besson[138], C. Betancourt[49], S. Bethke[103],
A.J. Bevan[78], W. Bhimji[15], R.M. Bianchi[127], L. Bianchini[24], M. Bianco[31], O. Biebel[102],
D. Biedermann[16], N.V. Biesuz[126a,126b], M. Biglietti[136a], J. Bilbao De Mendizabal[50], H. Bilokon[48],
M. Bindi[55], S. Binet[119], A. Bingul[19b], C. Bini[134a,134b], S. Biondi[21a,21b], D.M. Bjergaard[46],
C.W. Black[152], J.E. Black[145], K.M. Black[23], D. Blackburn[140], R.E. Blair[6], J.-B. Blanchard[138],

J.E. Blanco[79], T. Blazek[146a], I. Bloch[43], C. Blocker[24], W. Blum[85,*], U. Blumenschein[55],
S. Blunier[33a], G.J. Bobbink[109], V.S. Bobrovnikov[111,c], S.S. Bocchetta[83], A. Bocci[46], C. Bock[102],
M. Boehler[49], J.A. Bogaerts[31], D. Bogavac[13], A.G. Bogdanchikov[111], C. Bohm[148a], V. Boisvert[79],
T. Bold[39a], V. Boldea[27b], A.S. Boldyrev[101], M. Bomben[82], M. Bona[78], M. Boonekamp[138],
A. Borisov[132], G. Borissov[74], S. Borroni[43], J. Bortfeldt[102], V. Bortolotto[61a,61b,61c], K. Bos[109],
D. Boscherini[21a], M. Bosman[12], J. Boudreau[127], J. Bouffard[2], E.V. Bouhova-Thacker[74],
D. Boumediene[35], C. Bourdarios[119], N. Bousson[116], S.K. Boutle[54], A. Boveia[31], J. Boyd[31],
I.R. Boyko[67], I. Bozic[13], J. Bracinik[18], A. Brandt[8], G. Brandt[55], O. Brandt[59a], U. Bratzler[158],
B. Brau[88], J.E. Brau[118], H.M. Braun[175,*], W.D. Breaden Madden[54], K. Brendlinger[124],
A.J. Brennan[90], L. Brenner[109], R. Brenner[165], S. Bressler[172], T.M. Bristow[47], D. Britton[54],
D. Britzger[43], F.M. Brochu[29], I. Brock[22], R. Brock[92], G. Brooijmans[36], T. Brooks[79],
W.K. Brooks[33b], J. Brosamer[15], E. Brost[118], P.A. Bruckman de Renstrom[40], D. Bruncko[146b],
R. Bruneliere[49], A. Bruni[21a], G. Bruni[21a], M. Bruschi[21a], N. Bruscino[22], L. Bryngemark[83],
T. Buanes[14], Q. Buat[144], P. Buchholz[143], A.G. Buckley[54], I.A. Budagov[67], F. Buehrer[49],
L. Bugge[121], M.K. Bugge[121], O. Bulekov[100], D. Bullock[8], H. Burckhart[31], S. Burdin[76],
C.D. Burgard[49], B. Burghgrave[110], S. Burke[133], I. Burmeister[44], E. Busato[35], D. Büscher[49],
V. Büscher[85], P. Bussey[54], J.M. Butler[23], A.I. Butt[3], C.M. Buttar[54], J.M. Butterworth[80],
P. Butti[109], W. Buttinger[26], A. Buzatu[54], A.R. Buzykaev[111,c], S. Cabrera Urbán[167],
D. Caforio[130], V.M. Cairo[38a,38b], O. Cakir[4a], N. Calace[50], P. Calafiura[15], A. Calandri[138],
G. Calderini[82], P. Calfayan[102], L.P. Caloba[25a], D. Calvet[35], S. Calvet[35], R. Camacho Toro[32],
S. Camarda[43], P. Camarri[135a,135b], D. Cameron[121], R. Caminal Armadans[166], S. Campana[31],
M. Campanelli[80], A. Campoverde[150], V. Canale[106a,106b], A. Canepa[161a], M. Cano Bret[34e],
J. Cantero[84], R. Cantrill[128a], T. Cao[41], M.D.M. Capeans Garrido[31], I. Caprini[27b], M. Caprini[27b],
M. Capua[38a,38b], R. Caputo[85], R.M. Carbone[36], R. Cardarelli[135a], F. Cardillo[49], T. Carli[31],
G. Carlino[106a], L. Carminati[93a,93b], S. Caron[108], E. Carquin[33a], G.D. Carrillo-Montoya[31],
J.R. Carter[29], J. Carvalho[128a,128c], D. Casadei[80], M.P. Casado[12,h], M. Casolino[12], D.W. Casper[66],
E. Castaneda-Miranda[147a], A. Castelli[109], V. Castillo Gimenez[167], N.F. Castro[128a,i],
P. Catastini[58], A. Catinaccio[31], J.R. Catmore[121], A. Cattai[31], J. Caudron[85], V. Cavaliere[166],
D. Cavalli[93a], M. Cavalli-Sforza[12], V. Cavasinni[126a,126b], F. Ceradini[136a,136b],
L. Cerda Alberich[167], B.C. Cerio[46], A.S. Cerqueira[25b], A. Cerri[151], L. Cerrito[78], F. Cerutti[15],
M. Cerv[31], A. Cervelli[17], S.A. Cetin[19c], A. Chafaq[137a], D. Chakraborty[110], I. Chalupkova[131],
Y.L. Chan[61a], P. Chang[166], J.D. Chapman[29], D.G. Charlton[18], C.C. Chau[160],
C.A. Chavez Barajas[151], S. Che[113], S. Cheatham[74], A. Chegwidden[92], S. Chekanov[6],
S.V. Chekulaev[161a], G.A. Chelkov[67,j], M.A. Chelstowska[91], C. Chen[65], H. Chen[26], K. Chen[150],
L. Chen[34d,k], S. Chen[34c], S. Chen[157], X. Chen[34f], Y. Chen[69], H.C. Cheng[91], Y. Cheng[32],
A. Cheplakov[67], E. Cheremushkina[132], R. Cherkaoui El Moursli[137e], V. Chernyatin[26,*], E. Cheu[7],
L. Chevalier[138], V. Chiarella[48], G. Chiarelli[126a,126b], G. Chiodini[75a], A.S. Chisholm[18],
R.T. Chislett[80], A. Chitan[27b], M.V. Chizhov[67], K. Choi[62], S. Chouridou[9], B.K.B. Chow[102],
V. Christodoulou[80], D. Chromek-Burckhart[31], J. Chudoba[129], A.J. Chuinard[89],
J.J. Chwastowski[40], L. Chytka[117], G. Ciapetti[134a,134b], A.K. Ciftci[4a], D. Cinca[54], V. Cindro[77],
I.A. Cioara[22], A. Ciocio[15], F. Cirotto[106a,106b], Z.H. Citron[172], M. Ciubancan[27b], A. Clark[50],
B.L. Clark[58], P.J. Clark[47], R.N. Clarke[15], C. Clement[148a,148b], Y. Coadou[87], M. Cobal[164a,164c],
A. Coccaro[50], J. Cochran[65], L. Coffey[24], L. Colasurdo[108], B. Cole[36], S. Cole[110], A.P. Colijn[109],
J. Collot[56], T. Colombo[59c], G. Compostella[103], P. Conde Muiño[128a,128b], E. Coniavitis[49],
S.H. Connell[147b], I.A. Connelly[79], V. Consorti[49], S. Constantinescu[27b], C. Conta[123a,123b],
G. Conti[31], F. Conventi[106a,l], M. Cooke[15], B.D. Cooper[80], A.M. Cooper-Sarkar[122],
T. Cornelissen[175], M. Corradi[134a,134b], F. Corriveau[89,m], A. Corso-Radu[66], A. Cortes-Gonzalez[12],
G. Cortiana[103], G. Costa[93a], M.J. Costa[167], D. Costanzo[141], D. Côté[8], G. Cottin[29], G. Cowan[79],

B.E. Cox[86], K. Cranmer[112], S.J. Crawley[54], G. Cree[30], S. Crépé-Renaudin[56], F. Crescioli[82],
W.A. Cribbs[148a,148b], M. Crispin Ortuzar[122], M. Cristinziani[22], V. Croft[108], G. Crosetti[38a,38b],
T. Cuhadar Donszelmann[141], J. Cummings[176], M. Curatolo[48], J. Cúth[85], C. Cuthbert[152],
H. Czirr[143], P. Czodrowski[3], S. D'Auria[54], M. D'Onofrio[76],
M.J. Da Cunha Sargedas De Sousa[128a,128b], C. Da Via[86], W. Dabrowski[39a], A. Dafinca[122],
T. Dai[91], O. Dale[14], F. Dallaire[97], C. Dallapiccola[88], M. Dam[37], J.R. Dandoy[32], N.P. Dang[49],
A.C. Daniells[18], M. Danninger[168], M. Dano Hoffmann[138], V. Dao[49], G. Darbo[51a], S. Darmora[8],
J. Dassoulas[3], A. Dattagupta[62], W. Davey[22], C. David[169], T. Davidek[131], E. Davies[122,n],
M. Davies[155], P. Davison[80], Y. Davygora[59a], E. Dawe[90], I. Dawson[141],
R.K. Daya-Ishmukhametova[88], K. De[8], R. de Asmundis[106a], A. De Benedetti[115],
S. De Castro[21a,21b], S. De Cecco[82], N. De Groot[108], P. de Jong[109], H. De la Torre[84],
F. De Lorenzi[65], D. De Pedis[134a], A. De Salvo[134a], U. De Sanctis[151], A. De Santo[151],
J.B. De Vivie De Regie[119], W.J. Dearnaley[74], R. Debbe[26], C. Debenedetti[139], D.V. Dedovich[67],
I. Deigaard[109], J. Del Peso[84], T. Del Prete[126a,126b], D. Delgove[119], F. Deliot[138], C.M. Delitzsch[50],
M. Deliyergiyev[77], A. Dell'Acqua[31], L. Dell'Asta[23], M. Dell'Orso[126a,126b], M. Della Pietra[106a,l],
D. della Volpe[50], M. Delmastro[5], P.A. Delsart[56], C. Deluca[109], D.A. DeMarco[160], S. Demers[176],
M. Demichev[67], A. Demilly[82], S.P. Denisov[132], D. Derendarz[40], J.E. Derkaoui[137d], F. Derue[82],
P. Dervan[76], K. Desch[22], C. Deterre[43], K. Dette[44], P.O. Deviveiros[31], A. Dewhurst[133],
S. Dhaliwal[24], A. Di Ciaccio[135a,135b], L. Di Ciaccio[5], A. Di Domenico[134a,134b],
C. Di Donato[134a,134b], A. Di Girolamo[31], B. Di Girolamo[31], A. Di Mattia[154], B. Di Micco[136a,136b],
R. Di Nardo[48], A. Di Simone[49], R. Di Sipio[160], D. Di Valentino[30], C. Diaconu[87], M. Diamond[160],
F.A. Dias[47], M.A. Diaz[33a], E.B. Diehl[91], J. Dietrich[16], S. Diglio[87], A. Dimitrievska[13],
J. Dingfelder[22], P. Dita[27b], S. Dita[27b], F. Dittus[31], F. Djama[87], T. Djobava[52b], J.I. Djuvsland[59a],
M.A.B. do Vale[25c], D. Dobos[31], M. Dobre[27b], C. Doglioni[83], T. Dohmae[157], J. Dolejsi[131],
Z. Dolezal[131], B.A. Dolgoshein[100,*], M. Donadelli[25d], S. Donati[126a,126b], P. Dondero[123a,123b],
J. Donini[35], J. Dopke[133], A. Doria[106a], M.T. Dova[73], A.T. Doyle[54], E. Drechsler[55], M. Dris[10],
Y. Du[34d], J. Duarte-Campderros[155], E. Dubreuil[35], E. Duchovni[172], G. Duckeck[102], O.A. Ducu[27b],
D. Duda[109], A. Dudarev[31], L. Duflot[119], L. Duguid[79], M. Dührssen[31], M. Dunford[59a],
H. Duran Yildiz[4a], M. Düren[53], A. Durglishvili[52b], D. Duschinger[45], B. Dutta[43], M. Dyndal[39a],
C. Eckardt[43], K.M. Ecker[103], R.C. Edgar[91], W. Edson[2], N.C. Edwards[47], W. Ehrenfeld[22],
T. Eifert[31], G. Eigen[14], K. Einsweiler[15], T. Ekelof[165], M. El Kacimi[137c], M. Ellert[165], S. Elles[5],
F. Ellinghaus[175], A.A. Elliot[169], N. Ellis[31], J. Elmsheuser[102], M. Elsing[31], D. Emeliyanov[133],
Y. Enari[157], O.C. Endner[85], M. Endo[120], J. Erdmann[44], A. Ereditato[17], G. Ernis[175], J. Ernst[2],
M. Ernst[26], S. Errede[166], E. Ertel[85], M. Escalier[119], H. Esch[44], C. Escobar[127], B. Esposito[48],
A.I. Etienvre[138], E. Etzion[155], H. Evans[62], A. Ezhilov[125], L. Fabbri[21a,21b], G. Facini[32],
R.M. Fakhrutdinov[132], S. Falciano[134a], R.J. Falla[80], J. Faltova[131], Y. Fang[34a], M. Fanti[93a,93b],
A. Farbin[8], A. Farilla[136a], C. Farina[127], T. Farooque[12], S. Farrell[15], S.M. Farrington[170],
P. Farthouat[31], F. Fassi[137e], P. Fassnacht[31], D. Fassouliotis[9], M. Faucci Giannelli[79],
A. Favareto[51a,51b], L. Fayard[119], O.L. Fedin[125,o], W. Fedorko[168], S. Feigl[121], L. Feligioni[87],
C. Feng[34d], E.J. Feng[31], H. Feng[91], A.B. Fenyuk[132], L. Feremenga[8], P. Fernandez Martinez[167],
S. Fernandez Perez[12], J. Ferrando[54], A. Ferrari[165], P. Ferrari[109], R. Ferrari[123a],
D.E. Ferreira de Lima[54], A. Ferrer[167], D. Ferrere[50], C. Ferretti[91], A. Ferretto Parodi[51a,51b],
F. Fiedler[85], A. Filipčič[77], M. Filipuzzi[43], F. Filthaut[108], M. Fincke-Keeler[169], K.D. Finelli[152],
M.C.N. Fiolhais[128a,128c], L. Fiorini[167], A. Firan[41], A. Fischer[2], C. Fischer[12], J. Fischer[175],
W.C. Fisher[92], N. Flaschel[43], I. Fleck[143], P. Fleischmann[91], G.T. Fletcher[141], G. Fletcher[78],
R.R.M. Fletcher[124], T. Flick[175], A. Floderus[83], L.R. Flores Castillo[61a], M.J. Flowerdew[103],
G.T. Forcolin[86], A. Formica[138], A. Forti[86], D. Fournier[119], H. Fox[74], S. Fracchia[12],
P. Francavilla[82], M. Franchini[21a,21b], D. Francis[31], L. Franconi[121], M. Franklin[58], M. Frate[66],

M. Fraternali[123a,123b], D. Freeborn[80], S.T. French[29], S.M. Fressard-Batraneanu[31], F. Friedrich[45],
D. Froidevaux[31], J.A. Frost[122], C. Fukunaga[158], E. Fullana Torregrosa[85], T. Fusayasu[104],
J. Fuster[167], C. Gabaldon[56], O. Gabizon[175], A. Gabrielli[21a,21b], A. Gabrielli[15], G.P. Gach[18],
S. Gadatsch[31], S. Gadomski[50], G. Gagliardi[51a,51b], P. Gagnon[62], C. Galea[108],
B. Galhardo[128a,128c], E.J. Gallas[122], B.J. Gallop[133], P. Gallus[130], G. Galster[37], K.K. Gan[113],
J. Gao[34b,87], Y. Gao[47], Y.S. Gao[145,f], F.M. Garay Walls[47], C. García[167], J.E. García Navarro[167],
M. Garcia-Sciveres[15], R.W. Gardner[32], N. Garelli[145], V. Garonne[121], C. Gatti[48],
A. Gaudiello[51a,51b], G. Gaudio[123a], B. Gaur[143], L. Gauthier[97], I.L. Gavrilenko[98], C. Gay[168],
G. Gaycken[22], E.N. Gazis[10], Z. Gecse[168], C.N.P. Gee[133], Ch. Geich-Gimbel[22], M.P. Geisler[59a],
C. Gemme[51a], M.H. Genest[56], C. Geng[34b,p], S. Gentile[134a,134b], S. George[79], D. Gerbaudo[66],
A. Gershon[155], S. Ghasemi[143], H. Ghazlane[137b], B. Giacobbe[21a], S. Giagu[134a,134b],
P. Giannetti[126a,126b], B. Gibbard[26], S.M. Gibson[79], M. Gignac[168], M. Gilchriese[15],
T.P.S. Gillam[29], D. Gillberg[31], G. Gilles[35], D.M. Gingrich[3,d], N. Giokaris[9], M.P. Giordani[164a,164c],
F.M. Giorgi[21a], F.M. Giorgi[16], P.F. Giraud[138], P. Giromini[58], D. Giugni[93a], C. Giuliani[103],
M. Giulini[59b], B.K. Gjelsten[121], S. Gkaitatzis[156], I. Gkialas[156], E.L. Gkougkousis[119],
L.K. Gladilin[101], C. Glasman[84], J. Glatzer[31], P.C.F. Glaysher[47], A. Glazov[43],
M. Goblirsch-Kolb[103], J.R. Goddard[78], J. Godlewski[40], S. Goldfarb[91], T. Golling[50],
D. Golubkov[132], A. Gomes[128a,128b,128d], R. Gonçalo[128a], J. Goncalves Pinto Firmino Da Costa[138],
L. Gonella[22], S. González de la Hoz[167], G. Gonzalez Parra[12], S. Gonzalez-Sevilla[50], L. Goossens[31],
P.A. Gorbounov[99], H.A. Gordon[26], I. Gorelov[107], B. Gorini[31], E. Gorini[75a,75b], A. Gorišek[77],
E. Gornicki[40], A.T. Goshaw[46], C. Gössling[44], M.I. Gostkin[67], D. Goujdami[137c], A.G. Goussiou[140],
N. Govender[147b], E. Gozani[154], L. Graber[55], I. Grabowska-Bold[39a], P.O.J. Gradin[165],
P. Grafström[21a,21b], J. Gramling[50], E. Gramstad[121], S. Grancagnolo[16], V. Gratchev[125],
H.M. Gray[31], E. Graziani[136a], Z.D. Greenwood[81,q], C. Grefe[22], K. Gregersen[80], I.M. Gregor[43],
P. Grenier[145], J. Griffiths[8], A.A. Grillo[139], K. Grimm[74], S. Grinstein[12,r], Ph. Gris[35],
J.-F. Grivaz[119], S. Groh[85], J.P. Grohs[45], A. Grohsjean[43], E. Gross[172], J. Grosse-Knetter[55],
G.C. Grossi[81], Z.J. Grout[151], L. Guan[91], J. Guenther[130], F. Guescini[50], D. Guest[66], O. Gueta[155],
E. Guido[51a,51b], T. Guillemin[5], S. Guindon[2], U. Gul[54], C. Gumpert[31], J. Guo[34e], Y. Guo[34b,p],
S. Gupta[122], G. Gustavino[134a,134b], P. Gutierrez[115], N.G. Gutierrez Ortiz[80], C. Gutschow[45],
C. Guyot[138], C. Gwenlan[122], C.B. Gwilliam[76], A. Haas[112], C. Haber[15], H.K. Hadavand[8],
N. Haddad[137e], P. Haefner[22], S. Hageböck[22], Z. Hajduk[40], H. Hakobyan[177,*], M. Haleem[43],
J. Haley[116], D. Hall[122], G. Halladjian[92], G.D. Hallewell[87], K. Hamacher[175], P. Hamal[117],
K. Hamano[169], A. Hamilton[147a], G.N. Hamity[141], P.G. Hamnett[43], L. Han[34b], K. Hanagaki[68,s],
K. Hanawa[157], M. Hance[139], B. Haney[124], P. Hanke[59a], R. Hanna[138], J.B. Hansen[37],
J.D. Hansen[37], M.C. Hansen[22], P.H. Hansen[37], K. Hara[162], A.S. Hard[173], T. Harenberg[175],
F. Hariri[119], S. Harkusha[94], R.D. Harrington[47], P.F. Harrison[170], F. Hartjes[109], M. Hasegawa[69],
Y. Hasegawa[142], A. Hasib[115], S. Hassani[138], S. Haug[17], R. Hauser[92], L. Hauswald[45],
M. Havranek[129], C.M. Hawkes[18], R.J. Hawkings[31], A.D. Hawkins[83], T. Hayashi[162], D. Hayden[92],
C.P. Hays[122], J.M. Hays[78], H.S. Hayward[76], S.J. Haywood[133], S.J. Head[18], T. Heck[85],
V. Hedberg[83], L. Heelan[8], S. Heim[124], T. Heim[15], B. Heinemann[15], L. Heinrich[112], J. Hejbal[129],
L. Helary[23], S. Hellman[148a,148b], C. Helsens[31], J. Henderson[122], R.C.W. Henderson[74], Y. Heng[173],
C. Hengler[43], S. Henkelmann[168], A.M. Henriques Correia[31], S. Henrot-Versille[119], G.H. Herbert[16],
Y. Hernández Jiménez[167], G. Herten[49], R. Hertenberger[102], L. Hervas[31], G.G. Hesketh[80],
N.P. Hessey[109], J.W. Hetherly[41], R. Hickling[78], E. Higón-Rodriguez[167], E. Hill[169], J.C. Hill[29],
K.H. Hiller[43], S.J. Hillier[18], I. Hinchliffe[15], E. Hines[124], R.R. Hinman[15], M. Hirose[159],
D. Hirschbuehl[175], J. Hobbs[150], N. Hod[109], M.C. Hodgkinson[141], P. Hodgson[141], A. Hoecker[31],
M.R. Hoeferkamp[107], F. Hoenig[102], M. Hohlfeld[85], D. Hohn[22], T.R. Holmes[15], M. Homann[44],
T.M. Hong[127], B.H. Hooberman[166], W.H. Hopkins[118], Y. Horii[105], A.J. Horton[144],

J-Y. Hostachy[56], S. Hou[153], A. Hoummada[137a], J. Howard[122], J. Howarth[43], M. Hrabovsky[117],
I. Hristova[16], J. Hrivnac[119], T. Hryn'ova[5], A. Hrynevich[95], C. Hsu[147c], P.J. Hsu[153,t], S.-C. Hsu[140],
D. Hu[36], Q. Hu[34b], X. Hu[91], Y. Huang[43], Z. Hubacek[130], F. Hubaut[87], F. Huegging[22],
T.B. Huffman[122], E.W. Hughes[36], G. Hughes[74], M. Huhtinen[31], T.A. Hülsing[85], N. Huseynov[67,b],
J. Huston[92], J. Huth[58], G. Iacobucci[50], G. Iakovidis[26], I. Ibragimov[143], L. Iconomidou-Fayard[119],
E. Ideal[176], Z. Idrissi[137e], P. Iengo[31], O. Igonkina[109], T. Iizawa[171], Y. Ikegami[68], M. Ikeno[68],
Y. Ilchenko[32,u], D. Iliadis[156], N. Ilic[145], T. Ince[103], G. Introzzi[123a,123b], P. Ioannou[9,*],
M. Iodice[136a], K. Iordanidou[36], V. Ippolito[58], A. Irles Quiles[167], C. Isaksson[165], M. Ishino[70],
M. Ishitsuka[159], R. Ishmukhametov[113], C. Issever[122], S. Istin[19a], J.M. Iturbe Ponce[86],
R. Iuppa[135a,135b], J. Ivarsson[83], W. Iwanski[40], H. Iwasaki[68], J.M. Izen[42], V. Izzo[106a], S. Jabbar[3],
B. Jackson[124], M. Jackson[76], P. Jackson[1], M.R. Jaekel[31], V. Jain[2], K.B. Jakobi[85], K. Jakobs[49],
S. Jakobsen[31], T. Jakoubek[129], J. Jakubek[130], D.O. Jamin[116], D.K. Jana[81], E. Jansen[80],
R. Jansky[63], J. Janssen[22], M. Janus[55], G. Jarlskog[83], N. Javadov[67,b], T. Javůrek[49], L. Jeanty[15],
J. Jejelava[52a,v], G.-Y. Jeng[152], D. Jennens[90], P. Jenni[49,w], J. Jentzsch[44], C. Jeske[170],
S. Jézéquel[5], H. Ji[173], J. Jia[150], H. Jiang[65], Y. Jiang[34b], S. Jiggins[80], J. Jimenez Pena[167],
S. Jin[34a], A. Jinaru[27b], O. Jinnouchi[159], P. Johansson[141], K.A. Johns[7], W.J. Johnson[140],
K. Jon-And[148a,148b], G. Jones[170], R.W.L. Jones[74], T.J. Jones[76], J. Jongmanns[59a],
P.M. Jorge[128a,128b], K.D. Joshi[86], J. Jovicevic[161a], X. Ju[173], A. Juste Rozas[12,r], M.K. Köhler[172],
M. Kaci[167], A. Kaczmarska[40], M. Kado[119], H. Kagan[113], M. Kagan[145], S.J. Kahn[87],
E. Kajomovitz[46], C.W. Kalderon[122], A. Kaluza[85], S. Kama[41], A. Kamenshchikov[132],
N. Kanaya[157], S. Kaneti[29], V.A. Kantserov[100], J. Kanzaki[68], B. Kaplan[112], L.S. Kaplan[173],
A. Kapliy[32], D. Kar[147c], K. Karakostas[10], A. Karamaoun[3], N. Karastathis[10,109], M.J. Kareem[55],
E. Karentzos[10], M. Karnevskiy[85], S.N. Karpov[67], Z.M. Karpova[67], K. Karthik[112],
V. Kartvelishvili[74], A.N. Karyukhin[132], K. Kasahara[162], L. Kashif[173], R.D. Kass[113],
A. Kastanas[14], Y. Kataoka[157], C. Kato[157], A. Katre[50], J. Katzy[43], K. Kawade[105], K. Kawagoe[72],
T. Kawamoto[157], G. Kawamura[55], S. Kazama[157], V.F. Kazanin[111,c], R. Keeler[169], R. Kehoe[41],
J.S. Keller[43], J.J. Kempster[79], H. Keoshkerian[86], O. Kepka[129], B.P. Kerševan[77], S. Kersten[175],
R.A. Keyes[89], F. Khalil-zada[11], H. Khandanyan[148a,148b], A. Khanov[116], A.G. Kharlamov[111,c],
T.J. Khoo[29], V. Khovanskiy[99], E. Khramov[67], J. Khubua[52b,x], S. Kido[69], H.Y. Kim[8],
S.H. Kim[162], Y.K. Kim[32], N. Kimura[156], O.M. Kind[16], B.T. King[76], M. King[167], S.B. King[168],
J. Kirk[133], A.E. Kiryunin[103], T. Kishimoto[69], D. Kisielewska[39a], F. Kiss[49], K. Kiuchi[162],
O. Kivernyk[138], E. Kladiva[146b], M.H. Klein[36], M. Klein[76], U. Klein[76], K. Kleinknecht[85],
P. Klimek[148a,148b], A. Klimentov[26], R. Klingenberg[44], J.A. Klinger[141], T. Klioutchnikova[31],
E.-E. Kluge[59a], P. Kluit[109], S. Kluth[103], J. Knapik[40], E. Kneringer[63], E.B.F.G. Knoops[87],
A. Knue[54], A. Kobayashi[157], D. Kobayashi[159], T. Kobayashi[157], M. Kobel[45], M. Kocian[145],
P. Kodys[131], T. Koffas[30], E. Koffeman[109], L.A. Kogan[122], S. Kohlmann[175], Z. Kohout[130],
T. Kohriki[68], T. Koi[145], H. Kolanoski[16], M. Kolb[59b], I. Koletsou[5], A.A. Komar[98,*], Y. Komori[157],
T. Kondo[68], N. Kondrashova[43], K. Köneke[49], A.C. König[108], T. Kono[68,y], R. Konoplich[112,z],
N. Konstantinidis[80], R. Kopeliansky[154], S. Koperny[39a], L. Köpke[85], A.K. Kopp[49], K. Korcyl[40],
K. Kordas[156], A. Korn[80], A.A. Korol[111,c], I. Korolkov[12], E.V. Korolkova[141], O. Kortner[103],
S. Kortner[103], T. Kosek[131], V.V. Kostyukhin[22], V.M. Kotov[67], A. Kotwal[46],
A. Kourkoumeli-Charalampidi[156], C. Kourkoumelis[9], V. Kouskoura[26], A. Koutsman[161a],
R. Kowalewski[169], T.Z. Kowalski[39a], W. Kozanecki[138], A.S. Kozhin[132], V.A. Kramarenko[101],
G. Kramberger[77], D. Krasnopevtsev[100], M.W. Krasny[82], A. Krasznahorkay[31], J.K. Kraus[22],
A. Kravchenko[26], M. Kretz[59c], J. Kretzschmar[76], K. Kreutzfeldt[53], P. Krieger[160], K. Krizka[32],
K. Kroeninger[44], H. Kroha[103], J. Kroll[124], J. Kroseberg[22], J. Krstic[13], U. Kruchonak[67],
H. Krüger[22], N. Krumnack[65], A. Kruse[173], M.C. Kruse[46], M. Kruskal[23], T. Kubota[90], H. Kucuk[80],
S. Kuday[4b], S. Kuehn[49], A. Kugel[59c], F. Kuger[174], A. Kuhl[139], T. Kuhl[43], V. Kukhtin[67],

R. Kukla[138], Y. Kulchitsky[94], S. Kuleshov[33b], M. Kuna[134a,134b], T. Kunigo[70], A. Kupco[129],
H. Kurashige[69], Y.A. Kurochkin[94], V. Kus[129], E.S. Kuwertz[169], M. Kuze[159], J. Kvita[117],
T. Kwan[169], D. Kyriazopoulos[141], A. La Rosa[139], J.L. La Rosa Navarro[25d], L. La Rotonda[38a,38b],
C. Lacasta[167], F. Lacava[134a,134b], J. Lacey[30], H. Lacker[16], D. Lacour[82], V.R. Lacuesta[167],
E. Ladygin[67], R. Lafaye[5], B. Laforge[82], T. Lagouri[176], S. Lai[55], L. Lambourne[80], S. Lammers[62],
C.L. Lampen[7], W. Lampl[7], E. Lançon[138], U. Landgraf[49], M.P.J. Landon[78], V.S. Lang[59a],
J.C. Lange[12], A.J. Lankford[66], F. Lanni[26], K. Lantzsch[22], A. Lanza[123a], S. Laplace[82],
C. Lapoire[31], J.F. Laporte[138], T. Lari[93a], F. Lasagni Manghi[21a,21b], M. Lassnig[31], P. Laurelli[48],
W. Lavrijsen[15], A.T. Law[139], P. Laycock[76], T. Lazovich[58], O. Le Dortz[82], E. Le Guirriec[87],
E. Le Menedeu[12], M. LeBlanc[169], T. LeCompte[6], F. Ledroit-Guillon[56], C.A. Lee[147a], S.C. Lee[153],
L. Lee[1], G. Lefebvre[82], M. Lefebvre[169], F. Legger[102], C. Leggett[15], A. Lehan[76],
G. Lehmann Miotto[31], X. Lei[7], W.A. Leight[30], A. Leisos[156,aa], A.G. Leister[176], M.A.L. Leite[25d],
R. Leitner[131], D. Lellouch[172], B. Lemmer[55], K.J.C. Leney[80], T. Lenz[22], B. Lenzi[31], R. Leone[7],
S. Leone[126a,126b], C. Leonidopoulos[47], S. Leontsinis[10], C. Leroy[97], C.G. Lester[29],
M. Levchenko[125], J. Levêque[5], D. Levin[91], L.J. Levinson[172], M. Levy[18], A. Lewis[122],
A.M. Leyko[22], M. Leyton[42], B. Li[34b,ab], H. Li[150], H.L. Li[32], L. Li[46], L. Li[34e], S. Li[46], X. Li[86],
Y. Li[34c,ac], Z. Liang[139], H. Liao[35], B. Liberti[135a], A. Liblong[160], P. Lichard[31], K. Lie[166],
J. Liebal[22], W. Liebig[14], C. Limbach[22], A. Limosani[152], S.C. Lin[153,ad], T.H. Lin[85],
B.E. Lindquist[150], J.T. Linnemann[92], E. Lipeles[124], A. Lipniacka[14], M. Lisovyi[59b], T.M. Liss[166],
D. Lissauer[26], A. Lister[168], A.M. Litke[139], B. Liu[153,ae], D. Liu[153], H. Liu[91], H. Liu[26], J. Liu[87],
J.B. Liu[34b], K. Liu[87], L. Liu[166], M. Liu[46], M. Liu[34b], Y. Liu[34b], M. Livan[123a,123b], A. Lleres[56],
J. Llorente Merino[84], S.L. Lloyd[78], F. Lo Sterzo[153], E. Lobodzinska[43], P. Loch[7],
W.S. Lockman[139], F.K. Loebinger[86], A.E. Loevschall-Jensen[37], K.M. Loew[24], A. Loginov[176],
T. Lohse[16], K. Lohwasser[43], M. Lokajicek[129], B.A. Long[23], J.D. Long[166], R.E. Long[74],
K.A. Looper[113], L. Lopes[128a], D. Lopez Mateos[58], B. Lopez Paredes[141], I. Lopez Paz[12],
J. Lorenz[102], N. Lorenzo Martinez[62], M. Losada[20], P.J. Lösel[102], X. Lou[34a], A. Lounis[119],
J. Love[6], P.A. Love[74], H. Lu[61a], N. Lu[91], H.J. Lubatti[140], C. Luci[134a,134b], A. Lucotte[56],
C. Luedtke[49], F. Luehring[62], W. Lukas[63], L. Luminari[134a], O. Lundberg[148a,148b],
B. Lund-Jensen[149], D. Lynn[26], R. Lysak[129], E. Lytken[83], H. Ma[26], L.L. Ma[34d], G. Maccarrone[48],
A. Macchiolo[103], C.M. Macdonald[141], B. Maček[77], J. Machado Miguens[124,128b], D. Macina[31],
D. Madaffari[87], R. Madar[35], H.J. Maddocks[74], W.F. Mader[45], A. Madsen[43], J. Maeda[69],
S. Maeland[14], T. Maeno[26], A. Maevskiy[101], E. Magradze[55], K. Mahboubi[49], J. Mahlstedt[109],
C. Maiani[138], C. Maidantchik[25a], A.A. Maier[103], T. Maier[102], A. Maio[128a,128b,128d],
S. Majewski[118], Y. Makida[68], N. Makovec[119], B. Malaescu[82], Pa. Malecki[40], V.P. Maleev[125],
F. Malek[56], U. Mallik[64], D. Malon[6], C. Malone[145], S. Maltezos[10], V.M. Malyshev[111],
S. Malyukov[31], J. Mamuzic[43], G. Mancini[48], B. Mandelli[31], L. Mandelli[93a], I. Mandić[77],
J. Maneira[128a,128b], L. Manhaes de Andrade Filho[25b], J. Manjarres Ramos[161b], A. Mann[102],
A. Manousakis-Katsikakis[9], B. Mansoulie[138], R. Mantifel[89], M. Mantoani[55], S. Manzoni[93a,93b],
L. Mapelli[31], L. March[147c], G. Marchiori[82], M. Marcisovsky[129], M. Marjanovic[13], D.E. Marley[91],
F. Marroquim[25a], S.P. Marsden[86], Z. Marshall[15], L.F. Marti[17], S. Marti-Garcia[167], B. Martin[92],
T.A. Martin[170], V.J. Martin[47], B. Martin dit Latour[14], M. Martinez[12,r], S. Martin-Haugh[133],
V.S. Martoiu[27b], A.C. Martyniuk[80], M. Marx[140], F. Marzano[134a], A. Marzin[31], L. Masetti[85],
T. Mashimo[157], R. Mashinistov[98], J. Masik[86], A.L. Maslennikov[111,c], I. Massa[21a,21b],
L. Massa[21a,21b], P. Mastrandrea[5], A. Mastroberardino[38a,38b], T. Masubuchi[157], P. Mättig[175],
J. Mattmann[85], J. Maurer[27b], S.J. Maxfield[76], D.A. Maximov[111,c], R. Mazini[153],
S.M. Mazza[93a,93b], G. Mc Goldrick[160], S.P. Mc Kee[91], A. McCarn[91], R.L. McCarthy[150],
T.G. McCarthy[30], K.W. McFarlane[57,*], J.A. Mcfayden[80], G. Mchedlidze[55], S.J. McMahon[133],
R.A. McPherson[169,m], M. Medinnis[43], S. Meehan[140], S. Mehlhase[102], A. Mehta[76], K. Meier[59a],

C. Meineck[102], B. Meirose[42], B.R. Mellado Garcia[147c], F. Meloni[17], A. Mengarelli[21a,21b],
S. Menke[103], E. Meoni[163], K.M. Mercurio[58], S. Mergelmeyer[16], P. Mermod[50], L. Merola[106a,106b],
C. Meroni[93a], F.S. Merritt[32], A. Messina[134a,134b], J. Metcalfe[6], A.S. Mete[66], C. Meyer[85],
C. Meyer[124], J-P. Meyer[138], J. Meyer[109], H. Meyer Zu Theenhausen[59a], R.P. Middleton[133],
S. Miglioranzi[164a,164c], L. Mijović[22], G. Mikenberg[172], M. Mikestikova[129], M. Mikuž[77],
M. Milesi[90], A. Milic[31], D.W. Miller[32], C. Mills[47], A. Milov[172], D.A. Milstead[148a,148b],
A.A. Minaenko[132], Y. Minami[157], I.A. Minashvili[67], A.I. Mincer[112], B. Mindur[39a], M. Mineev[67],
Y. Ming[173], L.M. Mir[12], K.P. Mistry[124], T. Mitani[171], J. Mitrevski[102], V.A. Mitsou[167],
A. Miucci[50], P.S. Miyagawa[141], J.U. Mjörnmark[83], T. Moa[148a,148b], K. Mochizuki[87],
S. Mohapatra[36], W. Mohr[49], S. Molander[148a,148b], R. Moles-Valls[22], R. Monden[70],
M.C. Mondragon[92], K. Mönig[43], C. Monini[56], J. Monk[37], E. Monnier[87], A. Montalbano[150],
J. Montejo Berlingen[31], F. Monticelli[73], S. Monzani[134a,134b], R.W. Moore[3], N. Morange[119],
D. Moreno[20], M. Moreno Llácer[55], P. Morettini[51a], D. Mori[144], T. Mori[157], M. Morii[58],
M. Morinaga[157], V. Morisbak[121], S. Moritz[85], A.K. Morley[152], G. Mornacchi[31], J.D. Morris[78],
S.S. Mortensen[37], A. Morton[54], L. Morvaj[150], M. Mosidze[52b], J. Moss[145], K. Motohashi[159],
R. Mount[145], E. Mountricha[26], S.V. Mouraviev[98,*], E.J.W. Moyse[88], S. Muanza[87], R.D. Mudd[18],
F. Mueller[103], J. Mueller[127], R.S.P. Mueller[102], T. Mueller[29], D. Muenstermann[74], P. Mullen[54],
G.A. Mullier[17], F.J. Munoz Sanchez[86], J.A. Murillo Quijada[18], W.J. Murray[170,133],
H. Musheghyan[55], A.G. Myagkov[132,af], M. Myska[130], B.P. Nachman[145], O. Nackenhorst[50],
J. Nadal[55], K. Nagai[122], R. Nagai[159], Y. Nagai[87], K. Nagano[68], Y. Nagasaka[60], K. Nagata[162],
M. Nagel[103], E. Nagy[87], A.M. Nairz[31], Y. Nakahama[31], K. Nakamura[68], T. Nakamura[157],
I. Nakano[114], H. Namasivayam[42], R.F. Naranjo Garcia[43], R. Narayan[32], D.I. Narrias Villar[59a],
T. Naumann[43], G. Navarro[20], R. Nayyar[7], H.A. Neal[91], P.Yu. Nechaeva[98], T.J. Neep[86],
P.D. Nef[145], A. Negri[123a,123b], M. Negrini[21a], S. Nektarijevic[108], C. Nellist[119], A. Nelson[66],
S. Nemecek[129], P. Nemethy[112], A.A. Nepomuceno[25a], M. Nessi[31,ag], M.S. Neubauer[166],
M. Neumann[175], R.M. Neves[112], P. Nevski[26], P.R. Newman[18], D.H. Nguyen[6], R.B. Nickerson[122],
R. Nicolaidou[138], B. Nicquevert[31], J. Nielsen[139], N. Nikiforou[36], A. Nikiforov[16],
V. Nikolaenko[132,af], I. Nikolic-Audit[82], K. Nikolopoulos[18], J.K. Nilsen[121], P. Nilsson[26],
Y. Ninomiya[157], A. Nisati[134a], R. Nisius[103], T. Nobe[157], L. Nodulman[6], M. Nomachi[120],
I. Nomidis[30], T. Nooney[78], S. Norberg[115], M. Nordberg[31], O. Novgorodova[45], S. Nowak[103],
M. Nozaki[68], L. Nozka[117], K. Ntekas[10], E. Nurse[80], F. Nuti[90], F. O'grady[7], D.C. O'Neil[144],
V. O'Shea[54], F.G. Oakham[30,d], H. Oberlack[103], T. Obermann[22], J. Ocariz[82], A. Ochi[69],
I. Ochoa[36], J.P. Ochoa-Ricoux[33a], S. Oda[72], S. Odaka[68], H. Ogren[62], A. Oh[86], S.H. Oh[46],
C.C. Ohm[15], H. Ohman[165], H. Oide[31], W. Okamura[120], H. Okawa[162], Y. Okumura[32],
T. Okuyama[68], A. Olariu[27b], S.A. Olivares Pino[47], D. Oliveira Damazio[26], A. Olszewski[40],
J. Olszowska[40], A. Onofre[128a,128e], K. Onogi[105], P.U.E. Onyisi[32,u], C.J. Oram[161a], M.J. Oreglia[32],
Y. Oren[155], D. Orestano[136a,136b], N. Orlando[156], C. Oropeza Barrera[54], R.S. Orr[160],
B. Osculati[51a,51b], R. Ospanov[86], G. Otero y Garzon[28], H. Otono[72], M. Ouchrif[137d],
F. Ould-Saada[121], A. Ouraou[138], K.P. Oussoren[109], Q. Ouyang[34a], A. Ovcharova[15], M. Owen[54],
R.E. Owen[18], V.E. Ozcan[19a], N. Ozturk[8], K. Pachal[144], A. Pacheco Pages[12], C. Padilla Aranda[12],
M. Pagáčová[49], S. Pagan Griso[15], E. Paganis[141], F. Paige[26], P. Pais[88], K. Pajchel[121],
G. Palacino[161b], S. Palestini[31], M. Palka[39b], D. Pallin[35], A. Palma[128a,128b], Y.B. Pan[173],
E.St. Panagiotopoulou[10], C.E. Pandini[82], J.G. Panduro Vazquez[79], P. Pani[148a,148b], S. Panitkin[26],
D. Pantea[27b], L. Paolozzi[50], Th.D. Papadopoulou[10], K. Papageorgiou[156], A. Paramonov[6],
D. Paredes Hernandez[176], M.A. Parker[29], K.A. Parker[141], F. Parodi[51a,51b], J.A. Parsons[36],
U. Parzefall[49], V. Pascuzzi[160], E. Pasqualucci[134a], S. Passaggio[51a], F. Pastore[136a,136b,*],
Fr. Pastore[79], G. Pásztor[30], S. Pataraia[175], N.D. Patel[152], J.R. Pater[86], T. Pauly[31], J. Pearce[169],
B. Pearson[115], L.E. Pedersen[37], M. Pedersen[121], S. Pedraza Lopez[167], R. Pedro[128a,128b],

S.V. Peleganchuk[111,c], D. Pelikan[165], O. Penc[129], C. Peng[34a], H. Peng[34b], B. Penning[32], J. Penwell[62], D.V. Perepelitsa[26], E. Perez Codina[161a], M.T. Pérez García-Estañ[167], L. Perini[93a,93b], H. Pernegger[31], S. Perrella[106a,106b], R. Peschke[43], V.D. Peshekhonov[67], K. Peters[31], R.F.Y. Peters[86], B.A. Petersen[31], T.C. Petersen[37], E. Petit[43], A. Petridis[1], C. Petridou[156], P. Petroff[119], E. Petrolo[134a], F. Petrucci[136a,136b], N.E. Pettersson[159], R. Pezoa[33b], P.W. Phillips[133], G. Piacquadio[145], E. Pianori[170], A. Picazio[88], E. Piccaro[78], M. Piccinini[21a,21b], M.A. Pickering[122], R. Piegaia[28], D.T. Pignotti[113], J.E. Pilcher[32], A.D. Pilkington[86], A.W.J. Pin[86], J. Pina[128a,128b,128d], M. Pinamonti[164a,164c,ah], J.L. Pinfold[3], A. Pingel[37], S. Pires[82], H. Pirumov[43], M. Pitt[172], C. Pizio[93a,93b], L. Plazak[146a], M.-A. Pleier[26], V. Pleskot[85], E. Plotnikova[67], P. Plucinski[148a,148b], D. Pluth[65], R. Poettgen[148a,148b], L. Poggioli[119], D. Pohl[22], G. Polesello[123a], A. Poley[43], A. Policicchio[38a,38b], R. Polifka[160], A. Polini[21a], C.S. Pollard[54], V. Polychronakos[26], K. Pommès[31], L. Pontecorvo[134a], B.G. Pope[92], G.A. Popeneciu[27c], D.S. Popovic[13], A. Poppleton[31], S. Pospisil[130], K. Potamianos[15], I.N. Potrap[67], C.J. Potter[29], C.T. Potter[118], G. Poulard[31], J. Poveda[31], V. Pozdnyakov[67], M.E. Pozo Astigarraga[31], P. Pralavorio[87], A. Pranko[15], S. Prasad[31], S. Prell[65], D. Price[86], L.E. Price[6], M. Primavera[75a], S. Prince[89], M. Proissl[47], K. Prokofiev[61c], F. Prokoshin[33b], E. Protopapadaki[138], S. Protopopescu[26], J. Proudfoot[6], M. Przybycien[39a], D. Puddu[136a,136b], E. Pueschel[88], D. Puldon[150], M. Purohit[26,ai], P. Puzo[119], J. Qian[91], G. Qin[54], Y. Qin[86], A. Quadt[55], D.R. Quarrie[15], W.B. Quayle[164a,164b], M. Queitsch-Maitland[86], D. Quilty[54], S. Raddum[121], V. Radeka[26], V. Radescu[43], S.K. Radhakrishnan[150], P. Radloff[118], P. Rados[90], F. Ragusa[93a,93b], G. Rahal[178], S. Rajagopalan[26], M. Rammensee[31], C. Rangel-Smith[165], F. Rauscher[102], S. Rave[85], T. Ravenscroft[54], M. Raymond[31], A.L. Read[121], N.P. Readioff[76], D.M. Rebuzzi[123a,123b], A. Redelbach[174], G. Redlinger[26], R. Reece[139], K. Reeves[42], L. Rehnisch[16], J. Reichert[124], H. Reisin[28], C. Rembser[31], H. Ren[34a], M. Rescigno[134a], S. Resconi[93a], O.L. Rezanova[111,c], P. Reznicek[131], R. Rezvani[97], R. Richter[103], S. Richter[80], E. Richter-Was[39b], O. Ricken[22], M. Ridel[82], P. Rieck[16], C.J. Riegel[175], J. Rieger[55], O. Rifki[115], M. Rijssenbeek[150], A. Rimoldi[123a,123b], L. Rinaldi[21a], B. Ristić[50], E. Ritsch[31], I. Riu[12], F. Rizatdinova[116], E. Rizvi[78], S.H. Robertson[89,m], A. Robichaud-Veronneau[89], D. Robinson[29], J.E.M. Robinson[43], A. Robson[54], C. Roda[126a,126b], A. Rodriguez Perez[12], S. Roe[31], C.S. Rogan[58], O. Røhne[121], A. Romaniouk[100], M. Romano[21a,21b], S.M. Romano Saez[35], E. Romero Adam[167], N. Rompotis[140], M. Ronzani[49], L. Roos[82], E. Ros[167], S. Rosati[134a], K. Rosbach[49], P. Rose[139], O. Rosenthal[143], V. Rossetti[148a,148b], E. Rossi[106a,106b], L.P. Rossi[51a], J.H.N. Rosten[29], R. Rosten[140], M. Rotaru[27b], I. Roth[172], J. Rothberg[140], D. Rousseau[119], C.R. Royon[138], A. Rozanov[87], Y. Rozen[154], X. Ruan[147c], F. Rubbo[145], I. Rubinskiy[43], V.I. Rud[101], C. Rudolph[45], M.S. Rudolph[160], F. Rühr[49], A. Ruiz-Martinez[31], Z. Rurikova[49], N.A. Rusakovich[67], A. Ruschke[102], H.L. Russell[140], J.P. Rutherfoord[7], N. Ruthmann[31], Y.F. Ryabov[125], M. Rybar[166], G. Rybkin[119], N.C. Ryder[122], A. Ryzhov[132], A.F. Saavedra[152], G. Sabato[109], S. Sacerdoti[28], H.F-W. Sadrozinski[139], R. Sadykov[67], F. Safai Tehrani[134a], P. Saha[110], M. Sahinsoy[59a], M. Saimpert[138], T. Saito[157], H. Sakamoto[157], Y. Sakurai[171], G. Salamanna[136a,136b], A. Salamon[135a], J.E. Salazar Loyola[33b], M. Saleem[115], D. Salek[109], P.H. Sales De Bruin[140], D. Salihagic[103], A. Salnikov[145], J. Salt[167], D. Salvatore[38a,38b], F. Salvatore[151], A. Salvucci[61a], A. Salzburger[31], D. Sammel[49], D. Sampsonidis[156], A. Sanchez[106a,106b], J. Sánchez[167], V. Sanchez Martinez[167], H. Sandaker[121], R.L. Sandbach[78], H.G. Sander[85], M.P. Sanders[102], M. Sandhoff[175], C. Sandoval[20], R. Sandstroem[103], D.P.C. Sankey[133], M. Sannino[51a,51b], A. Sansoni[48], C. Santoni[35], R. Santonico[135a,135b], H. Santos[128a], I. Santoyo Castillo[151], K. Sapp[127], A. Sapronov[67], J.G. Saraiva[128a,128d], B. Sarrazin[22], O. Sasaki[68], Y. Sasaki[157], K. Sato[162], G. Sauvage[5,*], E. Sauvan[5], G. Savage[79], P. Savard[160,d], C. Sawyer[133], L. Sawyer[81,q], J. Saxon[32], C. Sbarra[21a], A. Sbrizzi[21a,21b], T. Scanlon[80], D.A. Scannicchio[66], M. Scarcella[152], V. Scarfone[38a,38b],

J. Schaarschmidt[172], P. Schacht[103], D. Schaefer[31], R. Schaefer[43], J. Schaeffer[85], S. Schaepe[22],
S. Schaetzel[59b], U. Schäfer[85], A.C. Schaffer[119], D. Schaile[102], R.D. Schamberger[150], V. Scharf[59a],
V.A. Schegelsky[125], D. Scheirich[131], M. Schernau[66], C. Schiavi[51a,51b], C. Schillo[49],
M. Schioppa[38a,38b], S. Schlenker[31], K. Schmieden[31], C. Schmitt[85], S. Schmitt[59b], S. Schmitt[43],
S. Schmitz[85], B. Schneider[161a], Y.J. Schnellbach[76], U. Schnoor[49], L. Schoeffel[138], A. Schoening[59b],
B.D. Schoenrock[92], E. Schopf[22], A.L.S. Schorlemmer[55], M. Schott[85], D. Schouten[161a],
J. Schovancova[8], S. Schramm[50], M. Schreyer[174], N. Schuh[85], M.J. Schultens[22],
H.-C. Schultz-Coulon[59a], H. Schulz[16], M. Schumacher[49], B.A. Schumm[139], Ph. Schune[138],
C. Schwanenberger[86], A. Schwartzman[145], T.A. Schwarz[91], Ph. Schwegler[103], H. Schweiger[86],
Ph. Schwemling[138], R. Schwienhorst[92], J. Schwindling[138], T. Schwindt[22], E. Scifo[119], G. Sciolla[24],
F. Scuri[126a,126b], F. Scutti[90], J. Searcy[91], G. Sedov[43], P. Seema[22], S.C. Seidel[107], A. Seiden[139],
F. Seifert[130], J.M. Seixas[25a], G. Sekhniaidze[106a], K. Sekhon[91], S.J. Sekula[41],
D.M. Seliverstov[125,*], N. Semprini-Cesari[21a,21b], C. Serfon[31], L. Serin[119], L. Serkin[164a,164b],
M. Sessa[136a,136b], R. Seuster[161a], H. Severini[115], T. Sfiligoj[77], F. Sforza[31], A. Sfyrla[50],
E. Shabalina[55], L.Y. Shan[34a], R. Shang[166], J.T. Shank[23], M. Shapiro[15], P.B. Shatalov[99],
K. Shaw[164a,164b], S.M. Shaw[86], A. Shcherbakova[148a,148b], C.Y. Shehu[151], P. Sherwood[80],
L. Shi[153,aj], S. Shimizu[69], C.O. Shimmin[66], M. Shimojima[104], M. Shiyakova[67,ak], A. Shmeleva[98],
D. Shoaleh Saadi[97], M.J. Shochet[32], S. Shojaii[93a,93b], S. Shrestha[113], E. Shulga[100], M.A. Shupe[7],
P. Sicho[129], P.E. Sidebo[149], O. Sidiropoulou[174], D. Sidorov[116], A. Sidoti[21a,21b], F. Siegert[45],
Dj. Sijacki[13], J. Silva[128a,128d], S.B. Silverstein[148a], V. Simak[130], O. Simard[5], Lj. Simic[13],
S. Simion[119], E. Simioni[85], B. Simmons[80], D. Simon[35], M. Simon[85], P. Sinervo[160], N.B. Sinev[118],
M. Sioli[21a,21b], G. Siragusa[174], S.Yu. Sivoklokov[101], J. Sjölin[148a,148b], T.B. Sjursen[14],
M.B. Skinner[74], H.P. Skottowe[58], P. Skubic[115], M. Slater[18], T. Slavicek[130], M. Slawinska[109],
K. Sliwa[163], V. Smakhtin[172], B.H. Smart[47], L. Smestad[14], S.Yu. Smirnov[100], Y. Smirnov[100],
L.N. Smirnova[101,al], O. Smirnova[83], M.N.K. Smith[36], R.W. Smith[36], M. Smizanska[74],
K. Smolek[130], A.A. Snesarev[98], G. Snidero[78], S. Snyder[26], R. Sobie[169,m], F. Socher[45],
A. Soffer[155], D.A. Soh[153,aj], G. Sokhrannyi[77], C.A. Solans Sanchez[31], M. Solar[130], J. Solc[130],
E.Yu. Soldatov[100], U. Soldevila[167], A.A. Solodkov[132], A. Soloshenko[67], O.V. Solovyanov[132],
V. Solovyev[125], P. Sommer[49], H.Y. Song[34b,ab], N. Soni[1], A. Sood[15], A. Sopczak[130], B. Sopko[130],
V. Sopko[130], V. Sorin[12], D. Sosa[59b], M. Sosebee[8], C.L. Sotiropoulou[126a,126b], R. Soualah[164a,164c],
A.M. Soukharev[111,c], D. South[43], B.C. Sowden[79], S. Spagnolo[75a,75b], M. Spalla[126a,126b],
M. Spangenberg[170], F. Spanò[79], W.R. Spearman[58], D. Sperlich[16], F. Spettel[103], R. Spighi[21a],
G. Spigo[31], L.A. Spiller[90], M. Spousta[131], R.D. St. Denis[54,*], A. Stabile[93a], S. Staerz[31],
J. Stahlman[124], R. Stamen[59a], S. Stamm[16], E. Stanecka[40], R.W. Stanek[6], C. Stanescu[136a],
M. Stanescu-Bellu[43], M.M. Stanitzki[43], S. Stapnes[121], E.A. Starchenko[132], J. Stark[56],
P. Staroba[129], P. Starovoitov[59a], R. Staszewski[40], P. Steinberg[26], B. Stelzer[144], H.J. Stelzer[31],
O. Stelzer-Chilton[161a], H. Stenzel[53], G.A. Stewart[54], J.A. Stillings[22], M.C. Stockton[89],
M. Stoebe[89], G. Stoicea[27b], P. Stolte[55], S. Stonjek[103], A.R. Stradling[8], A. Straessner[45],
M.E. Stramaglia[17], J. Strandberg[149], S. Strandberg[148a,148b], A. Strandlie[121], M. Strauss[115],
P. Strizenec[146b], R. Ströhmer[174], D.M. Strom[118], R. Stroynowski[41], A. Strubig[108], S.A. Stucci[17],
B. Stugu[14], N.A. Styles[43], D. Su[145], J. Su[127], R. Subramaniam[81], S. Suchek[59a], Y. Sugaya[120],
M. Suk[130], V.V. Sulin[98], S. Sultansoy[4c], T. Sumida[70], S. Sun[58], X. Sun[34a], J.E. Sundermann[49],
K. Suruliz[151], G. Susinno[38a,38b], M.R. Sutton[151], S. Suzuki[68], M. Svatos[129], M. Swiatlowski[32],
I. Sykora[146a], T. Sykora[131], D. Ta[49], C. Taccini[136a,136b], K. Tackmann[43], J. Taenzer[160],
A. Taffard[66], R. Tafirout[161a], N. Taiblum[155], H. Takai[26], R. Takashima[71], H. Takeda[69],
T. Takeshita[142], Y. Takubo[68], M. Talby[87], A.A. Talyshev[111,c], J.Y.C. Tam[174], K.G. Tan[90],
J. Tanaka[157], R. Tanaka[119], S. Tanaka[68], B.B. Tannenwald[113], S. Tapia Araya[33b], S. Tapprogge[85],
S. Tarem[154], F. Tarrade[30], G.F. Tartarelli[93a], P. Tas[131], M. Tasevsky[129], T. Tashiro[70],

E. Tassi[38a,38b], A. Tavares Delgado[128a,128b], Y. Tayalati[137d], A.C. Taylor[107], F.E. Taylor[96], G.N. Taylor[90], P.T.E. Taylor[90], W. Taylor[161b], F.A. Teischinger[31], P. Teixeira-Dias[79], K.K. Temming[49], D. Temple[144], H. Ten Kate[31], P.K. Teng[153], J.J. Teoh[120], F. Tepel[175], S. Terada[68], K. Terashi[157], J. Terron[84], S. Terzo[103], M. Testa[48], R.J. Teuscher[160,m], T. Theveneaux-Pelzer[87], J.P. Thomas[18], J. Thomas-Wilsker[79], E.N. Thompson[36], P.D. Thompson[18], R.J. Thompson[86], A.S. Thompson[54], L.A. Thomsen[176], E. Thomson[124], M. Thomson[29], M.J. Tibbetts[15], R.E. Ticse Torres[87], V.O. Tikhomirov[98,am], Yu.A. Tikhonov[111,c], S. Timoshenko[100], E. Tiouchichine[87], P. Tipton[176], S. Tisserant[87], K. Todome[159], T. Todorov[5,*], S. Todorova-Nova[131], J. Tojo[72], S. Tokár[146a], K. Tokushuku[68], K. Tollefson[92], E. Tolley[58], L. Tomlinson[86], M. Tomoto[105], L. Tompkins[145,an], K. Toms[107], E. Torrence[118], H. Torres[144], E. Torró Pastor[140], J. Toth[87,ao], F. Touchard[87], D.R. Tovey[141], T. Trefzger[174], L. Tremblet[31], A. Tricoli[31], I.M. Trigger[161a], S. Trincaz-Duvoid[82], M.F. Tripiana[12], W. Trischuk[160], B. Trocmé[56], C. Troncon[93a], M. Trottier-McDonald[15], M. Trovatelli[169], L. Truong[164a,164c], M. Trzebinski[40], A. Trzupek[40], C. Tsarouchas[31], J.C-L. Tseng[122], P.V. Tsiareshka[94], D. Tsionou[156], G. Tsipolitis[10], N. Tsirintanis[9], S. Tsiskaridze[12], V. Tsiskaridze[49], E.G. Tskhadadze[52a], K.M. Tsui[61a], I.I. Tsukerman[99], V. Tsulaia[15], S. Tsuno[68], D. Tsybychev[150], A. Tudorache[27b], V. Tudorache[27b], A.N. Tuna[58], S.A. Tupputi[21a,21b], S. Turchikhin[101,al], D. Turecek[130], D. Turgeman[172], R. Turra[93a,93b], A.J. Turvey[41], P.M. Tuts[36], A. Tykhonov[50], M. Tylmad[148a,148b], M. Tyndel[133], I. Ueda[157], R. Ueno[30], M. Ughetto[148a,148b], F. Ukegawa[162], G. Unal[31], A. Undrus[26], G. Unel[66], F.C. Ungaro[90], Y. Unno[68], C. Unverdorben[102], J. Urban[146b], P. Urquijo[90], P. Urrejola[85], G. Usai[8], A. Usanova[63], L. Vacavant[87], V. Vacek[130], B. Vachon[89], C. Valderanis[85], N. Valencic[109], S. Valentinetti[21a,21b], A. Valero[167], L. Valery[12], S. Valkar[131], S. Vallecorsa[50], J.A. Valls Ferrer[167], W. Van Den Wollenberg[109], P.C. Van Der Deijl[109], R. van der Geer[109], H. van der Graaf[109], N. van Eldik[154], P. van Gemmeren[6], J. Van Nieuwkoop[144], I. van Vulpen[109], M.C. van Woerden[31], M. Vanadia[134a,134b], W. Vandelli[31], R. Vanguri[124], A. Vaniachine[6], F. Vannucci[82], G. Vardanyan[177], R. Vari[134a], E.W. Varnes[7], T. Varol[41], D. Varouchas[82], A. Vartapetian[8], K.E. Varvell[152], F. Vazeille[35], T. Vazquez Schroeder[89], J. Veatch[7], L.M. Veloce[160], F. Veloso[128a,128c], T. Velz[22], S. Veneziano[134a], A. Ventura[75a,75b], D. Ventura[88], M. Venturi[169], N. Venturi[160], A. Venturini[24], V. Vercesi[123a], M. Verducci[134a,134b], W. Verkerke[109], J.C. Vermeulen[109], A. Vest[45,ap], M.C. Vetterli[144,d], O. Viazlo[83], I. Vichou[166], T. Vickey[141], O.E. Vickey Boeriu[141], G.H.A. Viehhauser[122], S. Viel[15], R. Vigne[63], M. Villa[21a,21b], M. Villaplana Perez[93a,93b], E. Vilucchi[48], M.G. Vincter[30], V.B. Vinogradov[67], I. Vivarelli[151], S. Vlachos[10], D. Vladoiu[102], M. Vlasak[130], M. Vogel[33a], P. Vokac[130], G. Volpi[126a,126b], M. Volpi[90], H. von der Schmitt[103], H. von Radziewski[49], E. von Toerne[22], V. Vorobel[131], K. Vorobev[100], M. Vos[167], R. Voss[31], J.H. Vossebeld[76], N. Vranjes[13], M. Vranjes Milosavljevic[13], V. Vrba[129], M. Vreeswijk[109], R. Vuillermet[31], I. Vukotic[32], Z. Vykydal[130], P. Wagner[22], W. Wagner[175], H. Wahlberg[73], S. Wahrmund[45], J. Wakabayashi[105], J. Walder[74], R. Walker[102], W. Walkowiak[143], V. Wallangen[148a,148b], C. Wang[153], F. Wang[173], H. Wang[15], H. Wang[41], J. Wang[43], J. Wang[152], K. Wang[89], R. Wang[6], S.M. Wang[153], T. Wang[22], T. Wang[36], X. Wang[176], C. Wanotayaroj[118], A. Warburton[89], C.P. Ward[29], D.R. Wardrope[80], A. Washbrook[47], C. Wasicki[43], P.M. Watkins[18], A.T. Watson[18], I.J. Watson[152], M.F. Watson[18], G. Watts[140], S. Watts[86], B.M. Waugh[80], S. Webb[86], M.S. Weber[17], S.W. Weber[174], J.S. Webster[6], A.R. Weidberg[122], B. Weinert[62], J. Weingarten[55], C. Weiser[49], H. Weits[109], P.S. Wells[31], T. Wenaus[26], T. Wengler[31], S. Wenig[31], N. Wermes[22], M. Werner[49], P. Werner[31], M. Wessels[59a], J. Wetter[163], K. Whalen[118], A.M. Wharton[74], A. White[8], M.J. White[1], R. White[33b], S. White[126a,126b], D. Whiteson[66], F.J. Wickens[133], W. Wiedenmann[173], M. Wielers[133], P. Wienemann[22], C. Wiglesworth[37], L.A.M. Wiik-Fuchs[22], A. Wildauer[103], H.G. Wilkens[31], H.H. Williams[124], S. Williams[109],

C. Willis[92], S. Willocq[88], J.A. Wilson[18], I. Wingerter-Seez[5], F. Winklmeier[118], B.T. Winter[22], M. Wittgen[145], J. Wittkowski[102], S.J. Wollstadt[85], M.W. Wolter[40], H. Wolters[128a,128c], B.K. Wosiek[40], J. Wotschack[31], M.J. Woudstra[86], K.W. Wozniak[40], M. Wu[56], M. Wu[32], S.L. Wu[173], X. Wu[50], Y. Wu[91], T.R. Wyatt[86], B.M. Wynne[47], S. Xella[37], D. Xu[34a], L. Xu[26], B. Yabsley[152], S. Yacoob[147a], R. Yakabe[69], M. Yamada[68], D. Yamaguchi[159], Y. Yamaguchi[120], A. Yamamoto[68], S. Yamamoto[157], T. Yamanaka[157], K. Yamauchi[105], Y. Yamazaki[69], Z. Yan[23], H. Yang[34e], H. Yang[173], Y. Yang[153], Z. Yang[14], W-M. Yao[15], Y.C. Yap[82], Y. Yasu[68], E. Yatsenko[5], K.H. Yau Wong[22], J. Ye[41], S. Ye[26], I. Yeletskikh[67], A.L. Yen[58], E. Yildirim[43], K. Yorita[171], R. Yoshida[6], K. Yoshihara[124], C. Young[145], C.J.S. Young[31], S. Youssef[23], D.R. Yu[15], J. Yu[8], J.M. Yu[91], J. Yu[65], L. Yuan[69], S.P.Y. Yuen[22], A. Yurkewicz[110], I. Yusuff[29,aq], B. Zabinski[40], R. Zaidan[34d], A.M. Zaitsev[132,af], J. Zalieckas[14], A. Zaman[150], S. Zambito[58], L. Zanello[134a,134b], D. Zanzi[90], C. Zeitnitz[175], M. Zeman[130], A. Zemla[39a], J.C. Zeng[166], Q. Zeng[145], K. Zengel[24], O. Zenin[132], T. Ženiš[146a], D. Zerwas[119], D. Zhang[91], F. Zhang[173], G. Zhang[34b,ab], H. Zhang[34c], J. Zhang[6], L. Zhang[49], R. Zhang[34b,k], X. Zhang[34d], Z. Zhang[119], X. Zhao[41], Y. Zhao[34d,119], Z. Zhao[34b], A. Zhemchugov[67], J. Zhong[122], B. Zhou[91], C. Zhou[46], L. Zhou[36], L. Zhou[41], M. Zhou[150], N. Zhou[34f], C.G. Zhu[34d], H. Zhu[34a], J. Zhu[91], Y. Zhu[34b], X. Zhuang[34a], K. Zhukov[98], A. Zibell[174], D. Zieminska[62], N.I. Zimine[67], C. Zimmermann[85], S. Zimmermann[49], Z. Zinonos[55], M. Zinser[85], M. Ziolkowski[143], L. Živković[13], G. Zobernig[173], A. Zoccoli[21a,21b], M. zur Nedden[16], G. Zurzolo[106a,106b] and L. Zwalinski[31]

1   Department of Physics, University of Adelaide, Adelaide, Australia
2   Physics Department, SUNY Albany, Albany NY, United States of America
3   Department of Physics, University of Alberta, Edmonton AB, Canada
4   [a] Department of Physics, Ankara University, Ankara; [b] Istanbul Aydin University, Istanbul; [c] Division of Physics, TOBB University of Economics and Technology, Ankara, Turkey
5   LAPP, CNRS/IN2P3 and Université Savoie Mont Blanc, Annecy-le-Vieux, France
6   High Energy Physics Division, Argonne National Laboratory, Argonne IL, United States of America
7   Department of Physics, University of Arizona, Tucson AZ, United States of America
8   Department of Physics, The University of Texas at Arlington, Arlington TX, United States of America
9   Physics Department, University of Athens, Athens, Greece
10 Physics Department, National Technical University of Athens, Zografou, Greece
11 Institute of Physics, Azerbaijan Academy of Sciences, Baku, Azerbaijan
12 Institut de Física d'Altes Energies (IFAE), The Barcelona Institute of Science and Technology, Barcelona, Spain, Spain
13 Institute of Physics, University of Belgrade, Belgrade, Serbia
14 Department for Physics and Technology, University of Bergen, Bergen, Norway
15 Physics Division, Lawrence Berkeley National Laboratory and University of California, Berkeley CA, United States of America
16 Department of Physics, Humboldt University, Berlin, Germany
17 Albert Einstein Center for Fundamental Physics and Laboratory for High Energy Physics, University of Bern, Bern, Switzerland
18 School of Physics and Astronomy, University of Birmingham, Birmingham, United Kingdom
19 [a] Department of Physics, Bogazici University, Istanbul; [b] Department of Physics Engineering, Gaziantep University, Gaziantep; [c] Department of Physics, Dogus University, Istanbul, Turkey
20 Centro de Investigaciones, Universidad Antonio Narino, Bogota, Colombia
21 [a] INFN Sezione di Bologna; [b] Dipartimento di Fisica e Astronomia, Università di Bologna, Bologna, Italy
22 Physikalisches Institut, University of Bonn, Bonn, Germany
23 Department of Physics, Boston University, Boston MA, United States of America
24 Department of Physics, Brandeis University, Waltham MA, United States of America

25 $^{(a)}$ *Universidade Federal do Rio De Janeiro COPPE/EE/IF, Rio de Janeiro;* $^{(b)}$ *Electrical Circuits Department, Federal University of Juiz de Fora (UFJF), Juiz de Fora;* $^{(c)}$ *Federal University of Sao Joao del Rei (UFSJ), Sao Joao del Rei;* $^{(d)}$ *Instituto de Fisica, Universidade de Sao Paulo, Sao Paulo, Brazil*

26 *Physics Department, Brookhaven National Laboratory, Upton NY, United States of America*

27 $^{(a)}$ *Transilvania University of Brasov, Brasov, Romania;* $^{(b)}$ *National Institute of Physics and Nuclear Engineering, Bucharest;* $^{(c)}$ *National Institute for Research and Development of Isotopic and Molecular Technologies, Physics Department, Cluj Napoca;* $^{(d)}$ *University Politehnica Bucharest, Bucharest;* $^{(e)}$ *West University in Timisoara, Timisoara, Romania*

28 *Departamento de Física, Universidad de Buenos Aires, Buenos Aires, Argentina*

29 *Cavendish Laboratory, University of Cambridge, Cambridge, United Kingdom*

30 *Department of Physics, Carleton University, Ottawa ON, Canada*

31 *CERN, Geneva, Switzerland*

32 *Enrico Fermi Institute, University of Chicago, Chicago IL, United States of America*

33 $^{(a)}$ *Departamento de Física, Pontificia Universidad Católica de Chile, Santiago;* $^{(b)}$ *Departamento de Física, Universidad Técnica Federico Santa María, Valparaíso, Chile*

34 $^{(a)}$ *Institute of High Energy Physics, Chinese Academy of Sciences, Beijing;* $^{(b)}$ *Department of Modern Physics, University of Science and Technology of China, Anhui;* $^{(c)}$ *Department of Physics, Nanjing University, Jiangsu;* $^{(d)}$ *School of Physics, Shandong University, Shandong;* $^{(e)}$ *Department of Physics and Astronomy, Shanghai Key Laboratory for Particle Physics and Cosmology, Shanghai Jiao Tong University, Shanghai; (also affiliated with PKU-CHEP);* $^{(f)}$ *Physics Department, Tsinghua University, Beijing 100084, China*

35 *Laboratoire de Physique Corpusculaire, Clermont Université and Université Blaise Pascal and CNRS/IN2P3, Clermont-Ferrand, France*

36 *Nevis Laboratory, Columbia University, Irvington NY, United States of America*

37 *Niels Bohr Institute, University of Copenhagen, Kobenhavn, Denmark*

38 $^{(a)}$ *INFN Gruppo Collegato di Cosenza, Laboratori Nazionali di Frascati;* $^{(b)}$ *Dipartimento di Fisica, Università della Calabria, Rende, Italy*

39 $^{(a)}$ *AGH University of Science and Technology, Faculty of Physics and Applied Computer Science, Krakow;* $^{(b)}$ *Marian Smoluchowski Institute of Physics, Jagiellonian University, Krakow, Poland*

40 *Institute of Nuclear Physics Polish Academy of Sciences, Krakow, Poland*

41 *Physics Department, Southern Methodist University, Dallas TX, United States of America*

42 *Physics Department, University of Texas at Dallas, Richardson TX, United States of America*

43 *DESY, Hamburg and Zeuthen, Germany*

44 *Institut für Experimentelle Physik IV, Technische Universität Dortmund, Dortmund, Germany*

45 *Institut für Kern- und Teilchenphysik, Technische Universität Dresden, Dresden, Germany*

46 *Department of Physics, Duke University, Durham NC, United States of America*

47 *SUPA - School of Physics and Astronomy, University of Edinburgh, Edinburgh, United Kingdom*

48 *INFN Laboratori Nazionali di Frascati, Frascati, Italy*

49 *Fakultät für Mathematik und Physik, Albert-Ludwigs-Universität, Freiburg, Germany*

50 *Section de Physique, Université de Genève, Geneva, Switzerland*

51 $^{(a)}$ *INFN Sezione di Genova;* $^{(b)}$ *Dipartimento di Fisica, Università di Genova, Genova, Italy*

52 $^{(a)}$ *E. Andronikashvili Institute of Physics, Iv. Javakhishvili Tbilisi State University, Tbilisi;* $^{(b)}$ *High Energy Physics Institute, Tbilisi State University, Tbilisi, Georgia*

53 *II Physikalisches Institut, Justus-Liebig-Universität Giessen, Giessen, Germany*

54 *SUPA - School of Physics and Astronomy, University of Glasgow, Glasgow, United Kingdom*

55 *II Physikalisches Institut, Georg-August-Universität, Göttingen, Germany*

56 *Laboratoire de Physique Subatomique et de Cosmologie, Université Grenoble-Alpes, CNRS/IN2P3, Grenoble, France*

57 *Department of Physics, Hampton University, Hampton VA, United States of America*

58 *Laboratory for Particle Physics and Cosmology, Harvard University, Cambridge MA, United States of America*

59 [a] *Kirchhoff-Institut für Physik, Ruprecht-Karls-Universität Heidelberg, Heidelberg;* [b] *Physikalisches Institut, Ruprecht-Karls-Universität Heidelberg, Heidelberg;* [c] *ZITI Institut für technische Informatik, Ruprecht-Karls-Universität Heidelberg, Mannheim, Germany*

60 *Faculty of Applied Information Science, Hiroshima Institute of Technology, Hiroshima, Japan*

61 [a] *Department of Physics, The Chinese University of Hong Kong, Shatin, N.T., Hong Kong;* [b] *Department of Physics, The University of Hong Kong, Hong Kong;* [c] *Department of Physics, The Hong Kong University of Science and Technology, Clear Water Bay, Kowloon, Hong Kong, China*

62 *Department of Physics, Indiana University, Bloomington IN, United States of America*

63 *Institut für Astro- und Teilchenphysik, Leopold-Franzens-Universität, Innsbruck, Austria*

64 *University of Iowa, Iowa City IA, United States of America*

65 *Department of Physics and Astronomy, Iowa State University, Ames IA, United States of America*

66 *Department of Physics and Astronomy, University of California Irvine, Irvine CA, United States of America*

67 *Joint Institute for Nuclear Research, JINR Dubna, Dubna, Russia*

68 *KEK, High Energy Accelerator Research Organization, Tsukuba, Japan*

69 *Graduate School of Science, Kobe University, Kobe, Japan*

70 *Faculty of Science, Kyoto University, Kyoto, Japan*

71 *Kyoto University of Education, Kyoto, Japan*

72 *Department of Physics, Kyushu University, Fukuoka, Japan*

73 *Instituto de Física La Plata, Universidad Nacional de La Plata and CONICET, La Plata, Argentina*

74 *Physics Department, Lancaster University, Lancaster, United Kingdom*

75 [a] *INFN Sezione di Lecce;* [b] *Dipartimento di Matematica e Fisica, Università del Salento, Lecce, Italy*

76 *Oliver Lodge Laboratory, University of Liverpool, Liverpool, United Kingdom*

77 *Department of Physics, Jožef Stefan Institute and University of Ljubljana, Ljubljana, Slovenia*

78 *School of Physics and Astronomy, Queen Mary University of London, London, United Kingdom*

79 *Department of Physics, Royal Holloway University of London, Surrey, United Kingdom*

80 *Department of Physics and Astronomy, University College London, London, United Kingdom*

81 *Louisiana Tech University, Ruston LA, United States of America*

82 *Laboratoire de Physique Nucléaire et de Hautes Energies, UPMC and Université Paris-Diderot and CNRS/IN2P3, Paris, France*

83 *Fysiska institutionen, Lunds universitet, Lund, Sweden*

84 *Departamento de Fisica Teorica C-15, Universidad Autonoma de Madrid, Madrid, Spain*

85 *Institut für Physik, Universität Mainz, Mainz, Germany*

86 *School of Physics and Astronomy, University of Manchester, Manchester, United Kingdom*

87 *CPPM, Aix-Marseille Université and CNRS/IN2P3, Marseille, France*

88 *Department of Physics, University of Massachusetts, Amherst MA, United States of America*

89 *Department of Physics, McGill University, Montreal QC, Canada*

90 *School of Physics, University of Melbourne, Victoria, Australia*

91 *Department of Physics, The University of Michigan, Ann Arbor MI, United States of America*

92 *Department of Physics and Astronomy, Michigan State University, East Lansing MI, United States of America*

93 [a] *INFN Sezione di Milano;* [b] *Dipartimento di Fisica, Università di Milano, Milano, Italy*

94 *B.I. Stepanov Institute of Physics, National Academy of Sciences of Belarus, Minsk, Republic of Belarus*

95 *National Scientific and Educational Centre for Particle and High Energy Physics, Minsk, Republic of Belarus*

96 *Department of Physics, Massachusetts Institute of Technology, Cambridge MA, United States of America*

97 *Group of Particle Physics, University of Montreal, Montreal QC, Canada*

98 *P.N. Lebedev Physical Institute of the Russian Academy of Sciences, Moscow, Russia*

99 *Institute for Theoretical and Experimental Physics (ITEP), Moscow, Russia*

100 *National Research Nuclear University MEPhI, Moscow, Russia*

101 *D.V. Skobeltsyn Institute of Nuclear Physics, M.V. Lomonosov Moscow State University, Moscow, Russia*

102 *Fakultät für Physik, Ludwig-Maximilians-Universität München, München, Germany*

103 *Max-Planck-Institut für Physik (Werner-Heisenberg-Institut), München, Germany*

104 *Nagasaki Institute of Applied Science, Nagasaki, Japan*

105 *Graduate School of Science and Kobayashi-Maskawa Institute, Nagoya University, Nagoya, Japan*

106 (a) *INFN Sezione di Napoli;* (b) *Dipartimento di Fisica, Università di Napoli, Napoli, Italy*

107 *Department of Physics and Astronomy, University of New Mexico, Albuquerque NM, United States of America*

108 *Institute for Mathematics, Astrophysics and Particle Physics, Radboud University Nijmegen/Nikhef, Nijmegen, Netherlands*

109 *Nikhef National Institute for Subatomic Physics and University of Amsterdam, Amsterdam, Netherlands*

110 *Department of Physics, Northern Illinois University, DeKalb IL, United States of America*

111 *Budker Institute of Nuclear Physics, SB RAS, Novosibirsk, Russia*

112 *Department of Physics, New York University, New York NY, United States of America*

113 *Ohio State University, Columbus OH, United States of America*

114 *Faculty of Science, Okayama University, Okayama, Japan*

115 *Homer L. Dodge Department of Physics and Astronomy, University of Oklahoma, Norman OK, United States of America*

116 *Department of Physics, Oklahoma State University, Stillwater OK, United States of America*

117 *Palacký University, RCPTM, Olomouc, Czech Republic*

118 *Center for High Energy Physics, University of Oregon, Eugene OR, United States of America*

119 *LAL, Univ. Paris-Sud, CNRS/IN2P3, Université Paris-Saclay, Orsay, France*

120 *Graduate School of Science, Osaka University, Osaka, Japan*

121 *Department of Physics, University of Oslo, Oslo, Norway*

122 *Department of Physics, Oxford University, Oxford, United Kingdom*

123 (a) *INFN Sezione di Pavia;* (b) *Dipartimento di Fisica, Università di Pavia, Pavia, Italy*

124 *Department of Physics, University of Pennsylvania, Philadelphia PA, United States of America*

125 *National Research Centre "Kurchatov Institute" B.P.Konstantinov Petersburg Nuclear Physics Institute, St. Petersburg, Russia*

126 (a) *INFN Sezione di Pisa;* (b) *Dipartimento di Fisica E. Fermi, Università di Pisa, Pisa, Italy*

127 *Department of Physics and Astronomy, University of Pittsburgh, Pittsburgh PA, United States of America*

128 (a) *Laboratório de Instrumentação e Física Experimental de Partículas - LIP, Lisboa;* (b) *Faculdade de Ciências, Universidade de Lisboa, Lisboa;* (c) *Department of Physics, University of Coimbra, Coimbra;* (d) *Centro de Física Nuclear da Universidade de Lisboa, Lisboa;* (e) *Departamento de Fisica, Universidade do Minho, Braga;* (f) *Departamento de Fisica Teorica y del Cosmos and CAFPE, Universidad de Granada, Granada (Spain);* (g) *Dep Fisica and CEFITEC of Faculdade de Ciencias e Tecnologia, Universidade Nova de Lisboa, Caparica, Portugal*

129 *Institute of Physics, Academy of Sciences of the Czech Republic, Praha, Czech Republic*

130 *Czech Technical University in Prague, Praha, Czech Republic*

131 *Faculty of Mathematics and Physics, Charles University in Prague, Praha, Czech Republic*

132 *State Research Center Institute for High Energy Physics (Protvino), NRC KI, Russia*

133 *Particle Physics Department, Rutherford Appleton Laboratory, Didcot, United Kingdom*

134 (a) *INFN Sezione di Roma;* (b) *Dipartimento di Fisica, Sapienza Università di Roma, Roma, Italy*

135 (a) *INFN Sezione di Roma Tor Vergata;* (b) *Dipartimento di Fisica, Università di Roma Tor Vergata, Roma, Italy*

136 (a) *INFN Sezione di Roma Tre;* (b) *Dipartimento di Matematica e Fisica, Università Roma Tre, Roma, Italy*

137 (a) *Faculté des Sciences Ain Chock, Réseau Universitaire de Physique des Hautes Energies - Université Hassan II, Casablanca;* (b) *Centre National de l'Energie des Sciences Techniques Nucleaires, Rabat;* (c) *Faculté des Sciences Semlalia, Université Cadi Ayyad, LPHEA-Marrakech;* (d) *Faculté des Sciences, Université Mohamed Premier and LPTPM, Oujda;* (e) *Faculté des sciences, Université Mohammed V, Rabat, Morocco*

138 *DSM/IRFU (Institut de Recherches sur les Lois Fondamentales de l'Univers), CEA Saclay (Commissariat à l'Energie Atomique et aux Energies Alternatives), Gif-sur-Yvette, France*

139 *Santa Cruz Institute for Particle Physics, University of California Santa Cruz, Santa Cruz CA, United States of America*

140 *Department of Physics, University of Washington, Seattle WA, United States of America*

141 *Department of Physics and Astronomy, University of Sheffield, Sheffield, United Kingdom*

142 *Department of Physics, Shinshu University, Nagano, Japan*

143 *Fachbereich Physik, Universität Siegen, Siegen, Germany*

144 *Department of Physics, Simon Fraser University, Burnaby BC, Canada*

145 *SLAC National Accelerator Laboratory, Stanford CA, United States of America*

146 (a) *Faculty of Mathematics, Physics & Informatics, Comenius University, Bratislava;* (b) *Department of Subnuclear Physics, Institute of Experimental Physics of the Slovak Academy of Sciences, Kosice, Slovak Republic*

147 (a) *Department of Physics, University of Cape Town, Cape Town;* (b) *Department of Physics, University of Johannesburg, Johannesburg;* (c) *School of Physics, University of the Witwatersrand, Johannesburg, South Africa*

148 (a) *Department of Physics, Stockholm University;* (b) *The Oskar Klein Centre, Stockholm, Sweden*

149 *Physics Department, Royal Institute of Technology, Stockholm, Sweden*

150 *Departments of Physics & Astronomy and Chemistry, Stony Brook University, Stony Brook NY, United States of America*

151 *Department of Physics and Astronomy, University of Sussex, Brighton, United Kingdom*

152 *School of Physics, University of Sydney, Sydney, Australia*

153 *Institute of Physics, Academia Sinica, Taipei, Taiwan*

154 *Department of Physics, Technion: Israel Institute of Technology, Haifa, Israel*

155 *Raymond and Beverly Sackler School of Physics and Astronomy, Tel Aviv University, Tel Aviv, Israel*

156 *Department of Physics, Aristotle University of Thessaloniki, Thessaloniki, Greece*

157 *International Center for Elementary Particle Physics and Department of Physics, The University of Tokyo, Tokyo, Japan*

158 *Graduate School of Science and Technology, Tokyo Metropolitan University, Tokyo, Japan*

159 *Department of Physics, Tokyo Institute of Technology, Tokyo, Japan*

160 *Department of Physics, University of Toronto, Toronto ON, Canada*

161 (a) *TRIUMF, Vancouver BC;* (b) *Department of Physics and Astronomy, York University, Toronto ON, Canada*

162 *Faculty of Pure and Applied Sciences, and Center for Integrated Research in Fundamental Science and Engineering, University of Tsukuba, Tsukuba, Japan*

163 *Department of Physics and Astronomy, Tufts University, Medford MA, United States of America*

164 (a) *INFN Gruppo Collegato di Udine, Sezione di Trieste, Udine;* (b) *ICTP, Trieste;* (c) *Dipartimento di Chimica, Fisica e Ambiente, Università di Udine, Udine, Italy*

165 *Department of Physics and Astronomy, University of Uppsala, Uppsala, Sweden*

166 *Department of Physics, University of Illinois, Urbana IL, United States of America*

167 *Instituto de Física Corpuscular (IFIC) and Departamento de Física Atómica, Molecular y Nuclear and Departamento de Ingeniería Electrónica and Instituto de Microelectrónica de Barcelona (IMB-CNM), University of Valencia and CSIC, Valencia, Spain*

168 *Department of Physics, University of British Columbia, Vancouver BC, Canada*

169 *Department of Physics and Astronomy, University of Victoria, Victoria BC, Canada*

170 *Department of Physics, University of Warwick, Coventry, United Kingdom*

171 Waseda University, Tokyo, Japan

172 Department of Particle Physics, The Weizmann Institute of Science, Rehovot, Israel

173 Department of Physics, University of Wisconsin, Madison WI, United States of America

174 Fakultät für Physik und Astronomie, Julius-Maximilians-Universität, Würzburg, Germany

175 Fakult[a]t für Mathematik und Naturwissenschaften, Fachgruppe Physik, Bergische Universität Wuppertal, Wuppertal, Germany

176 Department of Physics, Yale University, New Haven CT, United States of America

177 Yerevan Physics Institute, Yerevan, Armenia

178 Centre de Calcul de l'Institut National de Physique Nucléaire et de Physique des Particules (IN2P3), Villeurbanne, France

a Also at Department of Physics, King's College London, London, United Kingdom

b Also at Institute of Physics, Azerbaijan Academy of Sciences, Baku, Azerbaijan

c Also at Novosibirsk State University, Novosibirsk, Russia

d Also at TRIUMF, Vancouver BC, Canada

e Also at Department of Physics & Astronomy, University of Louisville, Louisville, KY, United States of America

f Also at Department of Physics, California State University, Fresno CA, United States of America

g Also at Department of Physics, University of Fribourg, Fribourg, Switzerland

h Also at Departament de Fisica de la Universitat Autonoma de Barcelona, Barcelona, Spain

i Also at Departamento de Fisica e Astronomia, Faculdade de Ciencias, Universidade do Porto, Portugal

j Also at Tomsk State University, Tomsk, Russia

k Also at CPPM, Aix-Marseille Université and CNRS/IN2P3, Marseille, France

l Also at Universita di Napoli Parthenope, Napoli, Italy

m Also at Institute of Particle Physics (IPP), Canada

n Also at Particle Physics Department, Rutherford Appleton Laboratory, Didcot, United Kingdom

o Also at Department of Physics, St. Petersburg State Polytechnical University, St. Petersburg, Russia

p Also at Department of Physics, The University of Michigan, Ann Arbor MI, United States of America

q Also at Louisiana Tech University, Ruston LA, United States of America

r Also at Institucio Catalana de Recerca i Estudis Avancats, ICREA, Barcelona, Spain

s Also at Graduate School of Science, Osaka University, Osaka, Japan

t Also at Department of Physics, National Tsing Hua University, Taiwan

u Also at Department of Physics, The University of Texas at Austin, Austin TX, United States of America

v Also at Institute of Theoretical Physics, Ilia State University, Tbilisi, Georgia

w Also at CERN, Geneva, Switzerland

x Also at Georgian Technical University (GTU),Tbilisi, Georgia

y Also at Ochadai Academic Production, Ochanomizu University, Tokyo, Japan

z Also at Manhattan College, New York NY, United States of America

aa Also at Hellenic Open University, Patras, Greece

ab Also at Institute of Physics, Academia Sinica, Taipei, Taiwan

ac Also at LAL, Univ. Paris-Sud, CNRS/IN2P3, Université Paris-Saclay, Orsay, France

ad Also at Academia Sinica Grid Computing, Institute of Physics, Academia Sinica, Taipei, Taiwan

ae Also at School of Physics, Shandong University, Shandong, China

af Also at Moscow Institute of Physics and Technology State University, Dolgoprudny, Russia

ag Also at Section de Physique, Université de Genève, Geneva, Switzerland

ah Also at International School for Advanced Studies (SISSA), Trieste, Italy

ai Also at Department of Physics and Astronomy, University of South Carolina, Columbia SC, United States of America

[aj] Also at School of Physics and Engineering, Sun Yat-sen University, Guangzhou, China

[ak] Also at Institute for Nuclear Research and Nuclear Energy (INRNE) of the Bulgarian Academy of Sciences, Sofia, Bulgaria

[al] Also at Faculty of Physics, M.V.Lomonosov Moscow State University, Moscow, Russia

[am] Also at National Research Nuclear University MEPhI, Moscow, Russia

[an] Also at Department of Physics, Stanford University, Stanford CA, United States of America

[ao] Also at Institute for Particle and Nuclear Physics, Wigner Research Centre for Physics, Budapest, Hungary

[ap] Also at Flensburg University of Applied Sciences, Flensburg, Germany

[aq] Also at University of Malaya, Department of Physics, Kuala Lumpur, Malaysia

[*] Deceased